DOE/BC/10845-10
(DE88001228)

FOSSIL ENERGY

ENHANCED OIL RECOVERY BY SURFACTANT-ENHANCED VOLUMETRIC SWEEP EFFICIENCY

Second Annual Report for the Period
September 30, 1986 to September 30, 1987

By
Jeffrey H. Harwell
John F. Scamehorn

April 1988

Performed Under Contract No. AC19-85BC10845

University of Oklahoma
Norman, Oklahoma

Bartlesville Project Office
U. S. DEPARTMENT OF ENERGY
Bartlesville, Oklahoma

DISCLAIMER

Printed in the United States of America. Available from:
National Technical Information Service
U.S. Department of Commerce
5285 Port Royal Road
Springfield, VA 22161

NTIS price codes
Paper copy: **A07**
Microfiche copy: **A01**

DOE/BC/10845-10
Distribution Category UC-122

ENHANCED OIL RECOVERY BY SURFACTANT-ENHANCED VOLUMETRIC SWEEP EFFICIENCY

Second Annual Report for the Period
September 30, 1986-September 30, 1987

By
Jeffrey H. Harwell
John F. Scamehorn

April 1988

Work Performed Under Contract No. AC19-85BC10845

Prepared for
U.S. Department of Energy
Assistant Secretary for Fossil Energy

Fred W. Burtch, Project Manager
Bartlesville Project Office
P.O. Box 1398
Bartlesville, OK 74005

Prepared by
University of Oklahoma
School of Chemical Engineering & Materials Science
Norman, OK 73019

ABSTRACT

It is widely known that heterogeneities in oil reservoirs occurring as a result of permeability variations in the rock can have a detrimental effect on an oil recovery process; preferential diversion of injected displacement fluid occurs through the high-permeability zones, leaving the lower-permeability zones at a high residual oil content at a time when it is no longer economically viable to continue the oil recovery process. A novel oil recovery process is described which aims to improve the volumetric sweep efficiency of oil recovery. High-permeability zones are partially or completely plugged off by using the chromatographic and phase behavior of surfactants and their mixtures and the preferential invasion of high-permeability areas by low-viscosity injected fluids. The plugging will divert flow into regions of higher oil saturation.

One possible combination of surfactants for this application is that of anionic and cationic surfactants.The effect of important process variables on the phase boundaries of such mixtures have been measured; such variables include pH, temperature, strength of electrolyte and molecular structure. Commercial surfactants occur almost always as mixtures of the members of a homologous series; this has important implications for the adsorptive and thus chromatographic properties of surfactant slugs. Measurements of the adsorption of binary mixtures of anionic surfactants of a homologous series have been predicted a priori using only the pure component adsorption isotherms.

Important phenomena pertaining to the new process include chromatographic transport, mixed micelle formation and surfactant precipitation. These phenomena have been studied experimentally while occurring simultaneously in a porous medium. The results of these studies have been successfully modeled, and this reinforces understanding of the basic physics of the process. A critical requirement in evaluating the technical feasibility of the process is the development of a mathematical simulation which is presented here. Case studies are presented which address different types of heterogeneous reservoirs. These studies examine the

effectiveness of the plugs in enhancing the net oil recovery, so that types of reservoirs which are potential candidates for the process may be delineated.

TABLE OF CONTENTS

ENHANCED OIL RECOVERY

BY

SURFACTANT-ENHANCED VOLUMETRIC SWEEP EFFICIENCY

CHAPTER 1

INTRODUCTION

In spite of the current ebb in oil prices, and as a direct result of diminishing oil reserves, it is still estimated by the U.S. Department of Energy that oil prices may reach forty or fifty dollars a barrel by the year 2000. However, it is widely known that conventional waterflooding technology leaves over two-thirds of the original oil in place in a reservoir unproduced at the point when it is no longer economic to continue its operation[1].This vast amount of unrecovered petroleum is the target of enhanced oil recovery. It is imperative that research into enhanced oil recovery processes begins now and reaches completion so that practical approaches can be formulated and implemented in good time.

The low efficiency of the waterflooding process is caused by both the difficulty of distributing injected displacement fluid throughout the reservoir (volumetric sweep efficiency) and the extent to which oil can be displaced from a portion of the reservoir when it is invaded by injected displacement fluid (microscopic displacement efficiency.) Improvements in the latter aim at overcoming capillary forces which arise from high oil/water interfacial tension and resist displacement of residual oil droplets from reservoir rocks. This microscopic problem is addressed by such techniques as surfactant flooding[2].

Volumetric sweep efficiencies arise because of the heterogeneous structure of real reservoirs[1].There are always areas of a reservoir which are more permeable (i.e.less resisting) to reservoir or injected fluids than the rest of

the reservoir; injected fluids tend to flow through the high-permeability areas, with little flow through the low-permeability areas. The oil is produced from the high-permeability areas, and the water-to-oil ratio in the production wells increases until it is no longer economically feasible to continue the waterflooding. At this point, there is still a relatively high content of unrecovered residual oil in the low permeability areas.

There are three basic ways to combat this phenomenon. One is to reduce the viscosity of the reservoir fluids by, for example, in-situ combustion and steam flooding. Another is to increase the viscosity of the displacement fluids by, for example, polymer flooding. A third approach is to partially or completely block off high-permeability regions. This will force the injected displacement fluids into the low permeability areas of high residual oil content, resulting in an decrease in the water-to-oil ratio and final recovery of the oil in place.

To date, no solution to the volumetric sweep problem has been without severe limitations. In-situ combustion is expensive and difficult to maintain. Using a high-viscosity drive fluid tends to reduce flow rates, and large volumes of solution are lost through the high permeability zones. Additionally, polymers degrade in reservoirs because of thermal action, microbial action, and shearing of the long polymer chains.[3-6].

Interest in selective plugging or isolation of the high permeability regions of a reservoir has increased over the last 40 years.[7-8] .The older methods have met with little success, but several new methods appear more promising. One of these involves the use of foams. Foams, however, are non-equilibrium structures and decay too early to be of use[9]. They are also difficult to form in-situ.Another procedure involves in-situ gelation of polymer/crosslinking agent[10,11]. However, it is difficult to control gelation time and prevent gelation from occurring near the injection well.If the plugging occurs only near the well bore, fluid diverted into the low permeability zones near the well bore moves back into the high permeability zones after bypassing the plug. Still another method involves the use of microbes[12-15]. Bacteria

are injected, and cell mass, cell debris and possibly metabolic byproducts are the blocking agents. Unfortunately, the majority of plugging has tended to occur at the inlet of laboratory cores due to the strong adsorption of the injected bacteria[14,15]

The objective of this research is to investigate a novel process of enhancing volumetric sweep efficiency[16] using surfactants (normally associated with microscopic recovery efficiency to plug the high permeability zones of a reservoir. In this new process, two very dilute surfactant slugs (concentrations on the order of hundredths of a weight percent) are sequentially injected into the reservoir formation, with a brine spacer injected between them. The two surfactant solutions have viscosities very little different from brine because they are so dilute. The two surfactants are chosen, however, so that the first surfactant has a lower chromatographic velocity of propagation than the second and so that upon mixing of the two solutions inside the reservoir, a physical or chemical interaction will occur resulting in the formation of either a solid precipitate, or a viscous, gel-like coacervate (known as "phase separation").

Since the viscosity of the injected fluids are relatively low compared to the residual oil, the injected fluids are preferentially diverted into the high-permeability zones and it is here that significant interaction between the two solutions will occur. The formation of a solid precipitate or a gel-like coacervate which occurs on in situ mixing can partially or completely block the high-permeability zones by sealing the pore throats of the permeable medium. The volumetric sweep efficiency will subsequently improve.

There are a number of potential advantages of this new method over current selective permeability reduction techniques. An important one is that it is possible to control the distance from the well bore at which plugging occurs; the mixing process is delayed until the surfactant solutions are an arbitrary distance from the well bore and deeply inside the high permeability areas. Such control exploits the tendency of different surfactant types to travel at different chromatographic velocities through the

reservoir, because of their different interactions with the reservoir minerals[17-19].

The blocking agents are, unlike foams, equilibrium structures. The surfactants are not sensitive to shear degradation (because of low molecular weight). Many commercially available surfactants are also thermally stable. Viscosity of injected fluids are little changed and injectivities may remain high relative to those of polymer solutions. Microbial degradation is less deleterious to the surfactant, and can be completely eliminated by adding side chains to the hydrophobic moeities[20,21].

Finally, it is important to distinguish between this process and classical surfactant flooding technology. Moreover, the new process should be much less sensitive to composition changes within the reservoir, and requires surfactant concentrations two or three orders of magnitude lower.

REFERENCES

(1) Craig.F.F.,Jr.,"Waterflooding,"**Secondary and Tertiary Oil Recovery Processes**,Interstate Oil Compact Commission,Oklahoma City(Sept.1974) 1-30.

(2) Shah,D.O. and R.S.Schecter,(eds.),**Improved Oil Recovery by Surfactant and Polymer Flooding** ,Academic Press,New York,N.Y.,1977.

(3) Wellington,S.L.,"Biopolymer Solution Viscosity Stabilization-Polymer Degradation and Antioxidant Use,"**Society of Petroleum Engineers Journal**, 23 (5),804,1983

(4) Prud'homme,R.K., J.T.Uhl, J.P.Poinsatte, and F.Halverson,"Rheological Monitoring of the Formation of Polyacrylamide/Cr^{+3} ,"**Society of Petroleum Engineers Journal**,23 (1), 42, 1983.

(5) Kohler,N.,M.Milas, and M.Rinaudo, "Elimination of Xanthan Microgels by New Enzymatic Treatments," **Society of Petroleum Engineers Journal**,23 (1), 42, 1983.

(6) Thomas,L.K.,T.N.DIxon,R.G.Pierson,"Fractured Reservoir Formulation,"**Society of Petroleum Engineer's Journal**,23(1),42,1983.

(7) Martin,D.,K.H.Anderson, and F.W.Ellenberger, "Recent Advances in Selective Exclusion of Water in Input wells,"1947.

(8) Yuster,S.T. and J.C.Calhoune,Jr.,"The Selective Plugging of Oil Sands,"**Producer's Monthly**,8 (7), 31, 1947.

(9) Rand,P.B. and A.M. Kyaynik, "Drainage of Aqueous Foams: Generation-Pressure and Cell-size effects,"

Society of Petroleum Engineer's Journal,23 (1), 152, 1983.

(10) Willhite,G.P.,P.W.Green,S.Vorshoughi,"Evaluation of Reducing Permeability in Porous Rocks by In-situ Polymer Treatment," Contracts for Field Projects and Supporting Research on Enhanced Oil Recovery and Improved Drilling Technology, Progress Review No.35, Bill Linville,ed.,DOE/BETC-83/3,p.38,October 1983.

(11) Sandiford,B.B."Selectively Controlling Fluid Flow Through the Higher Permeability Zones of Subterranean Reservoirs,'U.S.Pat. Appl.No.178911

(12) Crawford,P.B., "Possible Bacterial Correction of Stratification Problems",**Prod.Monthly(1961)**,25,10-11.

(13) Crawford,P.B.,"Water Technology:Continual Changes Observed in Bacterial Stratification Rectification," **Prod.Monthly(1962)**,26,123.

(14) Jennerman,G.E.,R.M.Knapp,M.J.McInerney, D.E.Menzie, and D.E.Revus,"Experimental Studies of In-situ Microbial Enhanced Oil Recovery," **Society of Petroleum Emgineer's Journal,24(1)**,33,1984.

(15) Freeman,C.D.,**The Use of Microorganisms to Increase The Recovery of Oil from Cores**,"M.S.Thesis,School of Petroleum and Geological Engineering,The University of Oklahoma,1984.

(16) Arshad,A.,**Improving Sweep Efficiency In Oil Reservoirs Using Surfactant Phase Behavior**", School of Chemical Engineering and Materials Science, The University of Oklahoma,1985.

(17) Harwell, J.H., **Surfactant Adsorption and Chromatographic Movement with Application in Enhanced Oil Recovery**, Ph.D.dissertation, The University of Texas at Austin,1983

(18) Harwell,J.H., F.G.Helfferich, and R.S.Schechter, "Effect of Mixed Micelle Formation on Chromatographic

Movement of Surfactant Mixtures,"**AICHE** J.,28 (3),448,1982.

(19) Harwell,J.H.,R.S.Schechter, and W.H.Wade, "Surfactant Chromatographic Movement:An Experimental Study," **AICHE** J.,**31**(3), 415., 1985.

(20) Sivak, A., M.goyer, J.Peawak, and P.Thayer, "Environmental and Human Health Aspects of Commercially Important Surfactants,"in **Solution Behavior of Surfactants**, Vol.1,K.L.Mittal,ed.,Plenum Press, New York,1982.

(21) Swisher,R.D., "Surfactants and the Environment: Biodegradation Aspects,"in **Solution Behavior of Surfactants,Vol.**1,K.L.Mittal, ed., Plenum Press, New York (1979.)

EFFECT OF EXPERIMENTAL VARIABLES ON THE PRECIPITATION PHASE BOUNDARIES OF ANIONIC/CATIONIC SURFACTANT MIXTURES

INTRODUCTION

The phase behavior of anionic/cationic surfactant mixtures was investigated by measuring the precipitation boundaries of the sodium dodecyl sulfate/dodecylpyridinium chloride (SDS/DPC) system over a wide range of concentrations. The effects of solution parameters on this system were studied by measuring the phase boundaries at two pH levels, two temperatures, and two salinities. Results showed that the precipitation boundaries were unaffected by pH changes. An increase in temperature reduced the precipitation region and a decrease in ionic strength increased it. The effect of anionic surfactant chain length was also studied and results showed that the precipitation boundaries shifted to higher anionic surfactant concentrations at decreasing chain length. A previously developed model for predicting the precipitation boundaries in anionic/cationic surfactant systems was tested using experimental data obtained in this study. The model described the precipitation phase boundaries well except in regions where coacervate and gels formed.

EXPERIMENTAL

Materials The anionic surfactants used were sodium dodecyl sulfate (SDS), sodium decyl sulfate (SDeS), and sodium octyl sulfate (SOS). SDS was obtained from Fisher Scientific and SDeS and SOS were obtained from Kodak Chemicals, Inc. The cationic surfactant used was dodecyl pyridinium chloride (DPC) obtained from Pfaltz and Bayer (technical grade).

All surfactants used in the experiments were purified by recrystallization. SDS and SDeS were recrystallized twice from ethanol and dried under vacuum for 72 hours. SOS was recrystallized twice in 2-propanol, washed with diethyl ether, and then dried under vacuum for 72 hours. DPC was recrystallized from a mixture of petroleum ether and ethanol

and then dried under vacuum for 72 hours.

Two brine solutions were used: a 0.15M sodium chloride (NaCl) solution and a 10% synthetic field brine (SFB) solution. Ten percent SFB is a dilution of full strength SFB whose composition is shown in Table 1. NaCl and other inorganic salts used for 100% SFB were obtained from Fisher Scientific, Inc. and were used as received. Deionized, distilled water was used in preparing all solutions and pH was adjusted with 0.1M NaOH and 0.1M HCl.

Methods

The experimental measurements has been described in an earlier paper (2). The SDS/DPC precipitation phase boundaries was initially measured at a pH of 8.4, 30° C, and 0.15M NaCl. Precipitation phase boundaries were then measured by varying one parameter at a time. The pH was changed to 6.9, temperature to 40° C, and the brine salinity to 10% SFB.

THEORY

Effect of pH

Two important parameters that affect the precipitation phase boundaries are the solubility product constant, K_{sp}, and the critical micelle concentration, CMC. If these parameters are affected by pH, a change in the precipitation phase boundaries will occur. If the charge of the surfactants are also affected by pH, the reaction stoichiometry between the two interacting surfactants will change.

Effect of Temperature

The two basic equilibria involved in anionic-cationic surfactant precipitation, monomer-precipitate and monomer-micelle equilibrium, are affected by changes in temperature. The effect of temperature on the monomer-precipitate equilibrium is reflected in the K_{sp}^{o} value which determines the location of the monomer-precipitate line shown in Figure 5 of ref. 2. In monomer-micelle equilibrium, temperature can affect the CMC of each surfactant which can displace the micelle boundary.

K_{sp}^{o}, as defined in eq. [1] of ref. 2, is the thermodynamic solubility product constant. K_{sp}^{o} can also be expressed as follows:

$$K_{sp}^{o} = K_{sp}' f_{\pm}^{2} \quad [1]$$

where K_{sp}' is the stoichiometric solubility product constant.

An increase in temperature generally favors the dissociation of precipitates into ions which consequently increases the solubility product, K_{sp}'. On the other hand, mean activity coefficients obtained using the extended Debye-Huckel equation (eqn. [2] of ref.2) decrease with increasing temperature which can offset the increase in K_{sp}^{o}. For small temperature changes, however, this effect is negligible. Hence, K_{sp}^{o} will increase with increasing temperature in general.

In anionic-cationic surfactant (3,4) and surfactant-salt (5,6) systems, this trend is observed with the solubility product constants increasing with increasing temperature. The logarithm of the solubility product, when plotted against reciprocal temperature in these systems, yields a straight line.

For surfactant-dye systems, Tomlinson et. al. (7) observed a minimum in the change of solubility product with temperature. A polynomial expression based on interaction data between sodium cromoglycate and a homologous series of alkylbenzenedimethylammonium chlorides was obtained which relates the solubility product and temperature as follows:

$$\log K_{sp}^{o} = A - BT + CT^{2} - DT^{3} \quad [2]$$

where A, B, C, and D are constants.

With expressions relating temperature and the solubility product constant such as equation [2], thermodynamic variables of the dissolution reaction can be calculated. The standard enthalpy of precipitation, ΔH^{o}, can be obtained from expressions such as equation [2] or data relating K_{sp}^{o} and temperature either by differentiation of the equation or by getting the slope of the log K_{sp}^{o} vs. 1/T plot. The standard free energy of precipitation, ΔG^{o}, can be calculated using the expression,

$$\Delta G^{o} = -RT\ln K_{sp}^{o}$$

from which the standard entropy, ΔS^{o} is calculated through the following relation:

$$\Delta G^{o} = \Delta H^{o} - T\Delta S^{o}$$

Calculation of these thermodynamic variables can help in understanding the dissolution or precipitation mechanism.

The effect of temperature on monomer-micelle equilibrium is evaluated by considering the CMC of the surfactants. For ionic surfactants, the effect of temperature is small (energies involved in micelle formation are small) but nevertheless complex in that CMC goes through a minimum with increasing temperature and then rises with further increases in temperature (8). Flockhart (9) measured the effect of temperature on the CMC of several alkyl sulfates and found that for SDS with no added salt, the minimum occurred at 25°C.

Effect of Ionic Strength

K_{sp}^{o}, the thermodynamic solubility product constant, is dependent only on temperature. Changes in ionic strength and consequently activity coefficient would therefore have to be compensated by adjustments in the solubility product constant, K_{sp}'. For a uni-univalent electrolyte, K_{sp}' values at different ionic strengths can be related as follows:

$$K_{sp}^{o} = K_{sp1}'(f_{\pm 1})^2 = K_{sp2}'(f_{\pm 2})^2 \qquad [3]$$

where the K_{sp}' value is obtained from the monomer-precipitate line and the activity coefficient is evaluated in the usual manner using equation [2] of ref. 2.

At decreasing ionic strength, the activity coefficient, $f_{\pm}$, will increase until a limiting value of unity is reached at zero ionic strength. From equation [3], K_{sp} has to decrease with increasing $f_{\pm}$ to maintain a constant K_{sp}^{o}. The result of a reduced K_{sp}' is a lowering of solubility or a downward shift of the monomer-precipitate line.

In mixed electrolyte systems like SFB, competing precipitation equilibria involving one or more ions reacting with only one oppositely charged ion can occur. For example, in the SDS/DPC system in synthetic field brine, DS^- monomers can precipitate not only with DP^+ monomers but with Ca^{2+} ions as well. In this case, the precipitation reaction with a higher equilibrium constant (lower solubility product constant) will preferentially occur.

The effect of electrolytes on the CMC of surfactants has been well studied. In the presence of additional electrolytes, the thickness of the electrical double layer surrounding the ionic headgroups decreases. A quenching of

the electrostatic repulsion between the headgroups will occur which favors micellization. Hence, an increase in electrolyte concentration decreases the CMC of pure ionic surfactants. The CMC of pure ionic surfactants is related to the unbound counterion concentration as follows (10):

$$\ln CMC = K_2 - K_g[\ln C_u] \qquad [4]$$

where C_u is the concentration of unbound counterions and K_2 and K_g are constants.

In previous model calculations of the precipitation phase boundaries, C_u was constant because of the swamping electrolyte assumption. When the counterion concentration contributed by the surfactants becomes significant, however, equation [4] should be included in model calculations.

The use of equation [4] requires a knowledge of counterion binding. A material balance on the precipitation phase boundary for the Na^+ counterion can be written as:

$$[Na^+]_{tot} = [NaCl] + C_{SDS} = [Na^+]_u + [Na^+]_b \qquad [5]$$

where $[Na^+]_{tot}$ is the total concentration of Na^+ ions, [NaCl] is the concentration of added electrolyte, $[Na^+]_u$ is the unbound Na^+ concentration, and $[Na^+]_b$ is the bound counterion concentration. This equation can also be written as:

$$[NaCl] + C_{SDS} = [Na^+]_u + B_{Na}\{[DS^-]_{mic} - [DP^+]_{mic}\} \qquad [6]$$

where B_{Na} is the fractional sodium ion binding on the micelles. B_{Na} is defined as the ratio of Na^+ ions bound on the mixed anionic-cationic micelle to the number of excess DS^- monomers in that mixed micelle, assuming a 1:1 charge neutralization of the DS^- and DP^+ monomers.

Equation [6] applies for the lower branch of the precipitation phase boundaries where previous calculations using regular solution theory have shown micelles in this branch to be SDS-rich. A similar equation for the Cl^- counterion can be written on the DPC-rich branch of the precipitation boundary:

$$[NaCl] + C_{DPC} = [Cl^-]_u + B_{Cl}\{[DP^+]_{mic} - [DS^-]_{mic}\} \qquad [7]$$

where $[Cl^-]_u$ is the concentration of unbound Cl^- ions and

B_{Cl} is the chloride ion fractional binding.

For model calculations, CMC_{DS} and CMC_{DP} can be expressed in the form of equation [4] where the constants are evaluated from independent CMC measurements. Equations [6] and [7] present some problems in that no counterion fractional binding for Na^+ and Cl^- have been found in the literature for mixed anionic-cationic micelles of SDS and DPC. It is even doubtful if binding has ever been measured for any anionic/cationic system since the possibility of counterion binding has not been generally considered in these systems.

Although a few studies (11,12) have shown through electrophoretic mobility and conductance measurements that anionic/cationic mixed micelles are charged, it has also been suggested that these mixed micelles consist of "nearly equal numbers of anions and cations so that no counterions are present which could form a diffuse layer" (13). No experimental data was measured in this study to support either contention; it may be possible though to study binding effects from emf data following experimental procedures (14) used for surfactant mixtures other than anionic/cationic systems.

Some models (14,15,16) have been proposed for calculating counterion binding. Models used for ionic/nonionic surfactant micelles can probably be extended to anionic/cationic surfactant micelles by assuming that neutralized anionic/cationic surfactant pairs in the mixed micelle behave as nonionic surfactants. For the purposes of this study, however, only a simplified model will be considered and counterion binding, although important for proper modeling of the precipitation phenomena, will be neglected. As such, equations [6] and [7] will not be incorporated into the model and only a modified form of equation [4] which follows will be included:

$$\ln CMC = K_2 - K_g \ln[C_{tot}]$$

where C_{tot} is the total counterion concentration. This equation can be written for SDS and DPC as follows:

$$\ln CMC_{DS} = K_2 - K_g \ln\{[Na^+]_{tot}\} \quad [8]$$

$$\ln CMC_{DP} = K_2' - K_g' \ln\{[Cl^-]_{tot} \quad [9]$$

where $[Na^+]_{tot}$ and $[Cl^-]_{tot}$ are calculated using the following equations:

$$[Na^+]_{tot} = [NaCl] + C_{SDS} \quad [10]$$

$$[Cl^-]_{tot} = [NaCl] + C_{DPC} \quad [11]$$

Equations [10] and [11] come from equations [6] and [7] where the bound counterions are neglected. Ionic strength is calculated from the following equation:

$$I = [NaCl] + C_{SDS} + C_{DPC} \quad [12]$$

Using equations [8-12] and equations [1-7] of ref. 2 C_{DPC} can be calculated for a given C_{SDS} to obtain the precipitation phase boundaries.

Aside from neglecting bound counterions in equations [8] and [9], it has also been assumed in these two expressions that the concentration of other inorganic ions present in 10% SFB are small enough to have a negligible effect on the CMC.

Effect of Surfactant Chain Length

One of the effects of surfactant chain length on precipitation phase behavior is an increase in the solubility of the precipitate with decreasing chain length. Stated differently, the tendency to precipitate increases as the chain length increases. This relationship is shown in an empirical equation obtained by Nakamura and Muramatsu (17) for the N-dodecyl-alanine/sodium alkyl sulfate complex:

$$\ln K = 0.79N + 1.65 \quad [13]$$

where K is the association constant for the complex and N is the number of carbon atoms in the hydrocarbon chain of the SAS molecule. The increased association can be viewed as an enhancement of the electrostatic attraction between the two oppositely charged ions due to the increased hydrophobic character of the anionic surfactant chain.

A similar effect is observed in micelle formation. As the chain length of the surfactant increases, the CMC in aqueous solution decreases. This relationship has been expressed as follows (18):

$$\log CMC = C - DN \quad [14]$$

where C and D are constants. The increasing hydrophobic character of the surfactant with increasing chain length favors micelle formation, thus lowering the CMC of the surfactant.

In surfactant-dye systems, correlations between the solubility product and the CMC of the surfactant have been obtained in the following form:

$$\log K_{sp}^{o} = A \log CMC - B \qquad [15]$$

where A and B are constants. Although this relationship has been obtained in systems where one of the interacting ions is surface inactive, it can also be applied to anionic/cationic systems. For instance, if the precipitation phase boundaries of each mixture of a cationic surfactant and a homolog of a certain type of anionic surfactant were to be measured, then the CMC of the anionic surfactants can be correlated with the K_{sp}^{o} of the mixture since the same the cationic surfactant is used and its CMC will remain constant if solution parameters remain constant.

RESULTS AND DISCUSSION

Effect of pH

The phase diagram measured at pH 6.9 (30°C and 0.15M NaCl) is shown in Figure 1 superimposed on the phase diagram measured at pH 8.4. The precipitation phase boundaries, as shown in Figure 1, are not affected by a change of pH from 8.4 to 6.9. Similar results by Peacock and Matijevic (5), who worked on the precipitation of alkylbenzene sulfonates with different metal ions , showed that the precipitation phase boundary is unaffected by pH over the range 3-11.

These results can be explained by considering the behavior of the two surfactants with changing pH. The primary alkyl sulfates are stable in neutral or alkaline solution but are readily hydrolyzed in the presence of acids (19). For the pH values considered here, no hydrolysis of SDS, which can reduce the amount of monomers available and hence alter the precipitation boundaries, is expected to occur. Similarly, quaternary ammonium salts are unaffected by pH changes with the positive charge remaining in acidic, neutral, and alkaline media (8). With SDS and DPC unaffected by pH changes, interaction between the two surfactant should remain the same despite changes in pH.

For other systems in which pH changes can alter the

charge of the surfactant head group or render an interacting molecule charged, a change in the precipitation phase boundary can be expected. For instance, Barry and Russell (20) found that the stoichiometry of the alkyltrimethylammonium:amaranth complex varied from 1:3, when the pH was less than 11, to 1:4 when the pH was greater than 11. In the former case, amaranth had three negatively charged sulfonate groups which interacted with three alkyltrimethylammonium groups;in the latter case, the phenolic OH of amaranth was completely dissociated increasing the negative charges of amaranth to four.

The effect of pH on the precipitation phase boundary can also be analyzed by considering the model in ref. 2. The parameters which can alter the precipitation phase boundaries are K_{sp}', CMC_{DS}, and CMC_{DP}. K_{sp}^{o}, the true or thermodynamic solubility product constant, is not affected by pH changes since it is only a function of temperature. The solution pH was adjusted with either HCl or NaCl aqueous solutions. Since activity coefficients are not affected by negligible amounts of electrolyte added for pH adjustments, the stoichiometric solubility product should remain constant to maintain a constant K_{sp}^{o}. Hence, the monomer-precipitate line which determines the stoichiometric solubility product constant should not shift with a change in pH. Results shown in Figure 1 prove that this is the case.

If there were a side reaction occurring , such as the hydrolysis of the dodecyl sulfate, a reduction in $[DS^{-}]_{mon}$ would occur due to the competing equilibria. The hydrolysis constant should be known in this case which can then be combined with K_{sp}^{o} to give a new solubility product constant that is a function of pH. The material balance for SDS would also have to be changed in this case to include the hydrolyzed monomers.

The other parameters that need to be considered are the CMC's of the pure surfactants. It can be seen from Figure 5 of ref. 2 that given a fixed monomer-precipitate line, a change in the monomer-micelle equilibrium can shift the micelle boundary and hence alter the position of the two branches of the precipitation boundary. If the CMC's of the two surfactants were to change with pH, regular solution theory would dictate a change in the monomer-micelle distribution of the surfactants.

To see if the CMC's of SDS and DPC changed with pH, surface tension measurements were made at pH 8.4 and 6.9 at the same temperature and salinity. The CMC of SDS measured at pH 8.4 and pH 6.9 are 7.7×10^{-4} M and 7.9×10^{-4} M, respectively. For DPC, the measured CMC at pH 8.4 was 4.0×10^{-3} M and that at pH 6.9 was 3.8×10^{-3} M. The changes are negligible and as shown in Figure 1, no change was observed experimentally in the precipitation phase boundaries.

Novich and Ring (21) investigated the effect of pH on the CMC of alkylamines and showed that the CMC decreases with increasing pH. This effect was attributed to neutral molecules formed by hydrolysis which reduces the repulsion between charged heads, enhancing micelle formation and lowering the CMC. Scamehorn (22) observed no detectable change in CMC values of alkylbenzene sulfonates with pH between a pH of 1 and 10. No data on the effect of pH on the CMC of other types of surfactants have been found in the literature. CMC lowering with increasing pH is probably limited to hydrolyzing surfactants.

Effect of Temperature

The measured phase boundaries at 40°C are shown in Figure 2 together with the modeled phase boundaries measured at 30°C. Both phase diagrams were measured at 0.15M NaCl and pH 8.4. For clarity, the data points at 40°C are connected with a dashed line and the coacervate region of the 30°C phase diagram was excluded.

At very low concentrations of SDS and DPC, the accuracy of data obtained through visual observations alone is limited and so laser measurements were used to obtain more accurate phase boundaries. For the 30°C phase diagram, only the data points obtained through surface tension measurements are shown other than those obtained through visual observation.

As shown in Figure 2, the lower branch of the precipitation boundaries moved to higher SDS concentrations and the upper branch shifted to lower DPC concentrations. The CMC of SDS increased from 7.7×10^{-4} M at 30°C to 8.9×10^{-4} M at 40°C. The CMC of DPC was little affected by temperature showing a very slight decrease from 4.0×10^{-3} M at 30°C to 3.9×10^{-3} M at 40°C.

In samples very near the upper branch of the precipitation boundaries, small balls of gel were seen floating either halfway up or near the surface of the solution. Going down from the upper branch at decreasing DPC concentration and constant SDS concentration, these balls turned into crystalline precipitates. These balls reappeared again in the transition region between the precipitate and coacervate regions in varying sizes starting with a huge ball mixed with precipitate at the bottom of the solution which then gradually became smaller as the precipitate dissolved and finally disappeared as two liquid phases or a coacervate was formed.

Hoyer et al (23) reported a similar observation in mixtures of sodium dodecyl sulfate and dodecyltrimethylammonium chloride. In their case, however, rings of coacervate halfway up in the solution were seen instead of balls. These rings appeared as the solutions were cooled down to room temperature in contrast to gel balls which appeared upon heating of the solution from 30° to $40^{\circ}C$.

The monomer-precipitate line shifted to higher concentrations of both SDS and DPC giving a higher K_{sp}° value as shown in Figure 3, a plot of the monomer-precipitate lines at 30° and $40^{\circ}C$. The effect on the activity coefficient with such a change in temperature is negligible.

From these two K_{sp}° values, the standard enthalpy, ΔH°, can be calculated by assuming that ΔH° is constant over the temperature range of 30°-$40^{\circ}C$. Using the following equation (45),

$$\ln (K_{sp1}/K_{sp2}) = -\Delta H^{\circ}(1/T_1-1/T_2)/R$$

ΔH° was calculated which, together with the other thermodynamic variables, are shown in Table 2.

The positive value of ΔH° indicates that the energy of hydration is less than the energy required to overcome the attractive forces between the SDS and DPC monomers. This value of ΔH° is much larger than the entropy term.

In Figure 4, the precipitation phase boundary points at $40^{\circ}C$ are shown with the model which was calculated using

equations [1-8] of ref. 2. The same procedure used in calculating the phase boundaries at 40°C. An average W/RT of -7.92 was obtained using the monomer concentrations at the intersection of each branch with the monomer-precipitate line.

For the SDS-rich branch, the calculated precipitation boundaries deviate from the experimental points which was also the case for the precipitation phase boundaries measured at 30°C. This deviation has been attributed to coacervation which was neglected in the development of the model.

For the DPC-rich branch, the calculated precipitation boundary describes well the experimental measurements at low concentrations but shows a substantial deviation at higher SDS concentrations starting at about $3x10^{-4}$M. For example, at a SDS concentration of $1x10^{-2}$M, the percentage error of the calculated DPC concentration is 100%. This result is in contrast with the calculated phase boundaries at 30°C which described well the experimental measurements along the DPC-rich branch throughout the concentration range studied.

This deviation could be the result of the appearance of balls of gel near the upper branch of the precipitation boundaries. It is possible that for the upper branch of the precipitation boundaries, colloidal precipitates not visible to the eye may exist as a result of the "balling" phenomena. If such precipitates exist, then the true precipitation boundary may actually be higher than is visually observed and could be that predicted by the model using regular solution theory.

However, results also indicate that regular solution theory may not be valid for this system. W, the interaction parameter which should be independent of temperature, increased from -21.7 $KJmol^{-1}$ at 30°C to -20.6$KJmol^{-1}$ at 40°C. Substantial evidence has been shown that regular solution theory is not thermodynamically valid in describing nonideal mixed micelles (24) but that it is a useful empirical model. In this study, the model provides a reasonable estimate of the precipitation boundaries considering the absence of experimental data on the distribution of surfactants between the micelle and monomer.

The empirical model previously used to account for coacervate can be used to obtain a better fit of the SDS-rich branch of the precipitation boundaries. Using equation [2] of ref. 2 and data in Figure 4, an X_{DS}^{*} value of 0.689 was obtained. Using this value of X_{DS}^{*}, the precipitation boundaries can be calculated using equation [15] of ref. 2. Similarly, the experimental points on the DPC-rich branch can be modelled by calculating the correct X_{DS} value which will fit the experimental measurements. Using equation [7] of ref. 2 and data in Figure 4, this X_{DS} value was calculated to be 0.240 which can then be used in equations [3], [4], and [7] of ref. 2 to calculate the DPC-rich precipitation phase boundary. Results are shown in Figure 5 where the calculated precipitation phase boundaries describe the experimental measurements on both the SDS-rich and DPC-rich branches well.

Effect of Ionic Strength

The precipitation phase boundaries measured at 10% SFB is shown in Figure 6 together with the precipitation boundaries measured at 0.15M NaCl. In addition to visual observation of the samples, laser and UV spectrophotometer were used at very low concentrations where difficulty in detecting precipitates was again encountered. As shown in Figure 6, the precipitation region increased with the upper and lower branches shifting to higher concentrations and the monomer-precipitate line moving down to lower concentrations.

In Figure 7, the monomer-precipitate line is shown with the calculated K_{sp}' value. To determine the activity coefficients for K_{sp}^{o} calculations, the ionic strength of 10% SFB needs to be calculated.

Table 3 shows the concentration of each component in 10% SFB. It can be seen that NaCl is present in a large excess over the other electrolytes and hence could be termed an "indifferent electrolyte". In cases like this, "the ionic atmospheres of all the ions are formed almost exclusively from ions of this excess" electrolyte which thus determines the ionic strength of the solution (25). A consequence is that the activity coefficient becomes a function of the concentration of the excess electrolyte alone.

With NaCl considered as an indifferent electrolyte, the ionic strength of 10% SFB becomes equal to the concentration

of NaCl which from Table 3 is 2.11×10^{-2} M. This value will be used in the extended Debye-Huckel equation to calculate the activity coefficient since the surfactant concentrations on the monomer-precipitate line are still negligible compared to the added salt concentration.

The activity coefficient was calculated to be 0.867 from which a K_{sp}^{o} value of 2.07×10^{-10} M^2 was obtained. Since the temperature was constant and only ionic strength was changed, the K_{sp}^{o} values at 10% SFB and 0.15M NaCl should be equal following equation [3]. At 0.15M NaCl, K_{sp}^{o} was previously calculated to be 2.24×10^{-10} which is greater that the K_{sp}^{o} value at 10% SFB. This difference may be attributed to activity coefficient calculations using the extended Debye-Huckel equation which becomes less accurate at higher ionic strengths. Since this relationship is valid at dilute concentrations, the K_{sp}^{o} value at 10% SFB is probably more accurate than that at 0.15M NaCl.

At this point, it is possible to infer from the calculated K_{sp}^{o} value if Ca^{2+} ions were precipitated out from solution. The K_{sp}^{o} value of the precipitation reaction between Ca^{2+} ions and DS^- monomers in 0.02M NaCl and 30°C has been calculated to be 5.02×10^{-10} M^3 (26). Since this value is lower than the K_{sp}^{o} value of 2.07×10^{-10} M^2 for the precipitation reaction between DP^+ and DS^- monomers, DS^- monomer precipitates preferentially to DP^+ monomers and not to Ca^{2+} ions.

From Figure 8, a CMC of 7.5×10^{-3} M was obtained for DPC and 1.6×10^{-3} M for SDS. The CMC of SDS is suspect as can be seen from the plot where a large minimum occurs. Since the necessary precautions were taken to maximize accuracy (27) and duplicate measurements showed the same minimum, the occurrence of the minimum may be attributed to highly surface active impurities or probably to the formation of precipitates of DS^- monomers and polyvalent ions in 10% SFB. SDS was obtained from a purified sample stock which did not show any minimum in surface tension measurements in 0.15M NaCl.

A more accurate value can probably be obtained by measuring surface tensions at shorter time intervals as has been suggested (28). Nevertheless, this value at 10% SFB will be used in model calculations.

To calculate the precipitation phase boundaries at 10% SFB, the constants in equations [8] and [9] which relates the CMC and the concentration of total counterion need to be evaluated. For SDS at 30°C, K_2 and K_g has been experimentally obtained (29) to give:

$$\ln CMC_{DS} = -8.52 - 0.696\ln\{[Na^+]_{tot}\} \qquad [13]$$

For DPC at 30°C, a rough approximation may be obtained for K_2 and K_g from the CMC values at 0.15M NaCl and 10% SFB (0.0211M NaCl) using equation [9]. The following equation is obtained for DPC:

$$\ln CMC_{DP} = -6.11 - 0.312\ln\{[Cl^-]_{tot}\} \qquad [14]$$

The K_g value of 0.696 for SDS in equation [13] is reasonable but K_g for DPC which is equal to 0.312 seems low. K_g, a constant relating actual to hypothetical electrical work of introducing a molecule into the micelle, is found to be in the range of 0.5 to 0.65, independent of the nature of the polar groups (30).

The calculated precipitation phase boundaries are shown in Figure 9. The DPC-rich branch of the precipitation phase boundaries, despite neglecting counterion binding, is described well. If counterion binding were considered, a decrease in the concentration of unbound counterions will occur and CMC will correspondingly increase as dictated by equations [4].

The effect of a higher CMC on the two branches of the precipitation boundaries is to shift them to higher concentrations. By neglecting counterion binding, the CMC decreases shifting the precipitation boundaries to lower concentration which results to a smaller region of precipitation. Since precipitation is desired, it is safe to neglect counterion binding for process design purposes as doing so can only underestimate the concentration ranges where precipitate forms.

The calculated precipitation boundary for the SDS-rich branch deviates substantially from the experimental points. As has been discussed, neglecting counterion binding shifts the phase boundaries to lower concentrations because of a lower CMC.

This deviation, however, is more than the effect of neglecting counterion binding. As shown in Figure 8, the measured CMC of pure SDS (1.6×10^{-3} M) is probably low because of the minimum in the surface tension-vs.-concentration plot. The position of the CMC of the pure SDS relative to the SDS-rich precipitation boundary also indicates that this value is lower than the true CMC.

Previous results and discussions have shown that mixed micelle formation results in a reversal in slope of the precipitation boundaries. This reversal occurs at the mixture CMC of SDS and DPC. Since mixed surfactant CMC's show negative deviations from ideality, which is predicted by regular solution theory, the pure SDS CMC should be greater than the mixture CMC of SDS and DPC. Hence, the pure SDS CMC should lie on or immediately to the right of the SDS-rich precipitation boundary. Because of a low pure SDS CMC, however, the opposite result is obtained as shown in Figure 6.

The pure SDS CMC obtained from Figure 6 was initially used to calculate the interaction parameter W/RT. If the measured SDS CMC is indeed lower than the true value, W/RT will also be low. A low value for W/RT will result to a shifting of the precipitation boundaries to lower concentrations because mixture CMC's predicted by regular solution theory will decrease.

By using a pure SDS CMC obtained from equation [9], W/RT increased from -10.19 to -9.23 which was then used to model the SDS-rich precipitation boundary. New results show a better fit of the SDS-rich branch as shown in Figure 10.

Effect of Surfactant Chain Length

The measured precipitation phase boundaries of the SDeS/DPC and SOS/DPC system are shown with the SDS/DPC phase boundaries in Figure 11. The precipitation phase boundaries have clearly shifted to higher anionic surfactant concentrations with a decrease in the chain length of the anionic surfactant. A coacervate and a transition region of mixed precipitate and coacervate were also observed in the SDeS/DPC system similar to that in the SDS/DPC system.

In the SOS/DPC system, however, balls of gel similar to that observed in the SDS/DPC system at 40°C were present in solution. It was difficult to distinguish between

crystalline and oily or viscous precipitate because of the turbidity of the solutions. Hence, the boundaries of the transition region between coacervate and crystalline precipitate regions could not be determined. The boundaries of the coacervate region where two liquid phases exist was distinct enough to be determined. Near the monomer-precipitate line, precipitates were crystalline which allowed an accurate determination of the precipitation boundary.

In Figure 12, the calculated K_{sp}^{o} values for each system are shown. The change in ionic strength due to the ions contributed by the surfactants have a negligible effect on the K_{sp}^{o} values. The K_{sp}^{o} values were correlated with N, the number of carbon atoms in the hydrocarbon chain, and the following empirical equation was obtained:

$$\log K_{sp}^{o} = -0.715N - 1.12 \qquad [16]$$

The CMC's of SDeS and SOS were obtained through surface tension measurements and was determined to be 1.1×10^{-2} M and 8.7×10^{-2} M, respectively. These CMC's and SDS CMC were also correlated with N and the following empirical relationship was obtained:

$$\log CMC = 3.08 - 0.513N \qquad [17]$$

Plots of K_{sp}^{o} and CMC versus the number of carbon atoms in the SAS chain are shown in Figure 13. A plot of K_{sp}^{o} versus CMC is shown in Figure 14 which is described by the following correlation:

$$\log K_{sp}^{o} = -5.45 + 1.38 \log CMC \qquad [18]$$

Equation [18] can also be obtained by combining equations [16] and [17].

Using the CMC of SDeS and the K_{sp}^{o} of the SDeS/DPC system, the precipitation phase boundaries for the SDeS/DPC system were calculated using equations [1-8] of ref. 2. The calculated phase boundaries are shown in Figure 15. The activity coefficients for the SDeS/DPC system were assumed constant as in the SDS/DPC because of swamping electrolyte.

The upper branch is fairly well-described but the calculated phase boundaries for the lower branch deviates again from experimental measurements where coacervation

occurred.

For the SOS/DPC system, data points of the lower branch were of relatively high concentrations compared to those of the SDS/DPC and SDeS/DPC systems. Swamping electrolyte cannot be assumed with an added salt concentration of 0.15M NaCl and so equation [9] was used to account for the change in the CMC of DPC with increasing electrolyte concentration. In this equation, counterion binding is neglected.

Only one CMC measurement was made for SOS and so an approximate expression to relate CMC and the counterion concentration was obtained from published SOS CMC data at 21^{o} (31). Since CMC is not a strong function of temperature, the following empirical correlation will be used at $30^{o}C$

$$\ln CMC_{OS} = -2.89 - 0.192\ln\{[Na^{+}]_{tot}\} \qquad [19]$$

where CMC_{OS} is the SOS CMC. Again, counterion binding will be neglected and $[Na^{+}]_{tot}$ will be calculated from the following expression:

$$[Na^{+}]_{tot} = 0.15 + C_{SOS} \qquad [20]$$

Equations [1-8] of ref. 2, [9], [11], [19], and [20] were used to calculate the precipitation boundaries and the results are shown in Figure 16.

The calculated precipitation boundaries for the SOS-rich branch deviates substantially from the experimental measurements. This deviation could not be the result of neglecting counterion binding because if it were considered the calculated precipitation boundaries will shift to even higher concentrations. Since the "balling" phenomena occurred in solutions near this precipitation boundary, possible explanations are that colloidal precipitate which cannot be seen exists or that regular solution theory fails to account for the monomer-micelle equilibrium because of the gel-ball formation. Another possible explanation is that the SOS micelles are inadequately described by the pseudo-phase separation model. This model works well with long-chain surfactants having low CMC's.

Deviations were also observed between the calculated phase boundaries and the experimental measurements where

coacervation occurred as in all the other phase diagrams.

CONCLUSIONS

Precipitation phase boundaries of aqueous mixtures of SDS and DPC were measured to study the effects of pH, temperature, ionic strength, and anionic surfactant chain length on phase behavior. Results showed that a change from an alkaline pH to a neutral pH does not affect the precipitation phase boundaries of the SDS/DPC system. An increase in temperature from 30^{o} to 40^{o}C results in a smaller region of precipitation. At decreasing ionic strengths, the precipitation region increases. The precipitation boundaries shifts to higher anionic surfactant concentrations with a decrease in the chain length of the anionic surfactant. From this result, an empirical equation was also obtained correlating the solubility product constant and CMC of anionic surfactant. The model developed in ref. 2 for predicting phase boundaries describes the precipitation phase boundaries well except in regions where coacervate and gels form in solution.

REFERENCES

1. Arshad, A. and Harwell, J.H., SPE Paper No. 14291 Presented at the 60th Annual Technical Conference of the Society of Petroleum Engineers, Las Vegas (September, 1985).

2. Stellner, K.L., Amante, J.C., Scamehorn, J.F., and Harwell, J.H., J. Colloid Interface Sci., (accepted).

3. Mitsuishi, M. and Hashizume, M., Bull. Chem. Soc. Japan 46, 1946 (1973).

4. Mandal, A.B., and Moulik, S.P., in "Solution Behavior of Surfactants" (K.L. Mittal and E.J. Fendler, Eds.), Vol.1, p. 521. Plenum, New York, 1980.

5. Peacock, J.M., and Matijevic, E., J. Colloid Interface Sci. 77, 548 (1980).

6. Kallay, N., Pastuovic, M., and Matijevic, E., J. Colloid Interface Sci. 106, 452 (1985).

7. Tomlinson, E., Davis, S.S., and Mukhayer, G.I., in "Solution Chemistry of Surfactants" (K.L. Mittal, Ed.), Vol. 1, p. 3. Plenum, New York, 1979.

8. Rosen, M.J., "Surfactants and Interfacial Phenomena", pp.15,108. Wiley, New York, 1978.

9. Flockhart, B.D., J. Colloid Interface Science 16, 484 (1961).

10. Shinoda, K., in "Colloidal Surfactants" (K. Shinoda, B. Tamamushi, T. Nakagawa, and T. Isemura, Eds.), p. 58. Academic Press, New York, 1963.

11. Hoyer, H.W., Marmo, A., and Zoellner, M., J. Physical Chem. 65, 1804 (1961).

12. Scott, A.B., Tartar, H.V., and Lingafelter, E.C., J. Amer. Chem. Soc. 65, 698 (1943).

13. Schwuger, M.J., in "Anionic Surfactants" (E. Lucassen-Reynders, Ed.), p.305. Marcel Dekker, New York, 1981.

14. Rathman, J.F. and Scamehorn, J.F., J. Physical Chem. 88, 5807 (1984).

15. Beunen, J.A., and Ruckenstein, E., J. Colloid Interface Sci. 96, 469 (1983).

16. Hall, D.G., and Price, T.J., J. Chem. Soc., Faraday Trans. 1 80, 1193 (1984).

17. Nakamura, A., and Muramatsu, M., J. Colloid Interface Sci. 62, 165 (1977).

18. Klevens, H.B., J. Amer. Oil Chem. Soc. 30, 74 (1953).

19. Swisher, R.D., "Surfactant Biodegradation", pp. 35-39. Marcel Dekker, New York, 1987.

20. Barry, B.W., and Russel, G.F.J., J. Pharm. Sci. 61, 502 (1972).

21. Novich, B.E., and Ring, T.A., Langmuir 1, 701 (1985).

22. Scamehorn, J.F., Ph.D. Dissertation, University of Texas at Austin, p.29 (1980).

23. Scamehorn, J.F. in "Phenomena in Mixed Surfactant Systems" (J.F. Scamehorn, Ed.), Vol. 311, p. 1. ACS Symp. Ser., ACS, Washington, 1986.

24. Koryta, J., and Dvorak, J., "Principles of Electrochemisty", p. 46. Wiley, Wichester, 1987.

25. Stellner, K.L., Ph.D. Dissertation, University of Oklahoma, p. 62 (1987).

26. Lukenheimer, K., and Wantke, K.D., Colloid Polym. Sci. 259, 354 (1981).

27. Mysels, K.J., Langmuir 2, 423 (1986).

28. Stellner, K.L., and Scamehorn, J.F., J. Amer. Oil Chemists Soc. 63, 566 (1986).

29. Shinoda, K., "Principles of Solution and Solubility", p. 169. Marcel Dekker, New York, 1978.

30. Mukerjee, P., and Mysels, K.J., "Critical Micelle Concentrations of Aqueous Surfactant Systems", p. 75 NSRDS-NBS, Washington D.C., 1971.

Table 1

Synthetic Field Brine (SFB) Composition

Component	kg/m^3
NaCl	12.31
$CaCl_2$	0.32
$MgCl_2.6H_2O$	0.44
NH_4Cl	0.07
$Na_2B_4O_7.10H_2O$	0.34

Table 2
Solubility Products and Standard Thermodynamic Functions for the Dissolution of the SDS/DPC Precipitate

Temperature (K)	K_{sp}^{o}	H^{o} (KJ/mol)	G^{o} (KJ/mol)	S^{o} (KJ/mol)
303	2.24×10^{-10}	95.0	56.0	0.129
313	7.47×10^{-10}	95.0	54.7	0.129

Table 3
Composition of 10% SFB

Component	Concentration (mol/L)	mole%
NaCl	2.11×10^{-2}	96.99
$CaCl_2.2H_2O$	2.18×10^{-4}	1.01
$MgCl_2.6H_2O$	2.16×10^{-4}	0.99
NH_4Cl	1.31×10^{-4}	0.60
$Na_2B_4O_7.10H_2O$	8.92×10^{-5}	0.41
		100.00%

LIST OF FIGURES

Values

Figure 13 Log K_{sp}^{o} of SAS/DPC Systems and Log CMC of SAS Versus N.

Figure 14. Log K_{sp}^{o} of SAS/DPC Systems Versus Log CMC of SAS.

Figure 15. SDeS/DPC Precipitation Data With Calculated Boundaries.

Figure 16. SOS/DPC Precipitation Data With Calculated Boundaries.

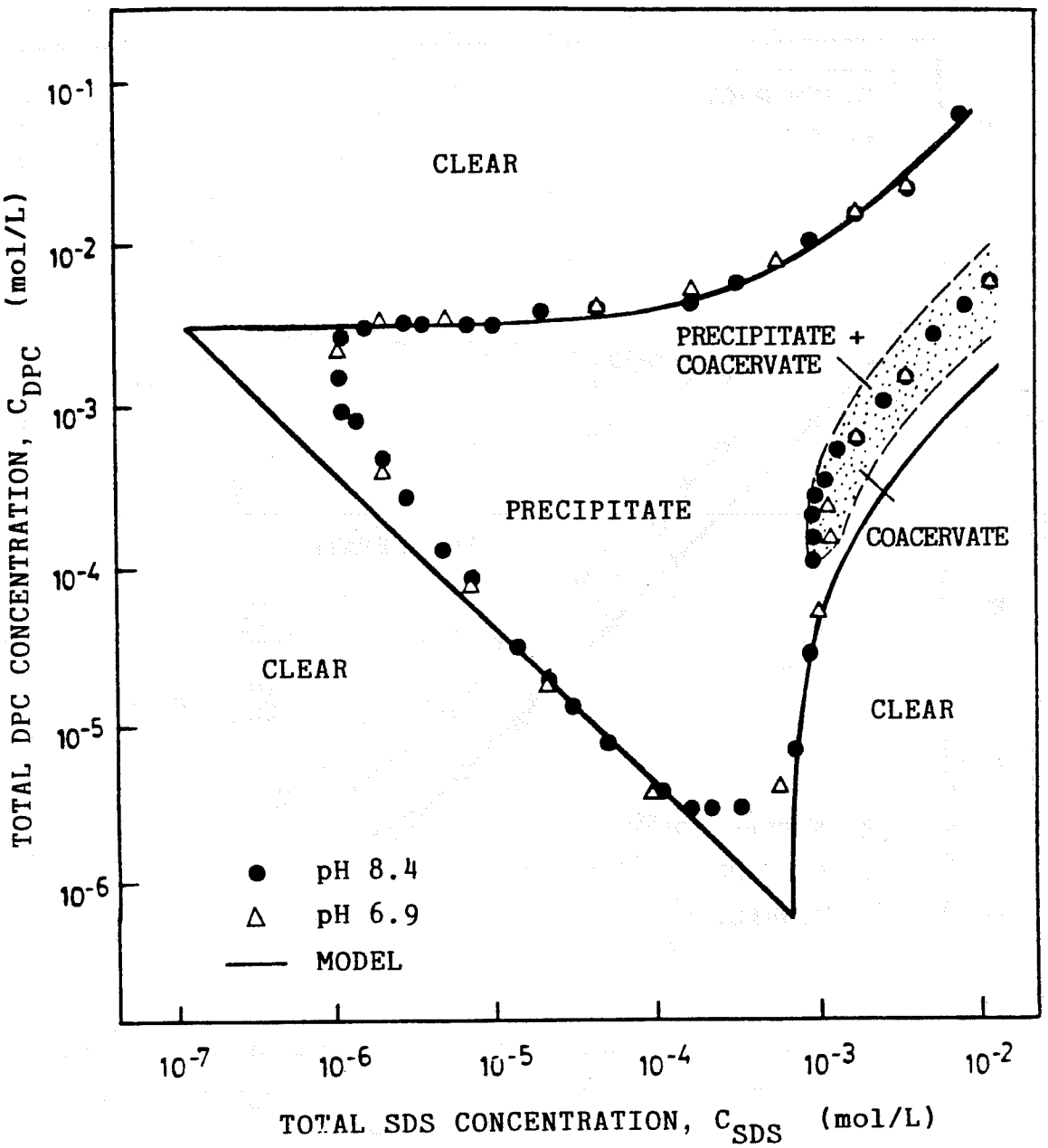

Figure 1. SDS/DPC Precipitation Data at pH 6.9 and pH 8.4 With Calculated Boundaries.

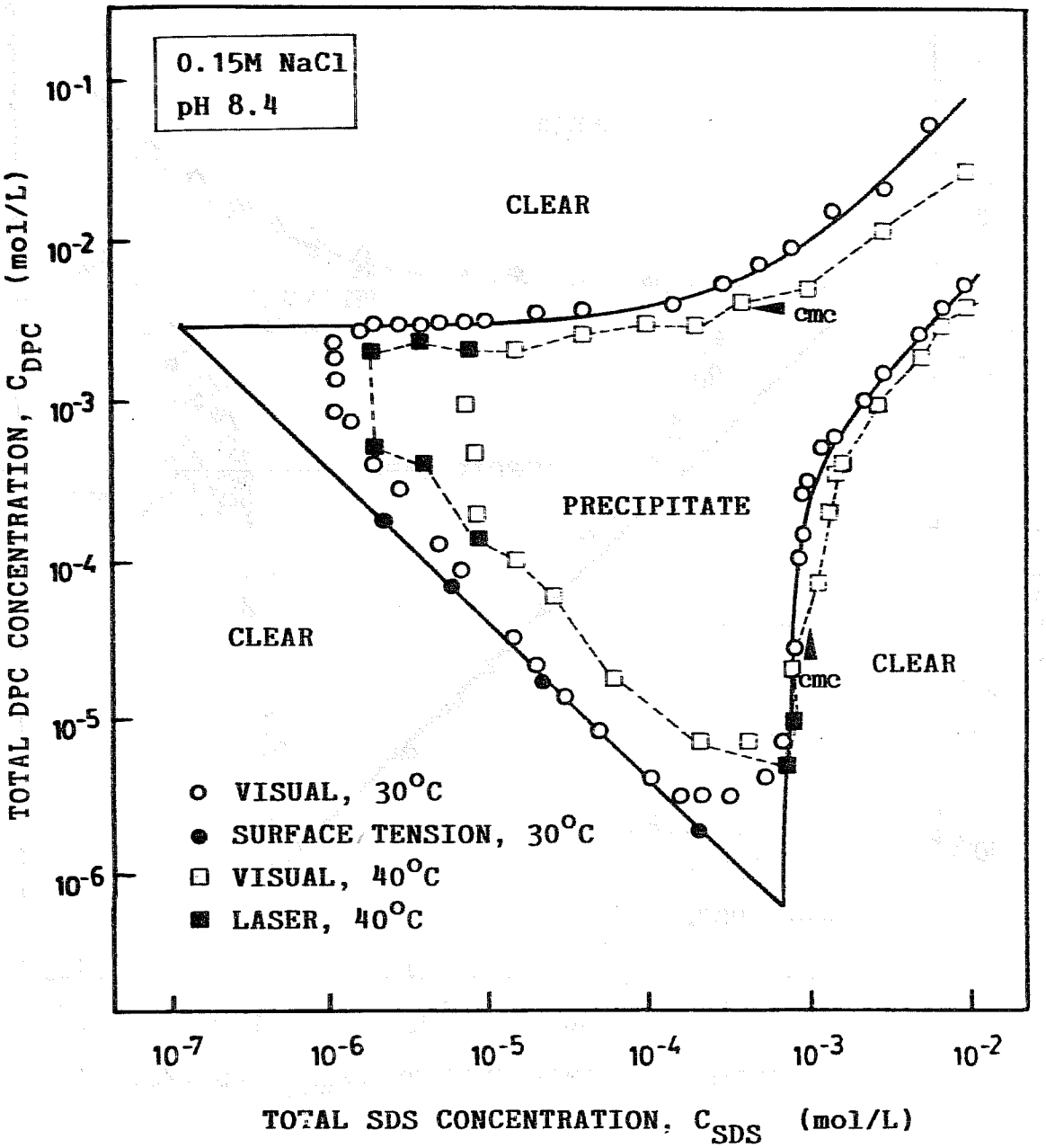

Figure 2. SDS/DPC Precipitation Phase Boundaries at 30° and 40°C.

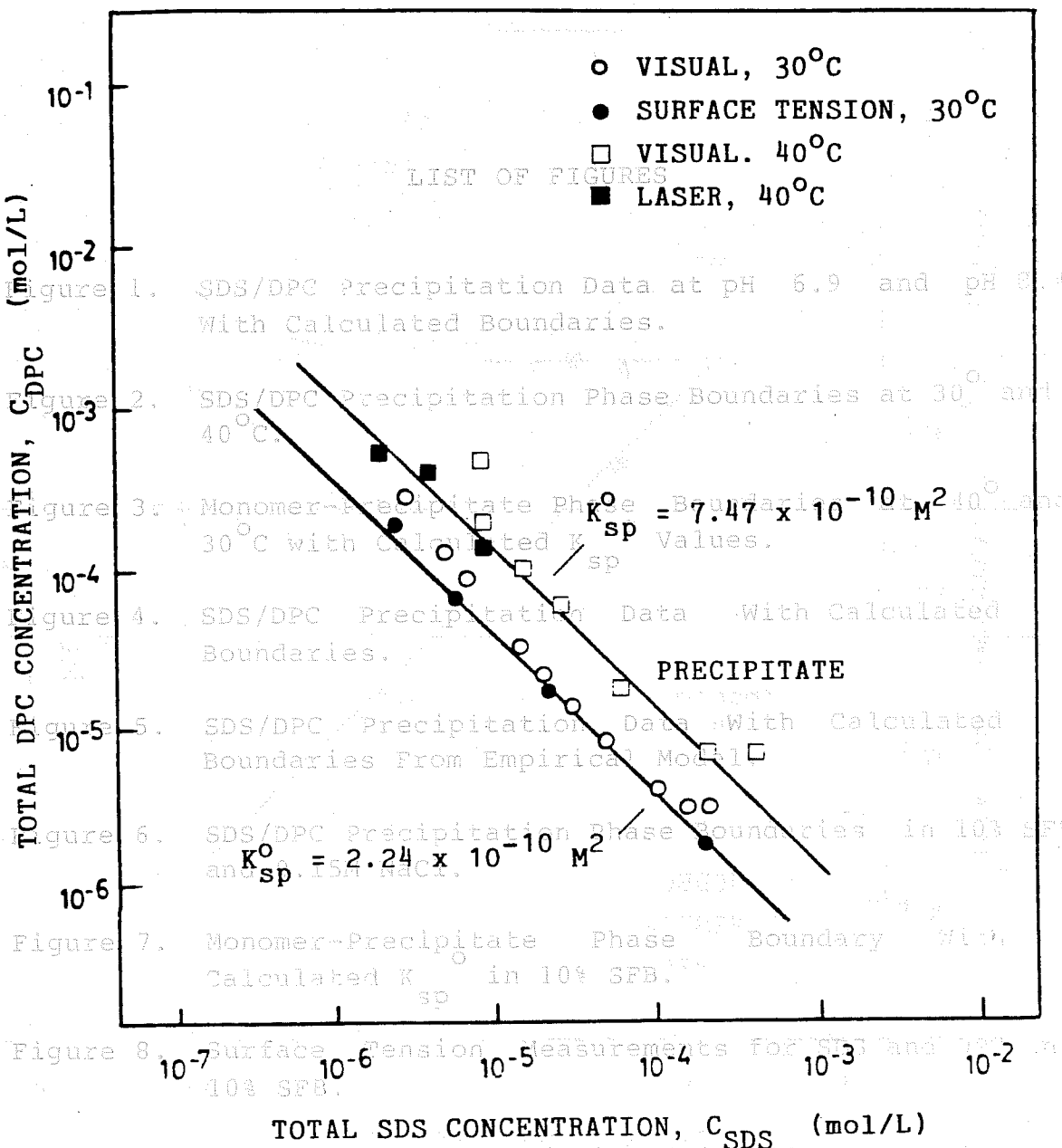

Figure 3. Monomer-Precipitate Phase Boundaries at 40° and 30°C with Calculated K^o_{sp} Values.

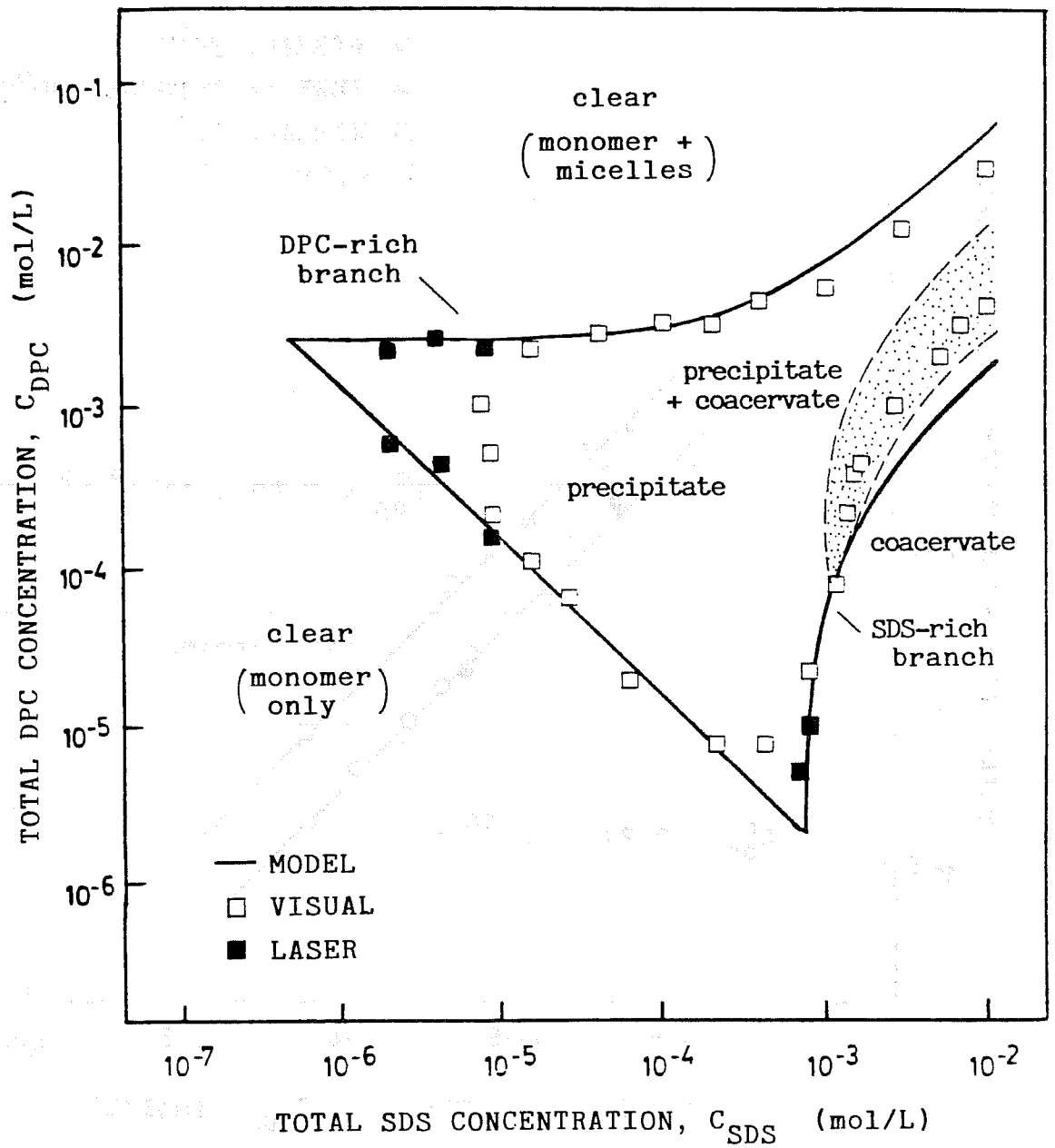

Figure 4. SDS/DPC Precipitation Data With Calculated Boundaries.

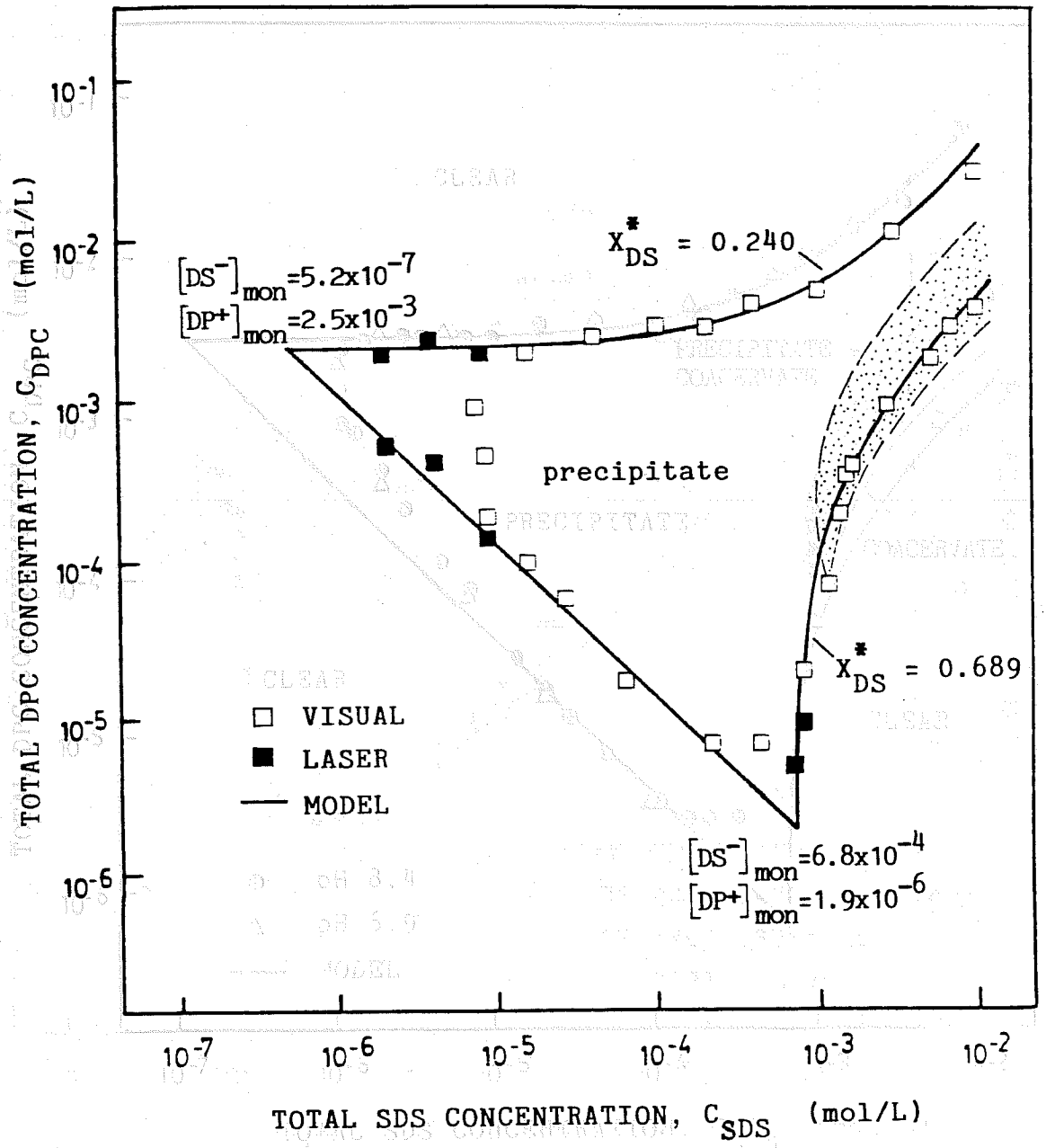

Figure 5. SDS/DPC Precipitation Data With Calculated Boundaries From Empirical Model.

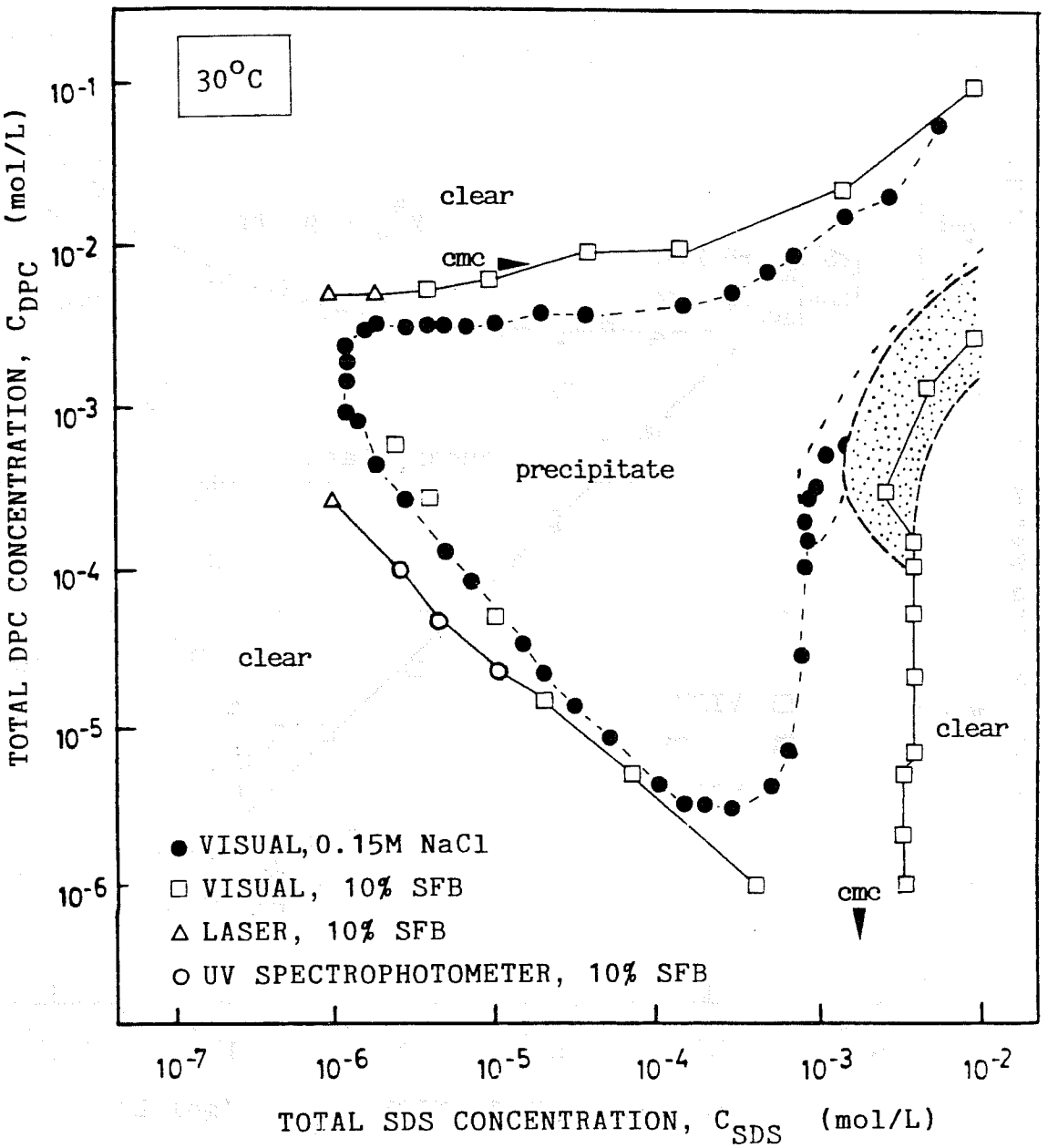

Figure 6. SDS/DPC Precipitation Phase Boundaries in 10% SFB and 0.15M NaCl.

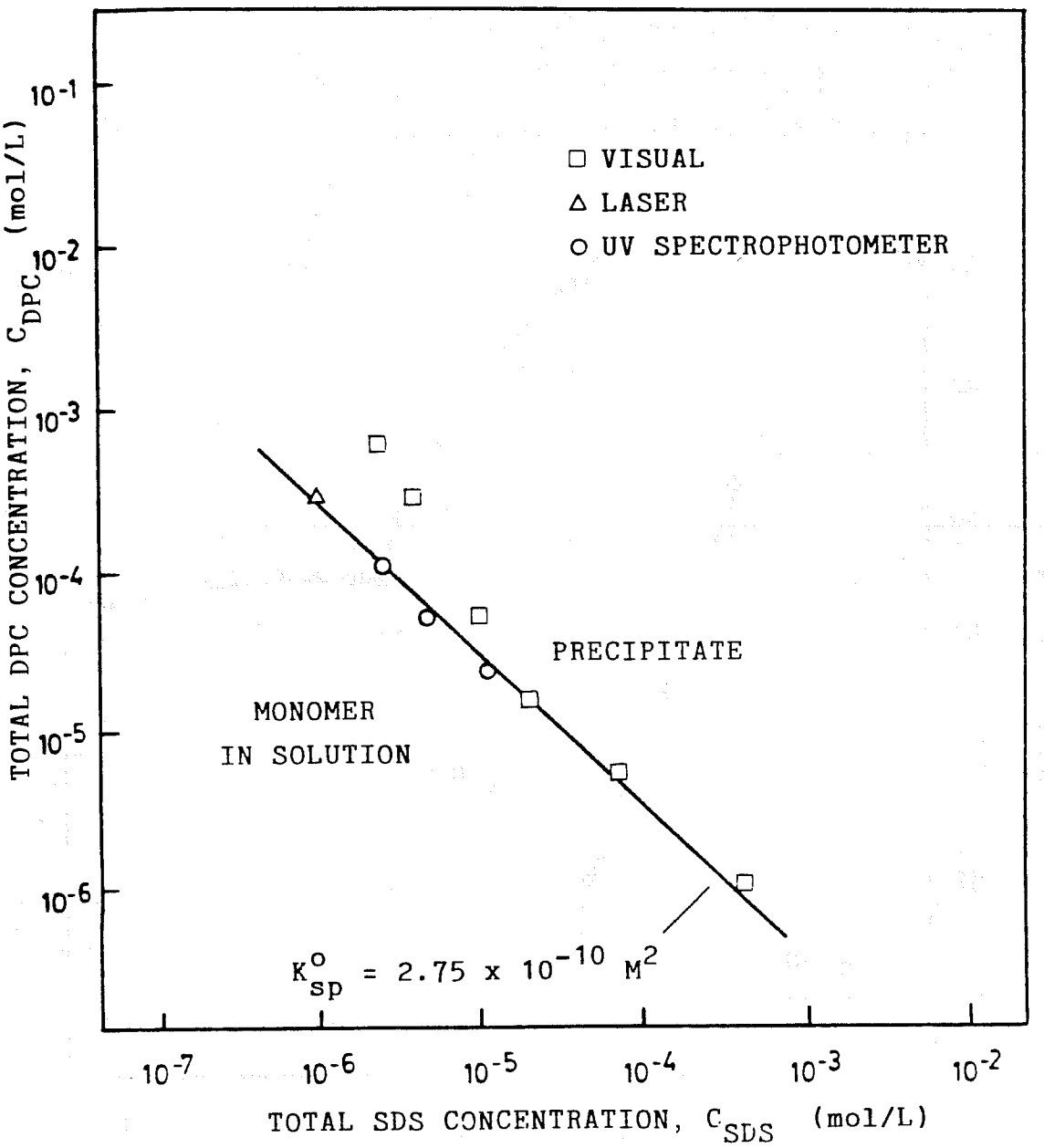

Figure 7. Monomer-Precipitate Phase Boundary With Calculated K_{sp}^{o} in 10% SFB.

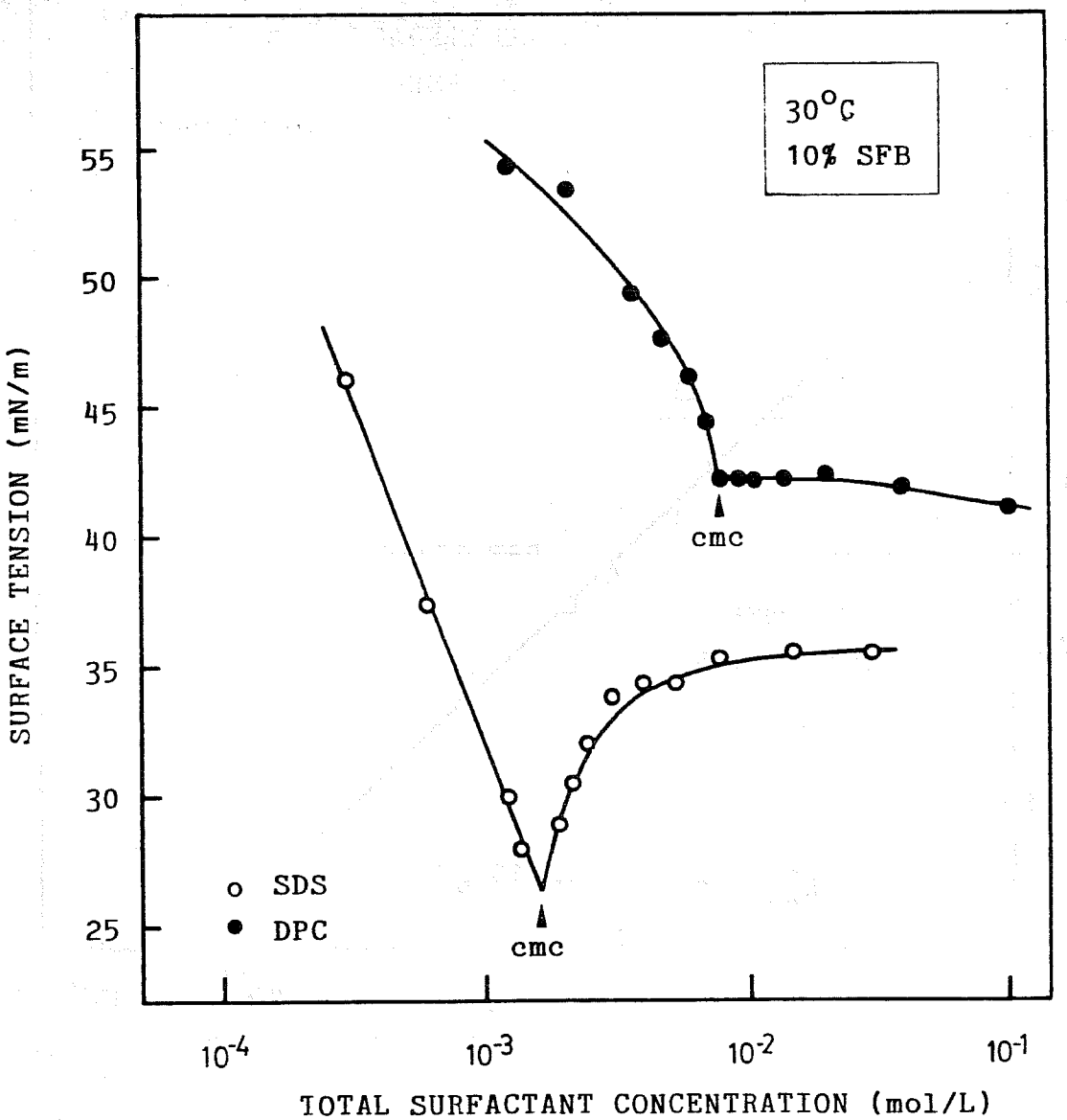

Figure 8. Surface Tension Measurements for SDS and DPC in 10% SFB.

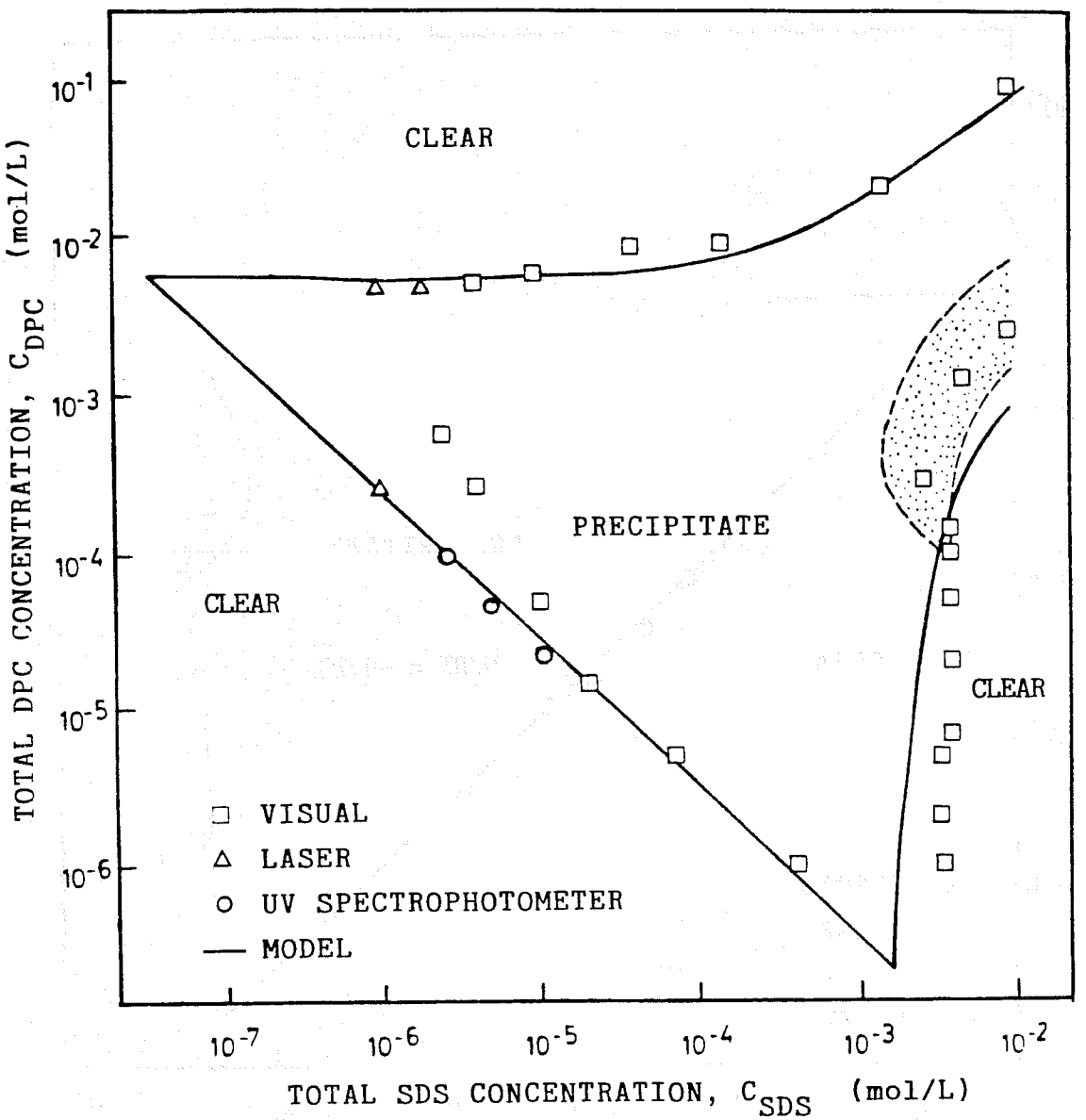

Figure 9. SDS/DPC Precipitation Data in 10% SFB With Calculated Boundaries.

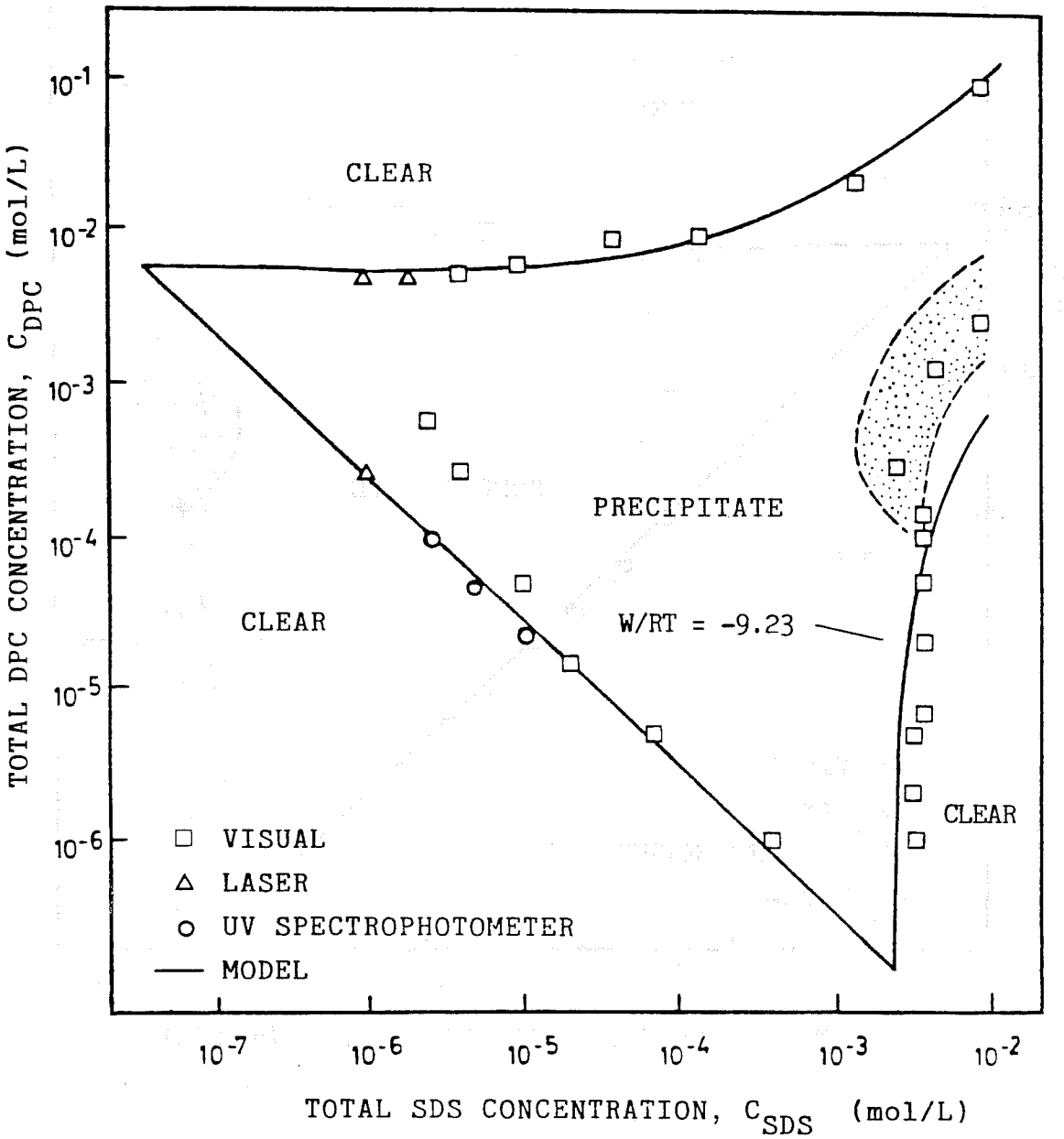

Figure 10. Calculated SDS/DPC Precipitation Boundaries in 10% SFB After W/RT Adjustment.

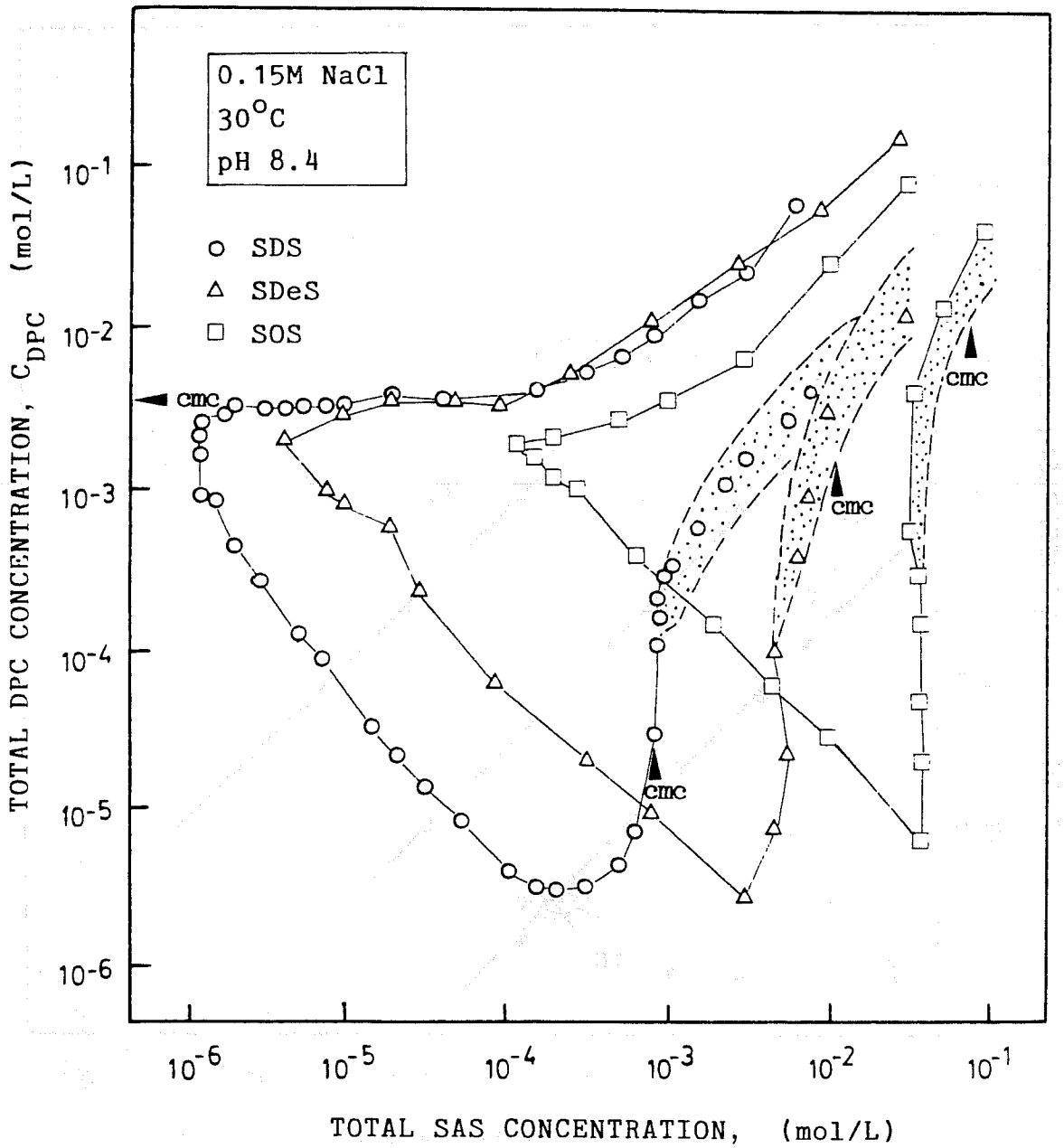

Figure 11. Precipitation Phase Boundaries of SDS/DPC, SDeS/DPC, and SOS/DPC Systems.

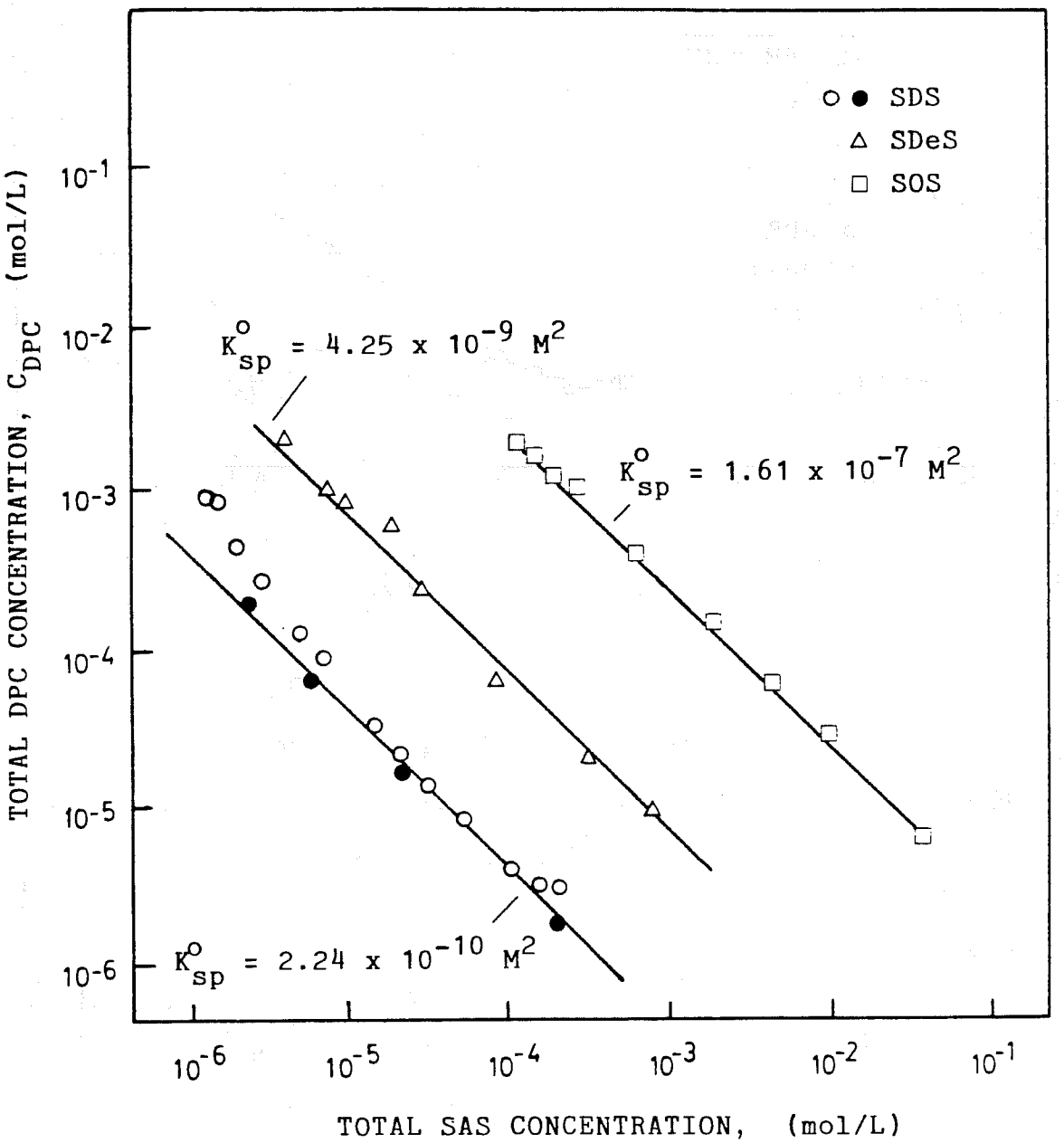

Figure 12. Monomer-Precipitate Phase Boundaries of SAS/DPC Systems With Calculated. K_{sp}^{o} Values

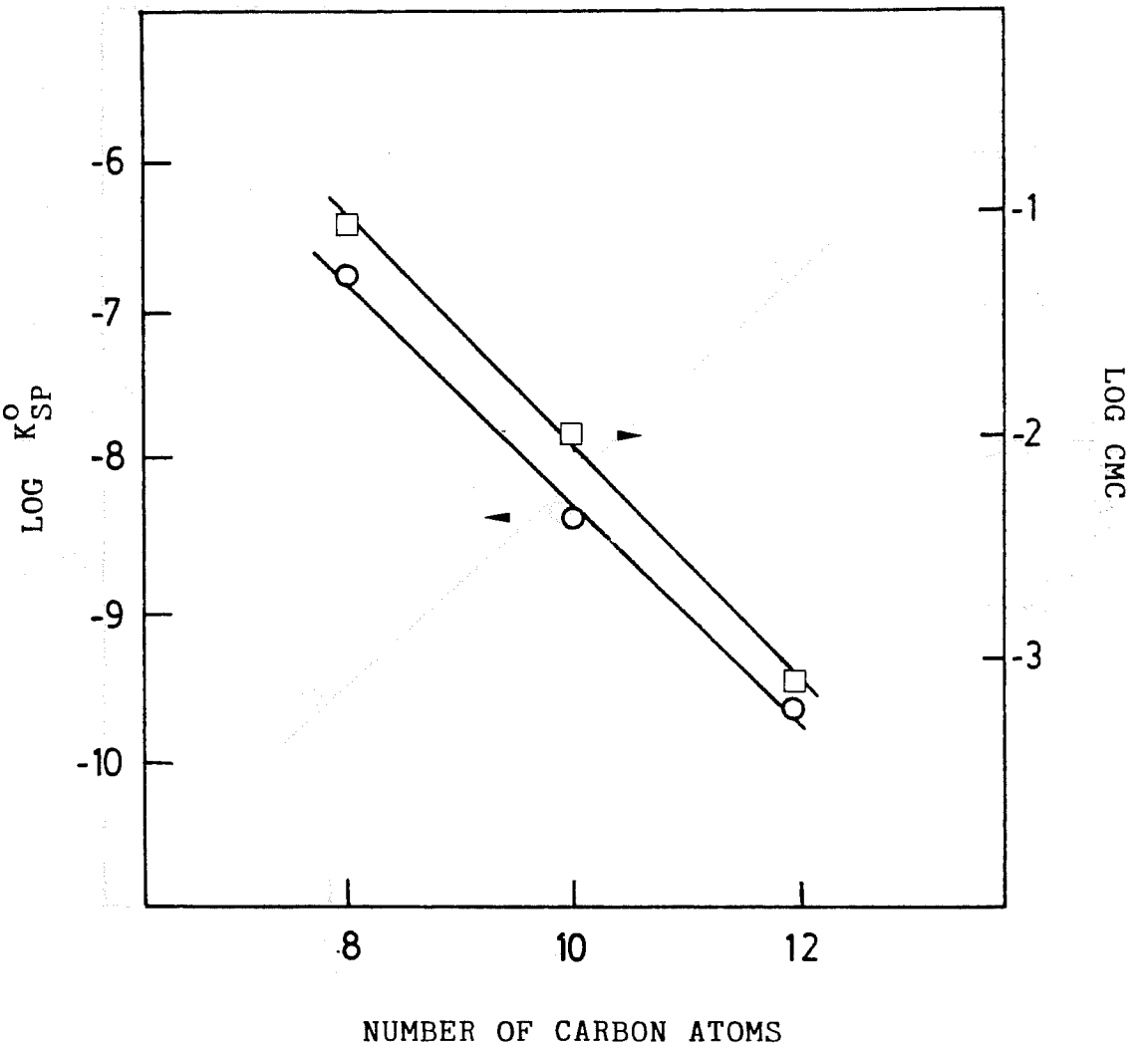

Figure 13 Log K_{mp}^{c} of SAS/DPC Systems and Log CMC of SAS Versus N.

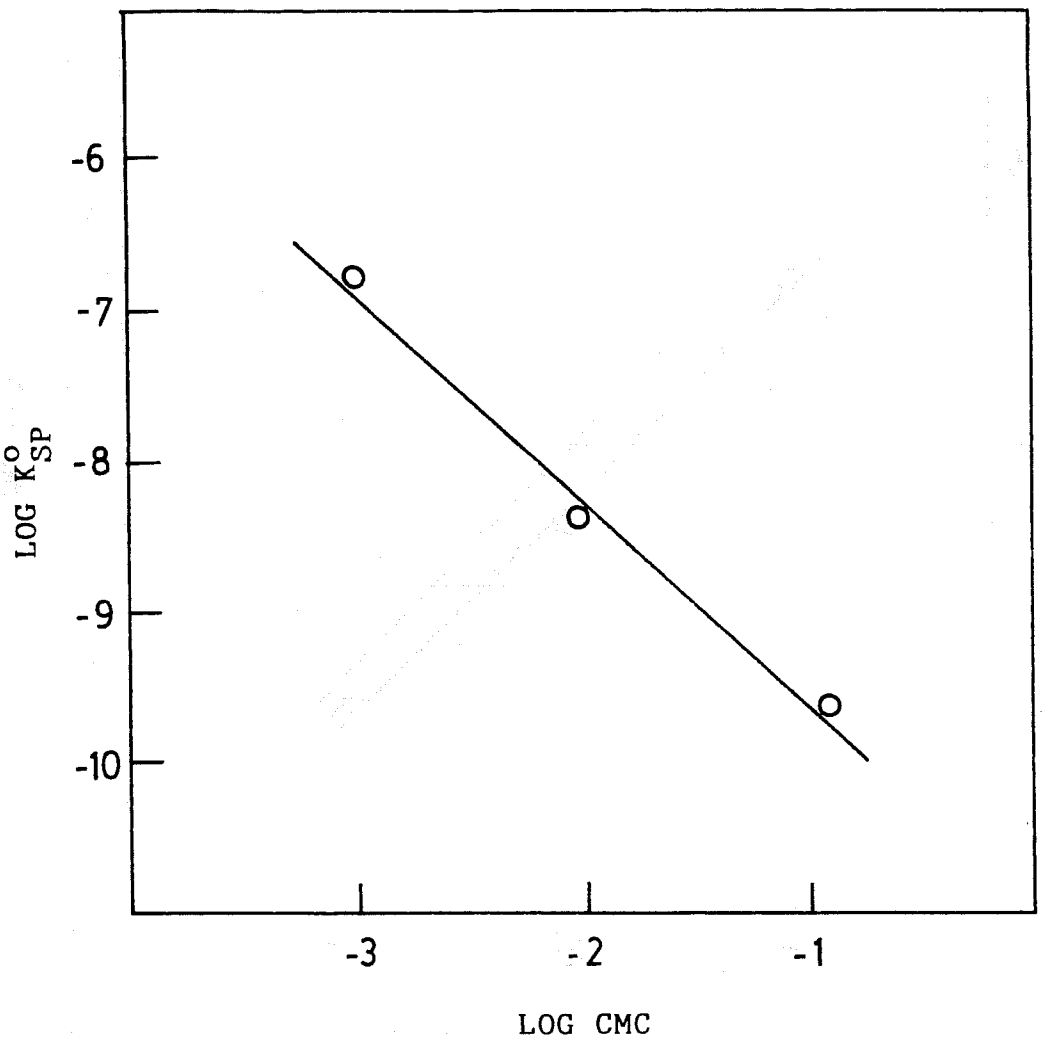

Figure 14. Log K_{sp}^{o} of SAS/DPC Systems Versus Log CMC of SAS.

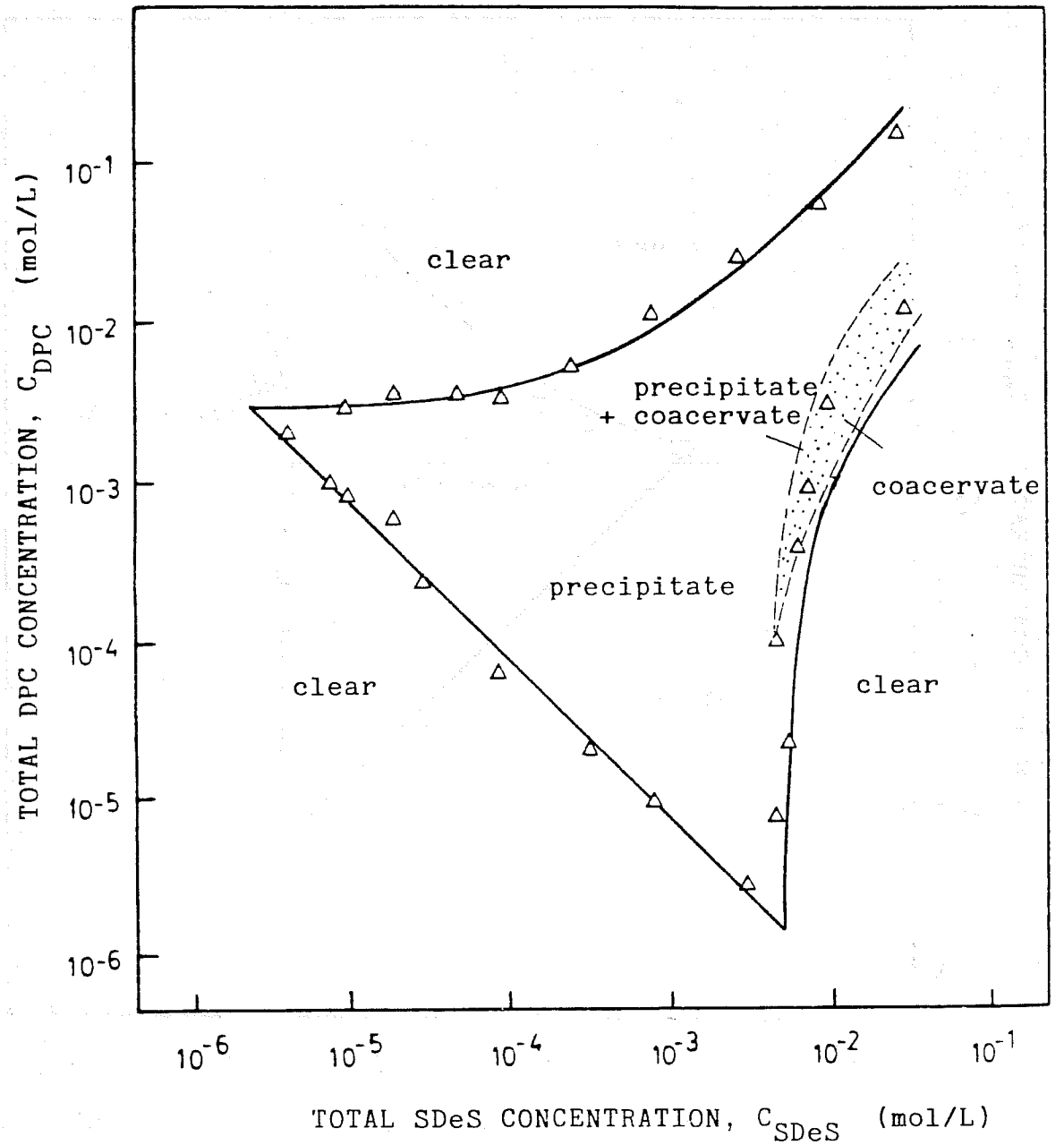

Figure 15. SDeS/DPC Precipitation Data With Calculated Boundaries.

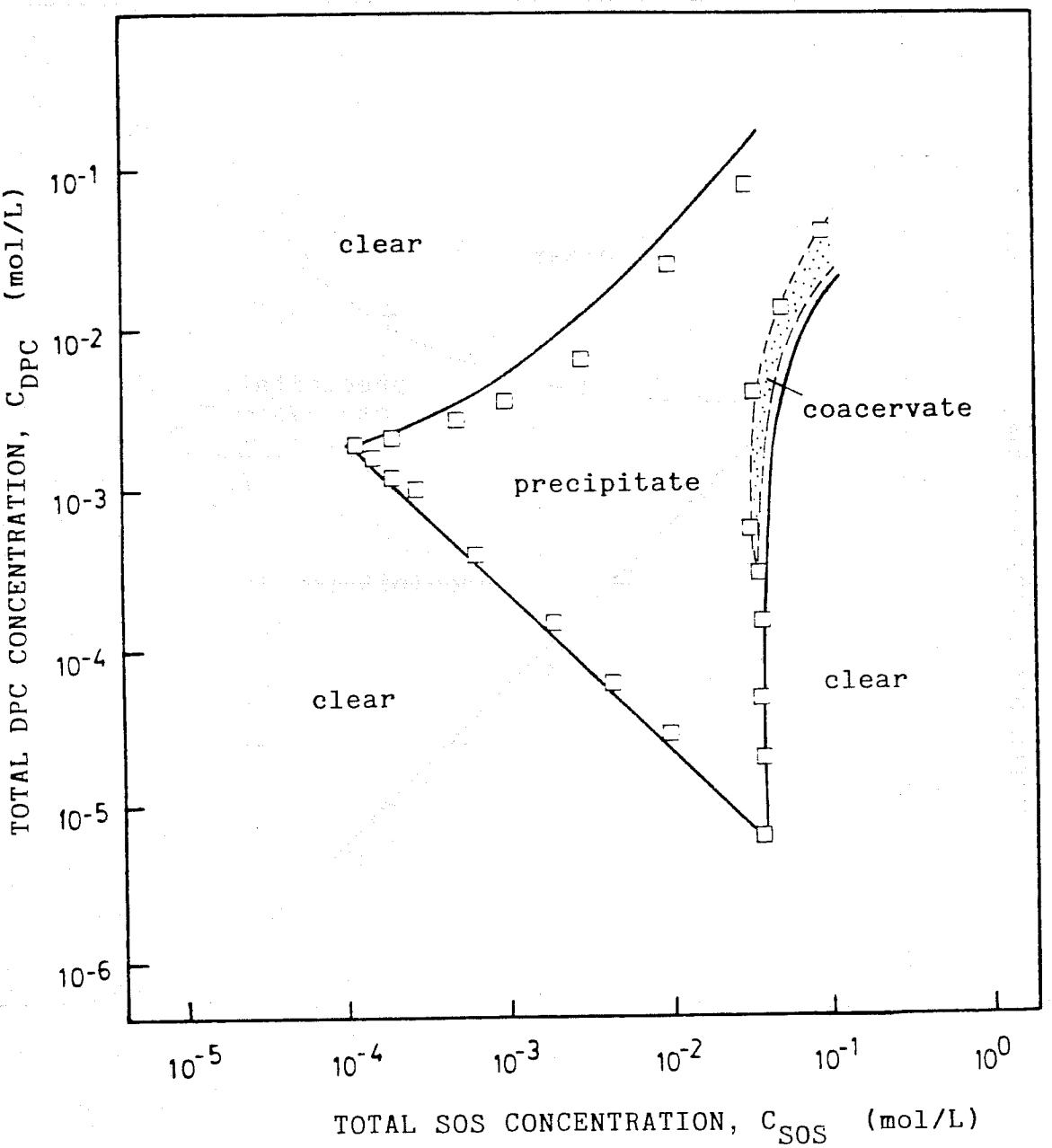

Figure 16. SOS/DPC Precipitation Data With Calculated Boundaries.

CHAPTER 3

ADSORPTION OF BINARY ANIONIC SURFACTANT MIXTURES ON ALPHA ALUMINA

ABSTRACT

The adsorption of binary mixtures of anionic surfactants of a homologous series (sodium octyl sulfate and sodium dodecyl sulfate) on alpha aluminum oxide was measured. A thermodynamic model was developed to describe ideal mixed admicelle (adsorbed surfactant bilayer) formation, for concentrations between the critical admicelle concentration and the critical micelle concentration. Specific homogeneous surface patches were examined by considering constant levels of adsorption. This model was shown to accurately describe the experimental results obtained, as well as previously reported results of another binary anionic/anionic surfactant system. Theoretical predictions of ideal mixture adsorption can be made on an *a priori* basis if the pure component adsorption isotherms are known.

The adsorption of mixtures of surfactants on mineral oxide surfaces is important in detergency, flotation, and enhanced oil recovery (EOR), among other technologies. If the thermodynamics of mixed surfactant adsorption on mineral surfaces were known, it might be possible to formulate mixtures to either enhance or reduce the total surfactant adsorption, thereby saving reagent costs in flotation (1-3) and enhanced oil recovery (4). Technical problems, such as the selectivity of mineral separation (3,5) and the chromatographic separation of surfactant slugs (6,7), could also be systematically addressed. Surfactants are almost always used as mixtures in practical applications, since surfactants are usually manufactured as mixtures. These mixtures are often comprised of homologs of a surfactant series that differ only by the alkyl chain length, and they are usually treated theoretically as a single component surfactant, with the mean properties of the mixture. A thermodynamic knowledge of the adsorption of homologous

mixtures of surfactants would allow better predictions to be made of the surfactant's performance.

Most oil-field experience with the use of surfactant derives from so-called micellar/polymer or chemical flooding EOR, in which surfactants are used to produce ultra-low interfacial tensions through the formation of a third phase, which coexists with the aqueous and oleic phase and contains most of the surfactant. By the phase rule, in a three-phase system of three components (or pseudocomponents) the compositions of the phases are fixed. So long as the system composition stays within the tie-triangle, removal of one of the components from the system does not change the compositions or physical properties of the phases. This stabilizes the properties of the system against loss of surfactant from the fluid phases due to adsorption on the very large surface area of the porous rock (8). Nevertheless, loss of surfactant due to adsorption has long been a major concern in micellar/polymer EOR (9-11).

The surfactant systems used for mobility control in, for example, the process addressed in this project, or in miscible flooding, do not form a surfactant rich third phase, and lack its "buffering" action against surfactant adsorption. Hence, surfactant adsorption is necessarily an even greater concern in the use of surfactants for mobility control in EOR. The importance of surfactant adsorption in surfactant-based mobility control is widely recognized by researchers. A decision tree has even been published for selection of a mobility-control surfactant based on adsorption characteristics (12).

Pure component surfactant adsorption has been widely studied (9,13-24). Figure 1 illustrates the four distinct adsorption regions that exist when an anionic surfactant adsorbs on a positively charged surface. Region I is called the Henry's Law region and the surfactant molecules adsorb because of the electrostatic attraction between the surfactant head groups and the oppositely charged surface, and the interaction of the surfactant tail groups with the surface. At a critical concentration, the adsorption is greatly enhanced by the association of the surfactant tail groups. A two-dimensional phase transition is believed to

take place on the highest energy patches on the solid surface. The concentration at which the first surfactant aggregate is formed is called the Critical Admicelle Concentration or CAC (18), or the Hemimicelle Concentration or HMC (20,23). At the CAC, the surfactant aggregate (or admicelle) forms on the most energetic patch on the surface. As the surfactant concentration increases, successively less energetic patches have admicelles form on them in Regions II and III. There is no fundamental significance to the Region II to Region III transition; Region III exists due to historical precedent as the region where the adsorption increases less rapidly with concentration on a log-log plot. With each adsorption level in Region II, there is a corresponding equilibrium concentration (CAC^*) that is required to form an admicelle on a patch of a specific energy level. Region IV begins with the formation of micelles. Micelles act as a chemical potential sink for any additional surfactant added to the solution, thereby keeping the monomer concentration nearly constant, and the adsorption level nearly constant. Hence, Region IV is sometimes called the plateau adsorption region (9).

The adsorption of mixtures of surfactants has received comparatively little attention. The adsorption of mixtures of nonionic and anionic surfactants has been studied (10,25-27) and strong negative deviations from ideality were observed (10,27). Attempts to model the degree of non-ideality using regular solution theory failed (27). The adsorption of mixtures of anionic and cationic surfactants would be expected to exhibit even larger deviations from ideality (28).

Wilson and co-workers developed a statistical mechanical model for single component surfactant adsorption (29-31) and expanded it to a binary system (2,3). Different adsorption curves were generated by varying the Van der Waals interaction parameters. The mixed adsorption equations that were developed were very complex and were not applied to experimental data.

Scamehorn et. al. expanded a single-component adsorption equation (9) to describe the adsorption of binary mixtures of anionic surfactants of a homologous series (11). Ideal

solution theory was found to describe the system fairly well. The mixed adsorption equations worked very well in predicting the mixture adsorption, but the equations were complex and would be difficult to extend beyond a binary system.

Scamehorn et. al. (32) also developed a reduced adsorption equation to describe the adsorption of mixtures of anionic surfactants, which are members of homologous series. The equations were semi-empirical and were based on ideal solution theory and the theory of corresponding states. To apply these equations, a critical concentration for each pure component in the mixture is chosen, so that when the equilibrium concentrations of the pure component adsorption isotherms are divided by their critical concentrations, the adsorption isotherms would coincide. The advantage of these equations is that little adsorption data is required to make approximate mixture predictions.

The adsorption of binary mixtures of anionic surfactants in the bilayer region has also been modeled by using just the pure component adsorption isotherms and ideal solution theory to describe the formation of mixed admicelles (33). Positive deviation from ideality in the mixed admicelle phase was reported, and the non-ideality was attributed to the planar shape of the admicelle. However, a computational error was made in comparison of the ideal solution theory equations to the experimental data, even though the theoretical equations presented were correct. Thus, the positive deviation from ideal mixed admicelle formation was in error.

Experimental

Materials. Sodium dodecyl sulfate ($C_{12}SO_4$) was purchased from Fisher Scientific with a manufacturer reported purity of at least 95.01%. The $C_{12}SO_4$ was recrystallized one time from reagent grade alcohol and water. Sodium decyl sulfate ($C_{10}SO_4$), from Eastman Kodak Company, was recrystallized twice using the same procedure as for the $C_{12}SO_4$. Sodium octyl sulfate (C_8SO_4), from Eastman Kodak Company, was recrystallized two times from boiling ACS grade 2-propanol and water, and then rinsed three times with ACS grade diethyl ether. The crystals were then dried in a hood for two days, and then under a vacuum for three days.

The alpha aluminum oxide was purchased from Alpha Products, Thiokol/Ventron Division. The aluminum oxide had a particle size of 40 microns, a surface area of 160 m^2/g, and consisted of 90% Al_2O_3 and 9% H_2O, according to the manufacturer. The aluminum oxide was dried in 50 g batches under a vacuum for two days before use.

Other materials used were ACS grade sodium chloride and sodium carbonate, HPLC grade methanol, and 0.1 N and 0.01 N hydrochloric acid and sodium hydroxide solutions. All of these chemicals were purchased from Fisher Scientific. The water was distilled and deionized.

Methods. The brine solutions that were used to make the sample solutions were 0.15 M sodium chloride and contained 0.0015 g/l sodium carbonate. Sodium carbonate was added to buffer the solutions against the carbonic acid that formed upon the absorption of carbon dioxide in the solutions. The pH of the brine solutions were adjusted to an initial value of 7.8, so that when the solution was equilibrated with the alumina, the equilibrium pH was 8.4. Ten milliliters of the sample solution were then pipetted to test tubes which contained 0.5 grams of aluminum oxide. The test tubes were then centrifuged for 45 minutes at 1000 rpm and placed in a water bath that was kept at a constant temperature of 30°C. After four to five days, the pH values of the equilibrated samples were measured and the supernatants of the samples were removed from the solids.

The concentrations of the anionic surfactants (C_8SO_4, $C_{10}SO_4$, and $C_{12}SO_4$) in the initial and equilibrated samples were measured using a high performance liquid chromatograph with a conductivity detector. Details of the analytical procedure may be found elsewhere (34).

Theory

The pure component adsorption isotherms of the surfactants used in this study (C_8SO_4, $C_{10}SO_4$, and $C_{12}SO_4$) are shown in Figure 2. All of the adsorption isotherms were continuous in Regions II and III, which suggests that the distribution of energy level patches on the surface of the

alpha aluminum oxide was nearly continuous.

The admicelle standard states are defined as the equilibrium monomer concentrations that are required to form the pure admicelles on a specific energy level patch. This particular patch is assumed to correspond to the same adsorption level for either pure surfactants or mixtures in Regions II and III. The equilibrium monomer concentration that is required to form the mixed admicelles on the same energy level patch, is then compared to the monomer concentration predicted from ideal solution theory. By defining the standard states at constant levels of adsorption, we can look at one homogeneous energy level patch on the surface at a time. As we look at increasingly higher adsorption levels, the effects of lower energy level patches and increasing total surface coverage on admicelle formation can be examined. The admicelle standard states were determined from the pure component adsorption isotherms by reading the equilibrium monomer concentrations that corresponded to an arbitrary adsorption level of interest (33).

The approach used to develop the ideal solution theory equations to describe binary mixed admicelle formation, was similar to that used by Roberts et. al. (33). The total monomer equilibrium concentration that it takes to reach a specified level of adsorption was used as the variable which was predicted from the model. The partial fugacities can be written for both the monomer and admicelle phases:

$$f_i^{mon} = Y_i \gamma_i^{mon} CAC_m^* \quad (1)$$

$$f_i^{adm} = Z_i \gamma_i^{adm} CAC_i^* \quad (2)$$

where f_i^{mon} and f_i^{adm} are the partial fugacities of component i in the monomer and admicelle phases, respectively; Y_i is the surfactant-only based mole fraction of component i in the equilibrium solution; Z_i is the surfactant-only based mole fraction of component i in the mixed admicelle; γ_i^{mon} and γ_i^{adm} are the activity coefficients of component i in the monomer and admicelle phases, respectively; CAC_m^* is the total equilibrium monomer concentration at the specified total adsorption level; and CAC_i^* is the pure surfactant i monomer concentration at the specified total adsorption

level. The asterisks above the critical admicelle concentrations (CAC_m^* and CAC_i^*) designate that these concentrations correspond to admicelle formation on a specific energy level patch, not necessarily the onset of aggregate formation (which is designated by CAC). The monomer concentration was extremely dilute, and swamping electrolyte was always present in the experiments. Therefore, the monomer was assumed to obey Henry's Law ($\gamma_i^{mon} = 1.0$).

At equilibrium, the partial fugacities of a component are equal in every phase. Therefore, Equations 1 and 2 can be equated to form Equation 3, which is valid for each surfactant component in the mixture.

$$Z_i \gamma_i^{adm} CAC_i^* = Y_i CAC_m^* \qquad (3)$$

It is desirable to obtain an a priori prediction of the total equilibrium monomer concentration (CAC_m^*) at set levels of adsorption based on the mixture feed mole fractions, instead of the equilibrium monomer mole fractions (Y_i). The equilibrium monomer mole fractions will differ from the feed mole fractions because of the preferential adsorption of some of the surfactants in the mixture. A mass balance on component i in the feed, equilibrium solution, and adsorbed phase is solved for the equilibrium monomer mole fraction to obtain Equation 4:

$$Y_i = \frac{Q_i (CAC_m^* V + W_g) - Z_i W_g}{CAC_m^* V} \qquad (4)$$

where Q_i is the feed mole fraction of component i, V is the volume of the liquid sample, is the total adsorption, and W_g is the weight of the aluminum sample. Equations can also be written for the surfactant-only based mole fractions in the monomer, admicelle, and feed. For a binary system,

$$Y_1 + Y_2 = 1.0 \qquad (5)$$

$$Z_1 + Z_2 = 1.0 \qquad (6)$$

$$Q_1 + Q_2 = 1.0 \qquad (7)$$

If ideal solution theory for mixed admicelle formation is assumed ($\gamma_i^{adm} = 1.0$), six independent equations can be written for a binary system. The set of equations consists of Equation 3 written for components 1 and 2, Equation 4 written for component 1, and Equations 5, 6, and 7. The six equations can be solved directly for the six unknowns (Y_1, Y_2, Z_1, Z_2, Q_2, and CAC_m^*) to completely describe the system. Equation 3 written for components 1 and 2 and Equations 4 - 7 can be combined to result in Equation 8.

$$CAC_m^* = \frac{CAC_1^* W_g Q_1 + CAC_2^* (CAC_1^* V + W_g(1-Q_1))}{V(1-Q_1)CAC_i^* + VCAC_2^* Q_1 + W_g} \quad (8)$$

Once CAC_m^* is known, Y_1 and Z_1 can be calculated by a simultaneous solution of Equations 3 and 4, and then Y_2 and Z_2 can be calculated from Equations 5 and 6, respectively. Equations 3-7 can easily be expanded to more than two components, and can describe non-ideal mixing in the admicelle phase by inserting the correct expressions for the admicellar activity coefficients for each component.

Except at concentrations near the CAC, the amount of surfactant adsorbed in the Henry's law region is small in comparison to the amount of surfactant present in the admicelles. This implies that nearly all of the adsorbed surfactant molecules are associated on the mineral surface in the form of admicelles. It is important to keep in mind that Equation 8 is valid only between the CAC and the CMC. Above the CMC, equations could be included to account for the formation of micelles, by including monomer-micelle equilibrium equations (11).

The only information needed to predict the mixture surfactant concentration to attain a specified adsorption level is the pure component adsorption isotherms measured at the same experimental conditions as the mixture isotherms. These isotherms are needed to obtain the pure component standard states.

The method of predicting the mixture adsorption isotherms is to first select the feed mole fractions of

interest and to pick an adsorption level within Region II. The pure component standard states are determined from the total equilibrium concentration that occurs at that set level of adsorption for the pure surfactant component adsorption isotherms. The total equilibrium mixture concentration corresponding to the selected adsorption level is then calculated from Equation 8. This procedure is repeated at different levels of adsorption until enough points are collected to completely describe the mixture adsorption isotherm curve.

Results and Discussion

The three pure component adsorption isotherms of the homologous series of sodium alkyl sulfates (C_8SO_4, $C_{10}SO_4$, and $C_{12}SO_4$) in Figure 2, were plotted at their reduced concentrations in Figure 3, to extrapolate the C_8SO_4 data to its CAC. The adsorption data for C_8SO_4 could not be measured below a certain concentration and the data was needed to obtain the C_8SO_4 standard state concentrations. The critical concentrations used to calculate the reduced concentrations were chosen for the best coincidence of the reduced adsorption isotherms. As seen in Figure 3, the corresponding states theory (32) worked very well for the pure component surfactants used in this study.

The adsorption isotherms of C_8SO_4 and $C_{12}SO_4$, and mixtures thereof, on alpha aluminum oxide are illustrated in Figure 4. Also shown in Figure 4 is the extrapolation of the C_8SO_4 pure component adsorption isotherm down to its CAC and the ideal solution theory predictions.

The agreement between the mixture adsorption data and ideal solution theory is excellent. It is important to remember that while looking at various constant levels of adsorption in Region II, we are looking at the CAC* of the mixed admicelle that has just formed on a particular patch. By looking at different adsorption levels, we are looking at how the two surfactants interact on different energy level patches on the surface.

Equation 8 was also used to predict the mixture adsorption isotherms in Region II of $C_{10}SO_4$ and $C_{12}SO_4$ on

gamma aluminum oxide and compared to experimental data from Roberts et. al. (33). Figure 5 is a plot of the total adsorption versus the total equilibrium concentration for two pure component and three mixture mole fractions from that work. The conditions under which the data were obtained were identical to those in this study, except for the substrate (gamma alumina) and the equilibrium pH (6.8). Once again, agreement between the data and ideal solution theory is excellent. It is no surprise that the adsorption of mixtures of $C_{10}SO_4$ and $C_{12}SO_4$ follow ideal solution theory, because the adsorption of mixtures of C_8SO_4 and $C_{12}SO_4$ follow ideal solution theory, and $C_{10}SO_4$ and $C_{12}SO_4$ are closer members of the homologous series. Roberts et. al., reported a positive deviation from ideality for the adsorption of mixtures of $C_{10}SO_4$ and $C_{12}SO_4$ due to a miscalculation, and attributed it to the planer shape of the admicelle. The results presented here clearly shows that the hydrophobic bonding in the admicelle is similar for mixed and single component admicelles.

Micelles and monolayers composed of homologous mixtures of anionic surfactants can be approximately described by ideal solution theory to model the mixed surfactant aggregate (35). Therefore, it is not surprising that mixed admicelles composed of these surfactants also obey ideal solution theory. It is also important to note that this is true at all adsorption levels within Region II, as seen by the excellent agreement between theory and experiment in Figures 4 and 5.

Literature Cited

1. Novich, B. E.; Ring, T. A. Langmuir 1985, 1, 701.
2. Wilson, D. J. Sep. Sci. Technol. 1982, 17, 1219.
3. Wilson, D. J.; Carter, K. N. Sep. Sci. Technol. 1983, 18, 657.
4. Meldrau, R. F., et. al. J. Pet. Technol. 1983, 35, 1279.
5. Aplan, F. F. In Flotation; Kirk-Othmer Encyclopedia of Chemical Technology; Wiley, Inc.: New York, Vol. 10, p 523.
6. Sharma, M. K.; Shah, D. O.; Brigham, W. E. SPE Reservoir Eng. 1986, 1, 253.
7. Harwell, J. H.; Helfferich, F. G.; Schechter, R. S. AIChE J. 1982, 28, 448.
8. Smith, D. H. SPE/DOE Paper No. 14914, Tulsa, April, 1986.
9. Scamehorn, J. F.; Schechter, R. S.; Wade, W. H. J. Colloid Interface Sci. 1982, 85, 463.
10. Scamehorn, J. F.; Schechter, R. S.; Wade, W. H. J. Colloid Interface Sci. 1982, 85, 494.
11. Scamehorn, J. F.; Schechter, R. S.; Wade, W. H. J. Colloid Interface Sci. 1982, 85, 479.
12. Wellington, S. L.; Vinegar, H. J. SPE Paper No. 14393, Las Vegas, September, 1985.
13. Hanna, H. S.; Somasundaran, P. J. Colloid Interface Sci. 1979, 70, 181.
14. Levitz, P.; Damme, H. V. J. Phys. Chem. 1986, 90, 1302.
15. Koopal, L. K.; Keltjens, L. Colloids Surf. 1986, 17, 371.
16. Rosen, M. J.; Nakamura, Y. J. Phys. Chem. 1977, 81, 873.
17. Trogus, F. J.; Thach, S.; Schechter, R. S.; Wade, W. H. Soc. Pet. Eng. J. 1977, 17, 337.
18. Harwell, J. H.; Hoskins, J. C.; Schechter, R. S.; Wade, W. H. Langmuir 1985, 1, 251.
19. Dick, S. G.; Fuerstenau, D. W.; Healy, T. W. J. Colloid Interface Sci. 1971, 37, 595.
20. Somasundaran, P.; Fuerstenau, D. W. J. Phys. Chem.

1966, 70, 90.
21. Wakamatsu, T.; Fuerstenau, D. W. in Adv. Chem. Ser. 1968, 79, 161.
22. Fuerstenau, D. W.; Wakamatsu, T. Farraday Discuss. Chem. Soc. 1976, 59, 157.
23. Chandar, S.; Fuerstenau, D. W.; Stigter, D. In Adsorption From Solution; Ottewill, R. H.; Rochester, C. H.; Smith, A. L., Eds.; Academic Press: London, 1983; p 197.
24. Dobias, B. Colloid Polym. Sci. 1978, 256, 465.
25. Schwuger, M. J.; Smolka, H. G. Colloid Polym. Sci. 1977, 255, 589.
26. Gao, Y.; Yue, C.; Lu, S.; Gu, W.; Gu T. J. Colloid Interface Sci. 1984, 100, 581.
27. Roberts, B. L.; Harwell, J. H.; Scamehorn, J. F. Colloids Surf., in press.
28. Schwuger, M. J. Kolloid - Z. Z.Polym. 1971, 243, 129.
29. Wilson, D. J. Sep. Sci. 1977, 12, 447.
30. Wilson, D. J.; Kennedy, R. M. Sep. Sci. Technol. 1979, 14, 319.
31. Kieffer, J. E.; Wilson, D. Sep. Sci. Technol. 1980, 15, 57.
32. Scamehorn, J. F.; Schechter, R. S.; Wade, W. H. J. Am. Oil Chem. Soc. 1983, 60, 1345.
33. Roberts, B. L.; Scamehorn, J. F.; Harwell, J. H. In Phenomena in Mixed Surfactant Systems; Scamehorn, J.F., Ed.; ACS Symp. Ser. Vol. 311, American Chemical Society: Washington, D. C., 1986, p 200.
34. Lopata, J. J. M.S. Thesis, University of Oklahoma, Oklahoma, 1987.
35. Scamehorn, J. F. In Phenomena in Mixed Surfactant Systems; Scamehorn, J. F. Ed.; ACS Symp. Ser., Vol. 311, American Chemical Society: Washington, D. C., 1986, p 1.

Figure 1. Typical Anionic Surfactant Adsorption Isotherm on a Positively Charged Mineral Oxide Surface.

Figure 2. Adsorption Isotherms of C_8SO_4, $C_{10}SO_4$, and $C_{12}SO_4$ on Alpha Aluminum Oxide.

Figure 3. Reduced Adsorption Isotherms of C_8SO_4, $C_{10}SO_4$, and $C_{12}SO_4$ on Alpha Aluminum Oxide.

Figure 4. Mixure Adsorption Isotherms of C_8SO_4 and $C_{12}SO_4$ on Alpha Aluminum Oxide.

Figure 5. Mixture Adsorption Isotherms of $C_{10}SO_4$ and $C_{12}SO_4$ on Gamma Aluminum Oxide (Data from (33)).

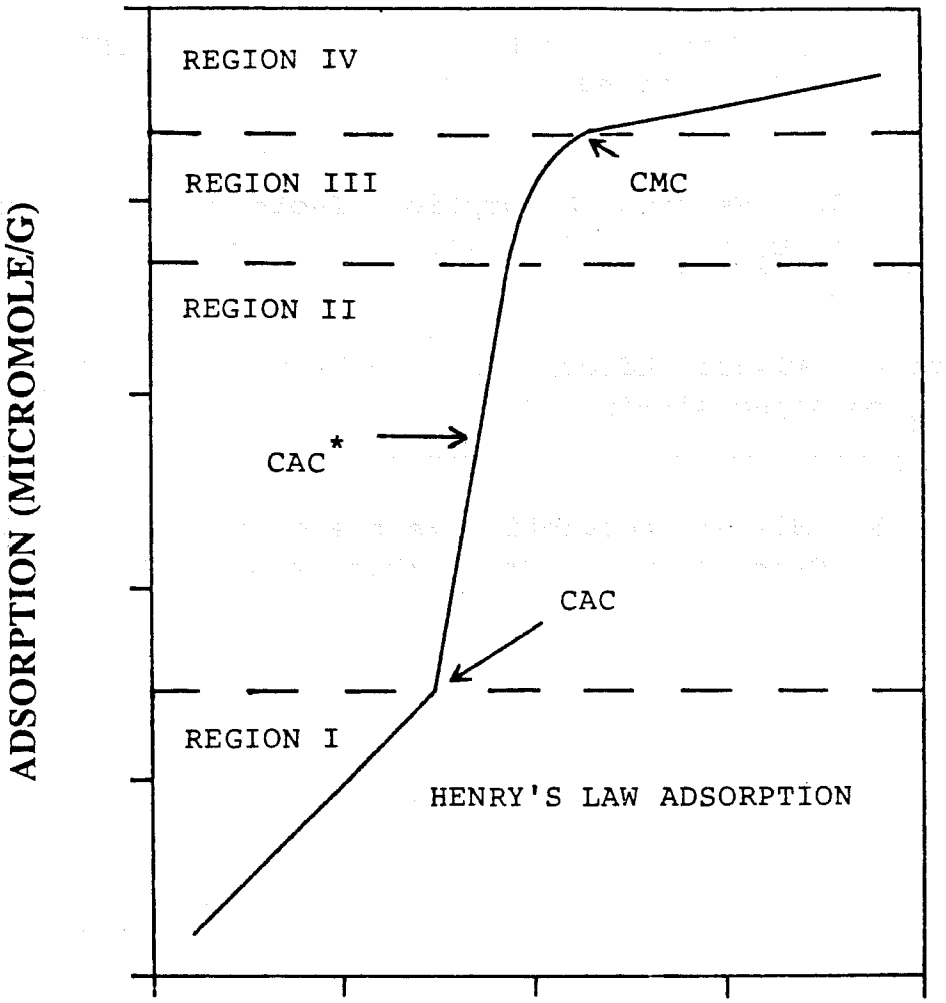

Figure 1. Typical Anionic Surfactant Adsorption Isotherm on a Positively Charged Mineral Oxide Surface.

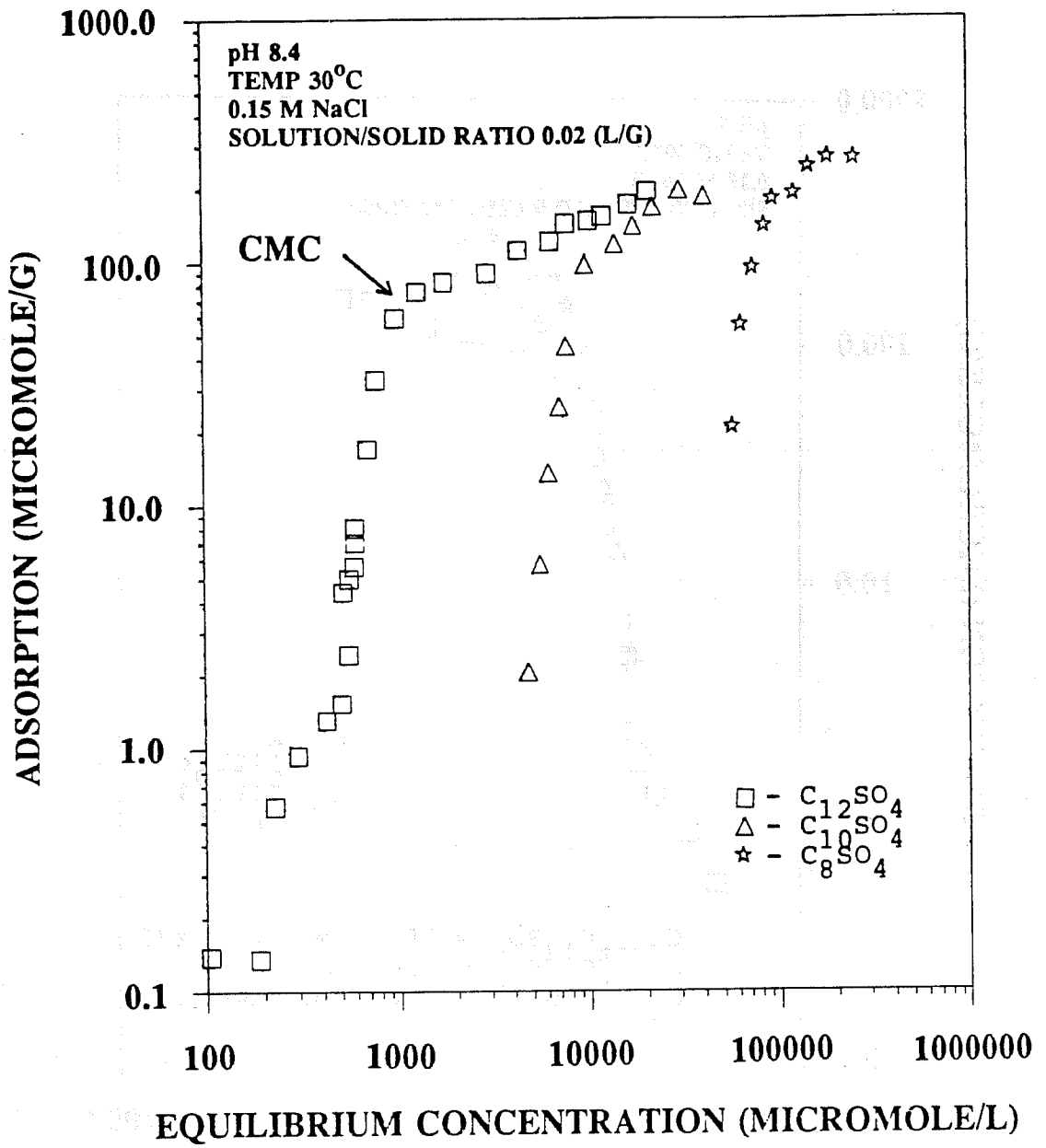

Figure 2. Adsorption Isotherms of C_8SO_4, $C_{10}SO_4$, and $C_{12}SO_4$ on Alpha Aluminum Oxide.

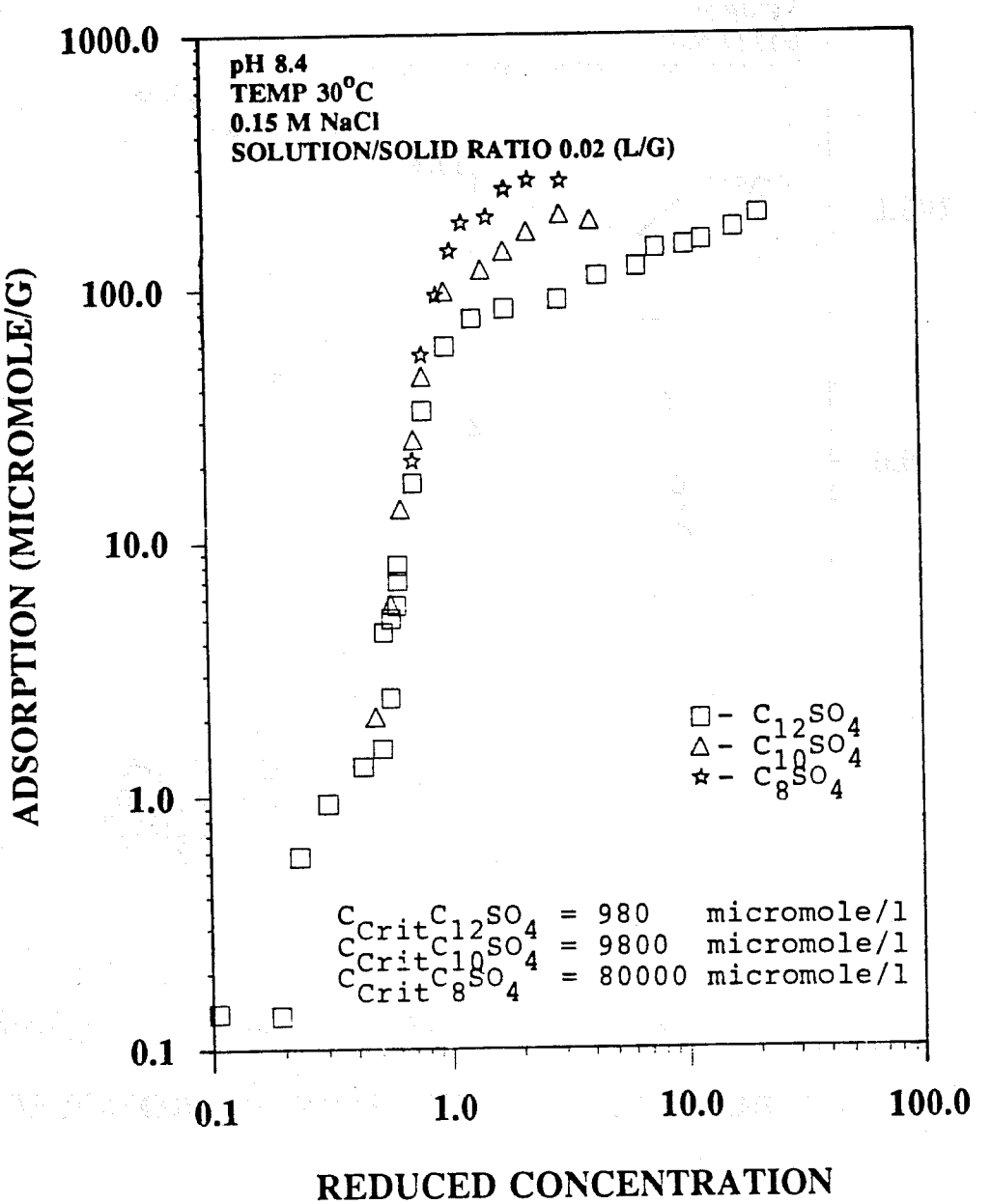

Figure 3. Reduced Adsorption Isotherms of C_8SO_4, $C_{10}SO_4$, and $C_{12}SO_4$ on Alpha Aluminum Oxide.

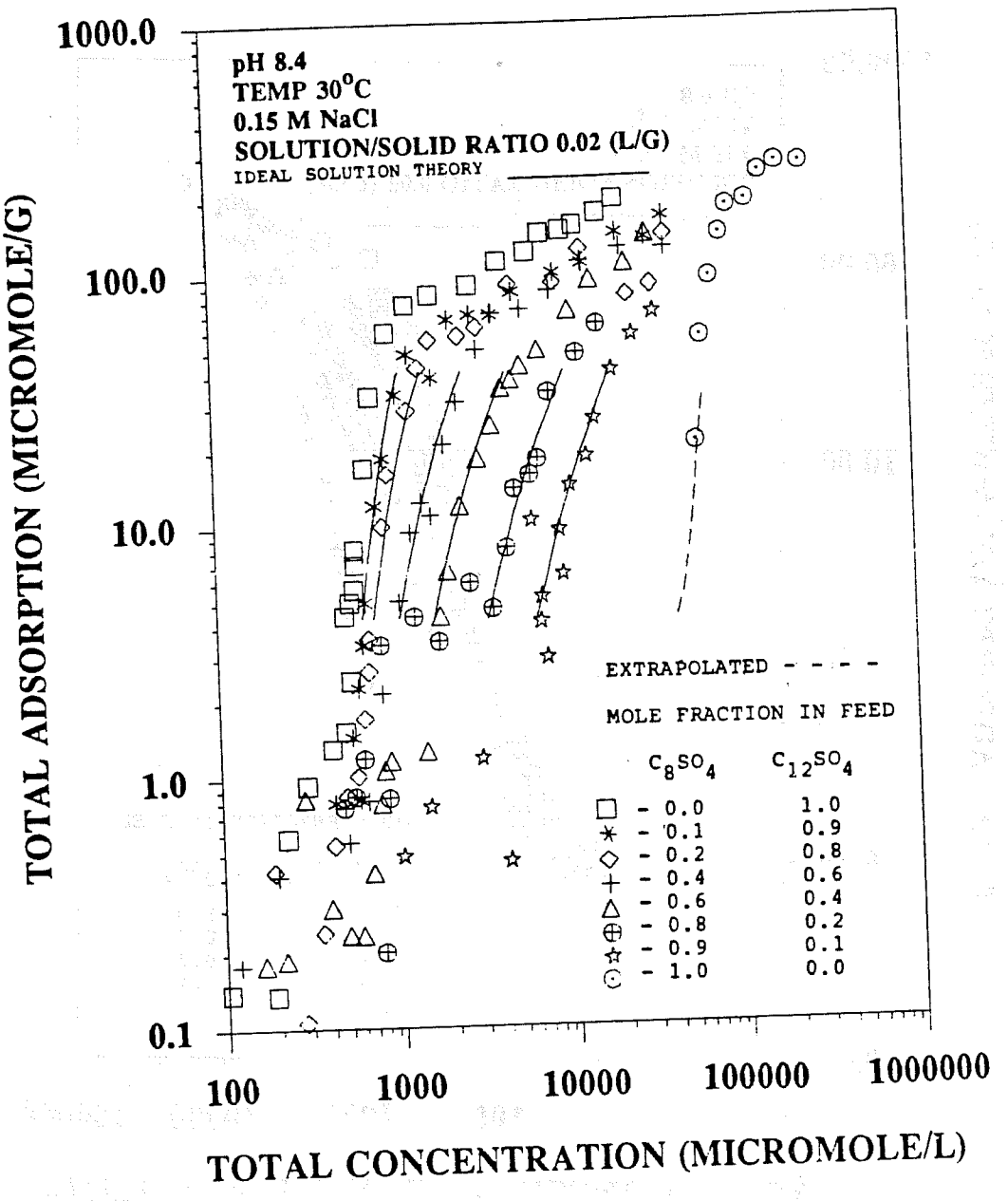

Figure 4. Mixure Adsorption Isotherms of C_8SO_4 and $C_{12}SO_4$ on Alpha Aluminum Oxide.

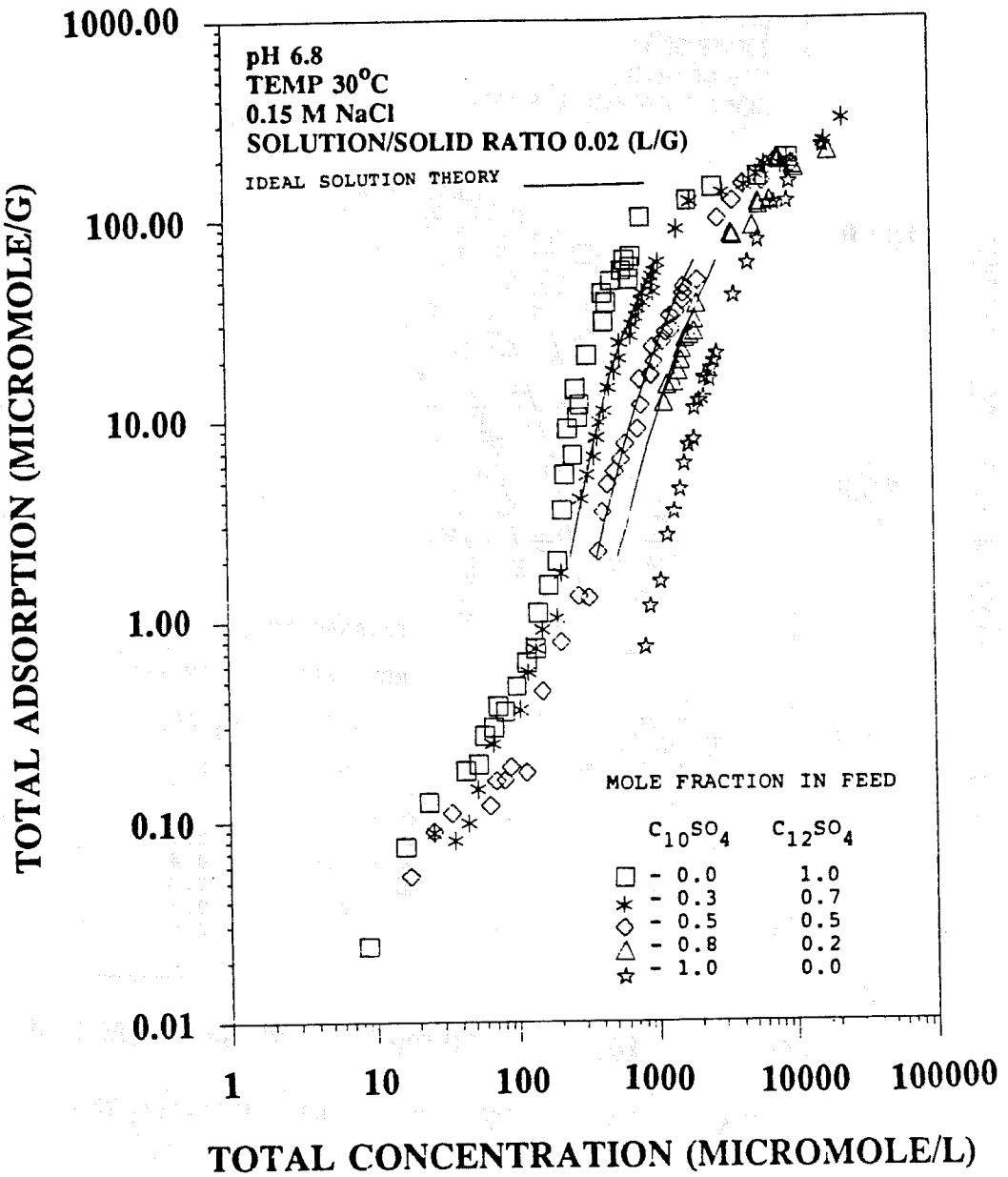

Figure 5. Mixture Adsorption Isotherms of $C_{10}SO_4$ and $C_{12}SO_4$ on Gamma Aluminum Oxide (Data from (33)).

CHAPTER 4

CHROMATOGRAPHIC MOVEMENT AND PRECIPITATION OF ANIONIC AND CATIONIC SURFACTANTS DURING PROPAGATION WITHIN A HOMOGENEOUS POROUS MEDIUM

INTRODUCTION

In this chapter, some studies are described on the behavior of anionic-cationic surfactant mixtures, during in-situ mixing inside a one dimensional, homogeneous, porous medium. A theoretical model is described which accounts for the pertinent phenomena including mixed micelle formation, chromatographic movement, and precipitate formation.This model is then used to predict the effluent surfactant profiles from the porous medium and the important features of these predictions are confirmed by some experimental results.

THEORY

1 Development of the mathematical model

The experiments that are being modeled here occur within a column packed with aluminum oxide. A solution of anionic surfactant SDS was injected, followed by a brine spacer, then a solution of cationic surfactant DPC, and finally an infinite brine slug. In these experiments, the mobile phase was a 0.15 M NaCl solution. To explain the experimental results, a theoretical model assuming the following was developed:

1. The column is one dimensional and the porous medium is homogeneous with constant porosity.

2. The surfactant solution is in plug flow.

3. There is a instantaneous reaction between the

SDS and the DPC monomers.

4. There is no supersaturation of the fluid phase.

5. The monomer and the adsorbate are in local equilibrium and the equilibrium is modeled assuming Henry's law adsorption.

6. The precipitate particles do not move through the column.

7. Mixed admicelles do not form.

In a real system, none of the above assumptions are completely correct but assumptions #3 and #6 have the most significant effect on the qualitative difference between the experimental and the theoretical results. It is clear that the reaction is not instantaneous and most probably, the precipitate does move through the column; nonetheless, the theoretical model does qualitatively predict every aspect of the experimental results except the fact that precipitate is seen in the effluent.

To model the experiments, the equilibrium relationships between monomer and micelle, monomer and admicelle, and monomer and precipitate, as well as the mass balance equations for the SDS and DPC are necessary (1,2).

To model the monomer-micelle equilibrium, regular solution theory was used.

$$[DS^-]_{mon} = X_{ds} CMC_{ds} \exp\{(1-X_{ds})^2 W/RT\} \quad [1]$$

$$[DP^+]_{mon} = (1-X_{ds}) CMC_{dp} \exp\{(X_{ds})^2 W/RT\} \quad [2]$$

where $[DS^-]_{mon}$ and $[DP^+]_{mon}$ are the monomer concentrations of SDS and DPC, respectively, X_{ds} is the mole fraction of SDS in the micellar phase, CMC_{ds} and CMC_{dp} are the critical micelle concentrations of pure SDS and DPC in 0.15 M brine, W is the interaction parameter, R is the ideal gas constant, and T is the absolute temperature.

It was assumed that Henry's law adsorption explains the

monomer-admicelle equilibrium. So,

$$[DS-]_a = ((1-E)/E)dH_{ds}[DS-]_{mon} \quad [3]$$

$$[DP+]_a = ((1-E)/E)dH_{dp}[DP+]_{mon} \quad [4]$$

where H_{ds} and H_{dp} are Henry's law constants for SDS and DPC, respectively, E is porosity, d is the density of the aluminum oxide, and $[DS-]_a$ and $[DP+]_a$ are the adsorbed concentrations of SDS and DPC, respectively, in units of micromoles per ml of solution.

The following equation was used to model the monomer-precipitate equilibrium:

$$[DS-]_{mon}[DP+]_{mon} < K_{sp}/f^2 \quad [5]$$

where k_{sp} is the solubility product, and f is the activity coefficient in solution.

The differential material balance equations for the SDS and DPC in their nondimensional forms are:

$$[DS-]^T/\ t^+ + [DS-]/\ z^+ = 0 \quad [6]$$

$$[DP+]^T/\ t^+ + [DP+]/\ z^+ = 0 \quad [7]$$

where

$$t^+ = tv/L$$

and

$$z^+ = z/L$$

and

$$[DS-]^T = [DS-]_{mon} + [DS-]_{agg} + [DS-]_a + [DSDP] \quad [8]$$

and

$$[DS-] = [DS-]_{mon} + [DS-]_{agg} \quad [9]$$

and

$$[DP+]^T = [DP+]_{mon} + [DP+]_{agg} + [DP+]_a + [DSDP] \quad [10]$$

and

$$[DP+] = [DP+]_{mon} + [DP+]_{agg} \quad [11]$$

where t is time, v is the pore velocity, L is length of the column, z is the length along the column, t^+ is the dimensionless time (pore volumes injected), Z^+ is the dimensionless length, $[DS-]^T$ and $[DP+]^T$ represent the total concentrations of SDS and DPC, respectively, [DS-] and [DP+] represent the total concentration of SDS and DPC in the solution, respectively, [DSDP] is the concentration of precipitate in units of micromoles per ml of solution, $[DS-]_{agg}$ and $[DP+]_{agg}$ are the concentrations of SDS and DPC in the aggregate phase, respectively.

In the experiments, SDS injection was started at time equal to zero ($t^+=0$) and DPC injection was started after the SDS and brine spacer were injected at $t=t^+_2$. The following boundary conditions were used to solve the respective mass balance equations for SDS and DPC. For the SDS:

$$\text{at } t^+=0 \quad [DS-]^T=[DS-]=0 \quad \text{for} \quad 0<z^+<1 \quad [12]$$

$$\text{at } z^+=0 \quad [DS-]^T=[DS-]=[DS-]_{inj} \quad \text{for} \quad 0<t^+<e_{ds}$$

$$\text{at } z^+=0 \quad [DS-]^T=[DS-]=0 \quad \text{for} \quad e_{ds}<t^+ \quad [13]$$

For the DPC:

$$\text{at} \quad t<t^+_2 \quad [DP+]^T=[DP+]=0 \quad \text{for} \quad 0<z^+<1 \quad [14]$$

$$\text{at } z^+=0 \quad [DP+]^T=[DP+]=[DP+]_{inj} \quad \text{for } t^+_2<t^+<t^+_2+e_{dp}$$

$$\text{at } z^+=0 \quad [DP+]^T=[DP+]=0 \quad \text{for } t^+_2+e_{dp}<t^+ \quad [15]$$

where e_{dp} and e_{ds} represent the pore volumes of DPC and SDS injected, respectively, and $[DS-]_{inj}$ and $[DP+]_{inj}$ are injected concentrations of SDS and DPC, respectively.

Substituting equation (3) into equation (8) results in the following:

$$[DS-]^T = u_{ds}[DS-]_{mon} + [DS-]_{agg} + [DSDP] \qquad [16]$$

where

$$u_{ds} = 1 + ((1-E)/E)dH_{ds}$$

Substituting equation (4) into equation (10) results in the following:

$$[DP+]^T = u_{dp}[DP+]_{mon} + [DP+]_{agg} + [DSDP] \qquad [17]$$

where

$$u_{dp} = 1 + ((1-E)/E)dH_{dp}$$

where u_{dp} and u_{ds} are a measure of adsorption of DPC and SDS by the adsorbent. Any increase in the value of u_{dp} or u_{ds} means the adsorption of DPC or SDS by the adsorbent have increased.

There are seven unknowns $[DP+]^T$, $[DP+]_{mon}$, $[DP+]_{agg}$, $[DSDP]$, $[DS-]^T$, $[DS-]_{mon}$, and $[DS-]_{agg}$ and there are seven equations; (1), (2), (5), (6), (7), (16), and (17). Equations (1), (2), and (5) are inequalities. So, it is necessary to ascertain the presence of micelle or precipitate before using the respective equations. Initial conditions set the values of the total concentration of SDS and DPC, $[DS-]^T$ and $[DP+]^T$, respectively, and the total concentration of SDS and DPC in the solution, [DS-] and [DP+], respectively, at time equal to zero; boundary conditions set the values of the total concentration of SDS and DPC in the solution at the beginning of the column at any time. Initial conditions, equations (12) and (14), and the mass balance equations can be used to calculate the total concentration of SDS and DPC at the next value of time. Then, equilibrium relationships are used to calculate the total concentration of SDS and DPC in the solution from the newly calculated values of the total concentration of SDS and DPC and this process is repeated for the entire value of time. In the next section , the solution technique for solving the mass balance equations will be discussed and in section 3 the

procedure for calculating the total concentrations of SDS and DPC in the solution knowing the total SDS and DPC concentrations using the equilibrium relationships will be explained.

2 Solution Technique

The mass balance equations, equations (6) and (7) were solved numerically using the explicit backward finite difference method. Dispersion was qualitatively approximated by numerical dispersion (3).

Finite difference expressions were substituted into equations (6) and (7).

$$[DS-]^T_{i+1,j}=[DS-]^T_{i,j}-(t^+/z^+([DS-]_{i,j}-[DS-]_{i,j-1})) \quad [18]$$

$$[DP+]^T_{i+1,j}=[DP+]^T_{i,j}-(t^+/z^+([DP+]_{i,j}-[DP+]_{i,j-1})) \quad [19]$$

i shows the time and its range of value is from 0 to m. j is the value of node along the length of the column and its range of value is from 0 to n.

To calculate the values of $[DS-]^T_{i=1,j}$ and $[DP+]^T_{i=1,j}$ for $1<j<n$ the initial conditions, equations (12) and (14), were used. Since the values of $[DS-]^T_{i,j=0}$ and $[DP+]^T_{i,j=0}$ are given by the boundary conditions, equations (13) and (15), it is not necessary to calculate them. To go any further, to calculate the values of $[DS-]^T_{i=2,j}$ and $[DP+]^T_{i=2,j}$, it is necessary to know the values of $[DS-]^T_{i=1,j}$ and $[DP+]^T_{i=1,j}$. The values of $[DS-]^T_{i=1,j}$ and $[DP+]^T_{i=1,j}$ are known and the equilibrium relationships have to be used to calculate $[DS-]_{i=1,j}$ and $[DP+]_{i=1,j}$ from $[DS-]^T_{i=1,j}$ and $[DP+]^T_{i=1,j}$ (the procedure is explained in the next section). Knowing $[DS-]_{i=1,j}$, $[DP+]_{i=1,j}$, $[DS-]^T_{i=1,j}$, and $[DP+]^T_{i=1,j}$, equations (18) and (19) can be used to calculate $[DS-]^T_{i=2,j}$ and $[DP+]^T_{i=2,j}$. These steps are continuously repeated for the entire value of time.

3 Equilibrium Relationship Calculations

In the previous section, the solution technique for solving the mass balance equations, equations (6) and (7), was explained. In this section, it will be explained how the concentration of SDS and DPC in the solution are calculated knowing the total concentration of SDS and DPC.

If the total concentration of SDS and DPC are known, equilibrium relationships are used to calculate the concentration of SDS and DPC in the solution. Equations (1), (2), and (5) are inequalities. So, before using these equilibrium relationships , it is necessary to ascertain the presence of micelles and precipitate. Equations (1) and (2) model the equilibrium between monomers and micelles. Equation (5) models the equilibrium between monomers and precipitate. The first step in calculating the concentration of SDS and DPC in the solution, knowing the total concentration of SDS and DPC, is to ascertain the presence or non-presence of precipitate or micelles. The second step is to calculate the amount of SDS and DPC in the solution using the appropriate equilibrium relationships.

The procedure, both the mentioned first and second step, used here to calculate the concentration of SDS and DPC in the solution knowing the total concentration of SDS and DPC, is based on the model developed by Stellner et. al. (4) to calculate the SDS-DPC phase boundaries at a pH of 8.4 and $T=30^{o}C$. To understand the details of the procedure used here to calculate the concentration of SDS and DPC in the solution a clear and detailed understanding of the Stellner et. al. (4) model is required.

To show how the SDS and DPC concentrations in the solution are calculated knowing $[DS-]^{T}$ and $[DP+]^{T}$, three new terms are introduced.

$$D = [DS-]^{T} - [DP+]^{T} \qquad [20]$$

$$D_1 = 600u_{ds} - 0.65u_{dp} \qquad [21]$$

$$D_2 = 0.13u_{ds} - 3000u_{dp} \qquad [22]$$

The full significance of numbers in equations (21) and (22) are explained in reference 4. The variable D is calculated using equation (20). The first possibility is that D is greater than D_1. If D is greater than D_1 then both precipitate and SDS rich micelles are present or there is no precipitate and only SDS rich micelles are present. To test whether there is any precipitate present or not, the following equations are used:

$$[DSS]_{agg} = \{[DS-]^T - [DP+]^T + u_{dp}[DP+]_{mon} - u_{ds}[DS-]_{mon}\} / (2x^*_{ds} - 1) \quad [23]$$

$$[DS-]_{agg} = (x^*_{ds})[DDS]_{agg} \quad [24]$$

$$[DSDP] = [DS-]^T - u_{ds}[DS-]_{mon} - [DS-]_{agg} \quad [25]$$

where $[DSS]_{agg}$ is the total aggregate concentration and x^*_{ds} is the mole fraction of SDS in the aggregate phase. The aggregate phase includes both the micelles and coacervate. The values used in the equations (23) through (25) for this case are:

$x^*_{ds} = 0.62$

$[DP+]_{mon} = 0.65$ Molar

$[DS-]_{mon} = 600.0$ Molar

Equation (23) was derived by subtracting equation (17) from equation (16) and using the fact that $[DS-]_{agg}$ and $[DP+]_{agg}$ are related by x^*_{ds}. The variables $[DP+]_{agg}$, $[DS-]_{agg}$, and [DSDP] are calculated using equations (23) through (25).

If [DSDP] calculated from equations (23) through (25) is negative, it indicates that the concentration of precipitate is equal to zero and only SDS rich micelles with a SDS mole fraction greater than 0.62 are present. A negative concentration does not have any physical significance but it is useful because it indicates no precipitate is present. To calculate [DS-] and [DP+], assuming no precipitate is present, equations (1) and (2) are substituted into equations

(16) and (17), respectively, and [DSDP] is set equal to zero in equations (16) and (17), the following equations result:

$$[DS-]^T = u_{ds} x^*_{ds} CMC_{ds} \exp\{(1-x^*_{ds})^2 W/RT\} + x^*_{ds}[DDS]_{agg} \quad [26]$$

$$[DP+]^T = u_{dp}(1-x^*_{ds}) CMC_{dp} \exp\{x^{*2}_{ds} W/RT\} + (1-x^*_{ds})[DDS]_{agg} \quad [27]$$

where

$W/RT = -8.62$ at $T = 30^{\circ}C$

Two unknowns in equations (26) and (27) are x^*_{ds} and $[DDS]_{agg}$. Equations (26) and (27) can be solved for x^*_{ds} using the Newton-Raphson root finding method. After calculating x^*_{ds} and $[DDS]_{agg}$, equations (16) and (17) can be used to calculate $[DS-]_{mon}$ and $[DP+]_{mon}$. Then, equations (9) and (11) are used to calculate $[DS-]_{mon}$ and $[DP+]_{mon}$.

If [DSDP] calculated using equations (23) through (25) is not negative, then both precipitate and SDS rich micelles with a SDS mole fraction equal to 0.62 are present and the $[DS-]_{mon}$ and $[DP+]_{mon}$ are equal to 600 and 0.65 micromolar, respectively. In this case equations (9) and (11) can be used to calculate [DS-] and [DP+]. If the calculated [DSDP] is zero then only SDS rich micelles with a SDS mole fraction of 0.62 are present.

The second possibility is that D is less than D_2. If D is less than D_2, both precipitate and DPC rich micelles are present, or the concentration of precipitate is zero and only DPC rich micelles are present. In any event, the same steps as in the previous case (D greater than D_1) have to be repeated with the exception that the values of x^*_{ds}, $[DS-]_{mon}$, and $[DP+]_{mon}$ used in the equations (23) through (25) are different. The values in this case are as follows:

$$x^*_{ds} = 0.107$$

$$[DS-]_{mon} = 0.13 \text{ Molar}$$

$[DP+]_{mon}$ = 3000.0 Molar

Now, if [DSDP] calculated using equations (23) through (25) is negative, DPC rich micelles with a SDS mole fraction less than 0.107 are present. If [DSDP] is positive or zero then DPC rich micelles with a SDS mole fraction of 0.107 are present and the SDS and DPC monomer concentration are 0.13 and 3000 micromolar, respectively.

The third possibility is that the calculated value of D is between D_2 and D_1. In this case, no micelles are present and the following equations are used to calculate [DSDP], [DS-], and [DP+]:

$$[DP+]_{mon} = \{([DP+]^T - [DS-]^T) + SQRT\{([DS-]^T - [DP+]^T)^2 + (4K_{sp} u_{ds} u_{dp}/f^2)\}\}/2u_{dp} \quad [28]$$

$$[DSDP] = [DP+]^T - u_{dp}[DP+]_{mon} \quad [29]$$

$$[DS-]_{mon} = \{[DS-]^T - [DSDP]\}/u_{ds} \quad [30]$$

where

K_{sp} = 115 $(M)^2$ at T=25°C

f=0.758 for 0.15 M NaCl solution

Equation (28) was derived by setting $[DS-]_{agg}$ and $[DP+]_{agg}$ in the equations (16) and (17) equal to zero, respectively, and substituting them in equation (5) assuming that precipitate is present. Since in this case concentration of micelles is equal to zero, $[DS-]_{mon}$ and $[DP+]_{mon}$ are equal to [DS-] and [DP+], respectively. If the calculated value of [DSDP] using equations (28) through (30) is negative or zero that means no precipitate is present. Then the following equations can be used to calculate [DS-] and [DP+]:

$$[DS-]_{mon} = [DS-]^T/u_{ds} \quad [31]$$

$$[DP+]_{mon} = [DP+]^T/u_{dp} \quad [32]$$

Equations (31) and (32) were derived by setting the

concentrations of micelle and precipitate in equations (16) and (17) equal to zero and solving them for $[DS-]_{mon}$ and $[DP+]_{mon}$, respectively. $[DS-]_{mon}$ and $[DP+]_{mon}$ are equal to [DS-] and [DP+], respectively.

EXPERIMENTAL WORK

In the experimental studies, both an SDS and a DPC slug were sequentially injected into the column. The purpose of these experiments was to form precipitate in the column and, therefore, reduce the column's permeability.

In all of the experiments, the column was dry packed with alpha aluminum oxide and equilibrated with 0.15 M brine at a pH of 5.2. The equilibration was stopped when the effluent pH was the same as the injected pH. To keep the air out of the injected solution, the solution was kept under a nitrogen environment. The effluent pH was measured using nitrogen, also.

In all cases, pH was adjusted using 0.01 and 0.1 N NaOH and HCl (Fisher Scientific) and it was measured by a Jenson pH meter and electrode (Jenson Products #R-6102A and #R-830B, respectively). The solvent for all of the surfactant solutions was a 0.15 M brine (NaCl, Fisher #S-271). The water was distilled and deionized.

In all of the experiments, SDS (Fisher #O-2674) was used as received. DPC (Pfaltz and Bauer #D 56650) was recrystallized four times from a mixture of petroleum ether and ethanol and was dried under vacuum for 72 hours before use.

In all of the experiments, the order of injection of solutions into the column was as follows, (1) SDS slug, (2) brine spacer, (3) DPC slug, (4) final brine solution. In all of the experiments, before a new solution was injected into the column, all of the remaining previous solution was flushed out of the tubes connecting the injection solution container to the column's inlet.

The solutions were pumped through the column using a constant flow rate pump with fluctuation in flow of less than

5%. The pressure drop across the column was measured using a pressure gauge. The pressure drop across the packing during the column equilibration was taken as the initial pressure. At the end of step 4, final brine injection, the pressure drop across the packing was measured again and it was taken as the final pressure drop, but usually, at the end of step 3, the DPC injection step, a new pressure drop across the packing stabilized and did not change. Any increase in the final pressure drop from the initial pressure drop was attributed to the formation of precipitate within the column. In all of the experiments, the effluent was collected in a fraction collector and later was analyzed.

In total, six experiments were performed and all of them were done at a pH of 5.2. The column was packed with low surface area aluminum oxide (Alpha Products #87354). In experiments 1, 2, 3, and 4, a 10mm x 25mm column (Alltech #9033D) was used and in experiments 5 and 6 a 6mm x 25mm column (Rainin #252-00) was used.

In experiments 1 through 5, a 0-30 psig pressure gauge (Cole Parmer #T-7380-22) was used. In experiment number 6 a 0-600 psig pressure gauge (Rainin #38-057) was used to measure the pressure drop across the packing.

Surfactant Analysis

SDS was analyzed using high-pressure liquid chromatography. The SDS solution containing NaCl was injected into a stainless steel column packed with C_{18}, polymeric silica gel (Alltech # 8251) and the effluent was analyzed by a conductivity detector (Wescan #213-505). The results were relayed to the integrator (Varian #4270) and it was recorded as peak heights or areas. The silica gel separated the SDS from NaCl and two separate peaks; one for each them was recorded by the integrator.

The peak heights for a set of SDS standards was found. A straight line was drawn through the plot of standard's concentration versus peak height and this plot was used to calculate the samples' SDS concentration knowing its peak height. Each sample, as well as standards, were injected

into the column more than once; usually, three times.

DPC was analyzed using a UV spectrophotometer (Bausch and Lomb 1001 Spectronic). The absorbence of the DPC pyridinium ring was measured at the wavelength of 260.1 nm. At this wavelength, the SDS and NaCl interference is negligible. Absorbence of a set of DPC standards was also measured and it was used to calculate the DPC concentrations in the solution knowing their absorbence. At DPC concentrations less than 200 micromolar and more than 10 micromolar, the plot of standard concentration versus absorbence is linear. All samples were diluted down into this concentration range.

RESULTS AND DISCUSSION

1 Experimental Results

The purpose of this section is to present and discuss the results of the experiments of formation of precipitate and coacervate in the column. As mentioned the order of the injection of the solutions into the column in these experiments was as follows: (1) The SDS solution, (2) the brine spacer, (3) the DPC solution, and (4) the final brine solution.

In tables 1 and 2, experimental data for experiments 1 through 6 are tabulated. Shown in the following figures, figures 1 through 6, are the plots of the concentrations of SDS and DPC in the effluent versus the cumulative pore volumes injected (pore volumes of SDS, brine spacer, DPC, and the final brine solution, respectively) for each of the mentioned six experiments. In figures 1 through 6, the zero in the abscissa (the pore volumes injected) marks the beginning of the injection of SDS and the end of the abscissa marks the end of step 4, injection of final brine solution.

Using SDS and CPC as the surfactant pair, Arshad (5) performed experiments similar to experiments 1 through 6. Arshad (5), in some cases, was able to reduce the column's permeability by more than 30% using smaller concentrations of SDS and CPC than the SDS and DPC concentrations used in experiment 13. CPC has a higher molecular weight than DPC,

and it reacts with SDS to form larger precipitate particles. SDS-CPC precipitate particles are larger than the SDS-DPC precipitate particles, so, smaller concentrations of SDS and CPC are necessary to cause the same permeability reduction.

In all of the experiments except experiment 6, a long tail of SDS and DPC were seen in the effluent (look at figures 1 through 5. In experiment 6 not enough brine in the fourth step was injected for the long tail of SDS and DPC seen in other experiments to show up in the effluent. It was not possible to measure the concentration of SDS in the mentioned tail accurately using available analysis techniques; but the concentration of DPC was measured to be 14 micromolar. A long tail of SDS or DPC can not be seen in any of the SDS or DPC breakthrough curves shown in the previous section. The tail of SDS and DPC seen in the effluent is due to precipitate dissolving. Using the value of K_{sp} at room temperature, the theory predicts that the concentrations of the SDS and the DPC coming out of the column when the precipitate is dissolving should be 14 micromolar. (In the next section, it will be shown that the model developed in chapter 3 predicts the long tail seen in the effluent and it predicts that the concentration of SDS and DPC in the tail should be 14 micromolar).

As mentioned above, the third step in all of the experiments was to inject a DPC slug into the column. In the experiments 2, 3, 5, and 6 (look at figures 2, 3, 5, and 6), no DPC wave came out of the column at the first pore volume. In the experiments, the concentration of DPC in the effluent goes to zero and the only DPC seen coming out of the column is due to precipitate dissolving. This phenomenon can be explained by the fact that the DPC wave catches up with the SDS wave and they react to form precipitate. Since all the DPC reacts with the SDS, the otherwise expected DPC wave disappears and the only DPC coming out of the column is due to precipitate dissolving.

It was believed that if precipitate has formed in the column, then the amount of SDS and DPC remaining in the column just before the precipitate started to dissolve should be equal. In the experiments 1, 2, and 4, the amount of SDS and DPC remaining in the column just before the long tail of

SDS and DPC appeared in the effluent were calculated (look at table 3). In each of these experiments, the amount of SDS and DPC remaining in the column was calculated by finding the amount of SDS and DPC that have come out the column before the precipitate started to dissolve and subtracting it from the total amount of SDS and DPC injected. To find out the total amount of SDS and DPC that have come out of the column, the area under the plots of concentrations of SDS and DPC versus the pore volumes injected in figures 1, 2, and 4 were graphically integrated. The calculated amount of the SDS and DPC remaining in the column just before the long tail of surfactants was seen in the effluent for experiments 2 and 4 are very close; suggesting that the SDS and DPC have formed precipitate. But, the calculated amount of SDS and DPC remaining in the column for experiment 1 are not as close as in experiment 2 or 4. There is probably some error involved in graphically estimating the amount of SDS and DPC that have come out of the column. In experiment 1, the injected concentrations of SDS and DPC were less than the injected SDS and DPC concentrations in experiments 2 and 4. So, the error has a more significant effect on the final calculated results in experiment 1 than experiments 2 and 4.

In the plot shown in figure 4, there are two SDS peaks which are split by a DPC peak. Notice that at the center of the DPC peak, the SDS concentration is at its minimum value for anywhere in the plot. In the next section, it will be explained why the concentration of SDS should go to a minimum when the concentration of DPC is at the maximum. Precipitate was seen in the effluent in experiment 4 at close to "pore volumes injected" equal to 4. There can only be two reasons for the presence of precipitate in the effluent: (1) Reaction between the SDS and the DPC is not instantaneous. (2) Precipitate move through the column.

All the mentioned aspects of the plots shown in figures 1 through 5, except the fact that any precipitate would be seen in the effluent, are predicted by the model developed previously. The mentioned aspects are: (1) In experiments 1 through 5, a long tail of SDS and DPC was seen in the effluent. (2) in experiments 2, 3, and 4, no DPC comes out of the column except for precipitate dissolving. (3) When the concentration of DPC goes to a maximum, the concentration of

SDS goes to a minimum (look at figure 4) and visa versa.

2 Theoretical Modeling

In this section, experimental results will be compared to the theoretical results obtained using the model developed previously. Theoretical data used to generate the plots shown in figures 7 through 12 is as follows: $[SDS]_{inj}$=2490 micromolar, $[DPC]_{inj}$=2980 micromolar, SDS slug=1.38 pore volumes, DPC slug=0.53 pore volume, and brine spacer=0.13 pore volume.

Figures 7 through 9 show the effluent profiles of SDS and DPC as SDS adsorption, u_{ds}, increases. As can be seen from figures 7 through 9, as u_{ds} is increased, the DPC concentration band gets smaller and it eventually disappears. As u_{ds} is increased, the SDS waves move slower and slower through the column. So, there is more time for the DPC wave to catch up with the SDS wave. Eventually, the SDS wave moves so slow that even the back of the DPC concentration band catches up with the SDS wave and it reacts with SDS to form precipitate. The same thing happens in experiments 2,3,5, and 6. In these experiments, the DPC wave disappears. The disappearance of the DPC concentration band in the experiments is due to all the DPC reacting with SDS and forming precipitate within the column. In figures 7 through 9, just to show that it is possible for the expected DPC wave to disappear, u_{ds} was increased while every other parameter was kept a constant. It is also possible to cause the DPC concentration band to disappear by keeping u_{ds} a constant and changing one or combination of other parameters. Except for u_{ds}, the other parameters that could have been changed to cause the DPC concentration band to disappear are the amount brine spacer injected, injected concentrations of SDS and DPC, and the amount of the SDS and DPC slugs injected.

A long tail of SDS and DPC is seen in the effluent profiles shown in figures 7 through 9. The concentrations of SDS and DPC in the tail of the effluent profiles shown in figures 7 through 9 are 14 micromolar. The concentrations of SDS and DPC in the effluent have to satisfy the following constraint:

$$[DP+].[DS-] < k_{sp}/f^2 \qquad [33]$$

where

$k_{sp}=115\ (M)^2$ at $T=25^{o}C$ (room temperature)

$f=0.758$

For a 0.15 M NaCl solution [DP+] and [DS-] are the concentrations of DPC and SDS in the solution. In the fourth step of the experiments (brine injection), precipitate starts dissolving from the beginning of the column. Due to the values of K_{sp} and f at $T=25^{o}C$, the model predicts that the concentrations of SDS and DPC in the effluent when the precipitate is dissolving have to be equal to 14 micromolar. In experiments 1 through 5 (previous section), the concentration of DPC in the tail was measured to be 14 micromolar.

Equation 33 can easily explain the SDS and DPC effluent profiles shown in figure 4, experiment 4. In the effluent profiles shown in figure 4, when the concentration of DPC in the DPC band is at the maximum, the concentration of SDS is at the minimum. This is to satisfy the equality in the equation 33.

Shown in figures 2 through 4 are the concentrations of SDS, DPC, and precipitate within the column at "pore volumes injected" equal to 2.8 and different values of u_{ds}. As can be seen from the concentration profiles in the mentioned figures, as the value of u_{ds} increases, the average amount of precipitate formed in the column increases as well. Increasing the value of u_{ds} means the amount of adsorbed SDS in equilibrium with the same concentration of SDS monomer in the solution has increased. Since the SDS monomer is in equilibrium with the adsorbed SDS, any reduction in the concentration of SDS monomer in the solution due to the reaction causes the adsorbed SDS monomer to desorb, and they in turn react with the DPC monomer. So, the total amount of precipitate formed at any point in the column is dependent on the total amount of SDS present, both in the solution and adsorbed. By increasing the value of u_{ds}, not only does the SDS wave slow down to allow the DPC wave to completely react with it but, also, the increase in the value of u_{ds} causes the amount of precipitate formed at any point in the column

to increase, as well. Unfortunately, increasing the value of u_{ds} causes an increase in the spreading of the SDS wave, also.

The model also predicts that it is possible to control where in the column the precipitate forms by varying the amount of the brine spacer injected between the SDS and the DPC slugs. Shown in figure 13 is the plot of concentrations of SDS, DPC, and precipitate versus dimensionless length at "pore volumes injected" equal to 2.8. The only difference between the data used to generate the plots shown in figures 13 and 10 is the value of the brine spacer. The values of the brine spacer used to generate the plots shown in figures 13 and 10 are 0.62 and 0.13 pore volumes, respectively. In figure 13, concentration of precipitate in the first half of the column is zero. In figure 10, the amount of brine spacer is smaller, and concentration of precipitate in the first half of the column is not zero. By comparing the concentrations of precipitate in both the plots shown in these figures, it can be concluded that the greater the amount of the brine spacer injected, the further away from the beginning of the column the precipitate forms.

CONCLUSIONS

1. When SDS and DPC are injected into a packed column, they react and form precipitate.

2. Only at very high injected SDS and DPC concentrations is there a significant reduction in permeability.

3. With the exception of seeing precipitate in the column effluent, every other aspect of the experimental SDS and DPC effluent profiles is predicted by the theoretical model.

4. Anionic-cationic surfactants with high molecular weights form larger precipitate particles, and cause greater reductions in permeability.

5. The model predicts that the average amount of precipitate formed within the column increases with an

increase in the adsorption of the first surfactant by the mineral oxide. Increasing adsorption causes an increase in the spreading of the surfactant concentration wave also.

REFERENCES

1. Walsh, M.P.; Bryant, S.L.; Schechter, R.S.; Lake, L.W. AIChE J. 1984, No. 2, 30, (3), 317.

2. Bryant, S.L.; Schechter, R.S.; Lake, L.W. AIChE J. 1986, No. 5, 32, (5), 751.

3. Anderson, D.A.; Tannehill, J.C.; Pletch, R.H. "Computational Fluid Mechanics and Heat Transfer"; McGraw-Hill: New York, 1984.

4. Stellner, K.L.; Amante, J.C.; Scamehorn, J.F.; Harwell, J.H. "Precipitation Phenomena in Mixtures of Anionic and Cationic Surfactants in Aqueous Solution", J.Colloid Interface Sci., In press.

5. Arshad,A. "Improving sweep efficiency in oil reservoirs using surfactant phase separation",M.S. Thesis, University of Oklahoma, 1985.

Table 1. Experimental Data for Experiments 1 Through 3

	Experiment#		
	1	2	3
$[SDS]_{inj}$ (M)	310	2490	9000
$[DPC]_{inj}$ (M)	1200	2980	10000
SDS Slug (pv)	1.61	1.38	2.86
DPC Slug (pv)	0.68	0.53	0.65
Brine Spacer (pv)	0.31	0.13	0.17
Velocity (ft/day)	6	12	12
Initial Permeability (md)	217	197	172
Final Permeability (md)	210	188	151
Porosity	0.84	0.84	0.84

Table 2. Experimental Data for Experiments 4 Through 6

	Experiment#		
	4	5	6
$[SDS]_{inj}$ (M)	20000	2000	2000
$[DPC]_{inj}$ (M)	40000	400	400
SDS Slug (pv)	1.51	9.2	28
DPC Slug (pv)	0.62	1.1	1.3
Brine Spacer (pv)	0.23	0.17	0.19
Velocity (ft/day)	12	17	17
Initial Permeability (md)	157	125	11
Final Permeability (md)	105	120	8
Porosity	0.83	0.83	0.83

Table 3. Amount of SDS and DPC Remaining in the Column at a Certain Pore Volumes Injected for Experiments 1, 2, and 4.

Experiment # 1:

Amount of SDS remaining in
the column (at pv injected=4.1) = 5 Mole

Amount of DPC remaining in
the column (at pv injected=4.1) = 4 Mole

Experiment # 2:

Amount of SDS remaining in
the column (at pv injected=20) = 21 Mole

Amount of DPC remaining in
the column (at pv injected=20) = 21 Mole

Experiment # 3:

Amount of SDS remaining in
the column (at pv injected=17) = 431 Mole

Amount of DPC remaining in
the column (at pv injected=17) = 420 Mole

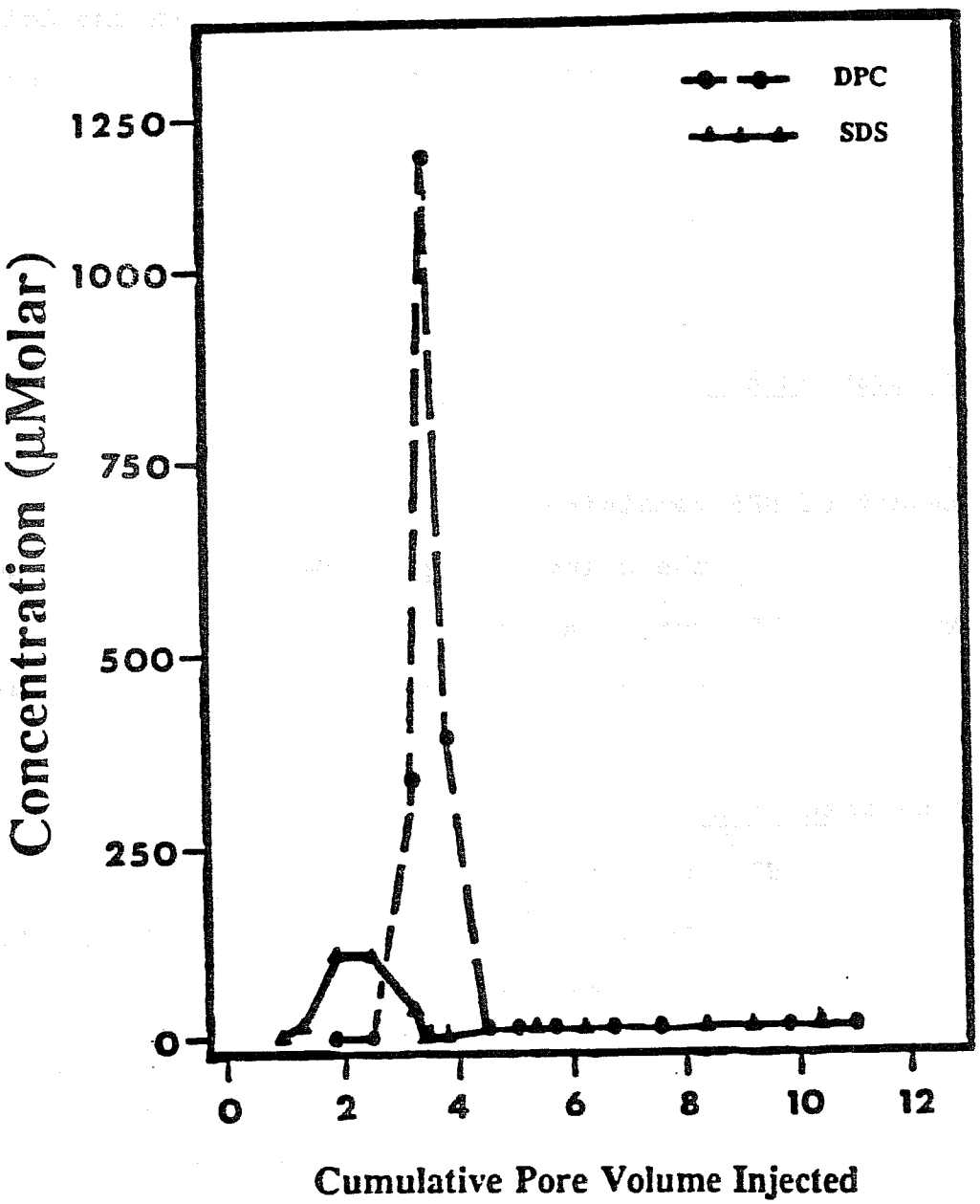

Figure 1 SDS and DPC Effluent Profiles (Experiment 1).

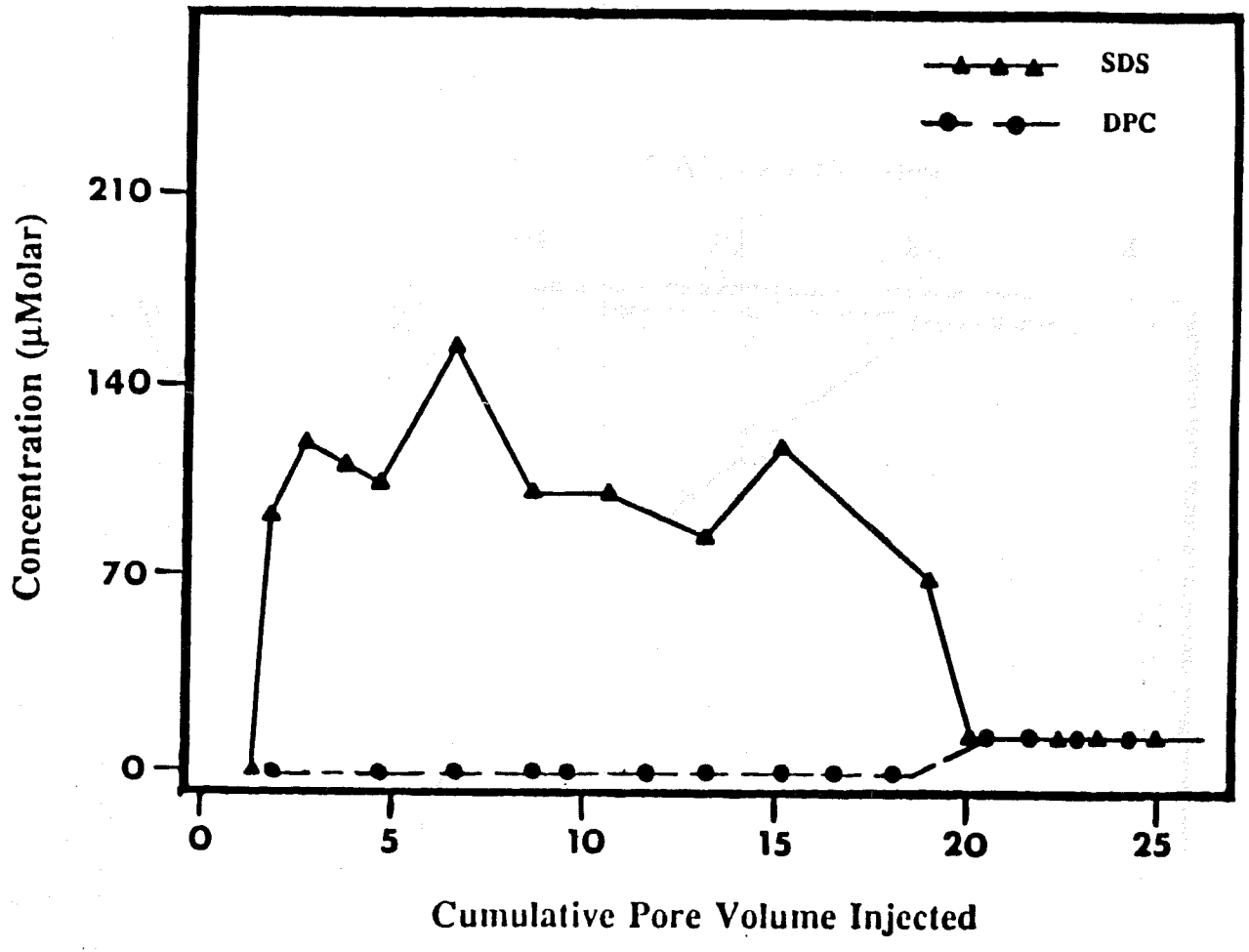

Figure 2. SDS and DPC Effluent Profiles (Experiment 2).

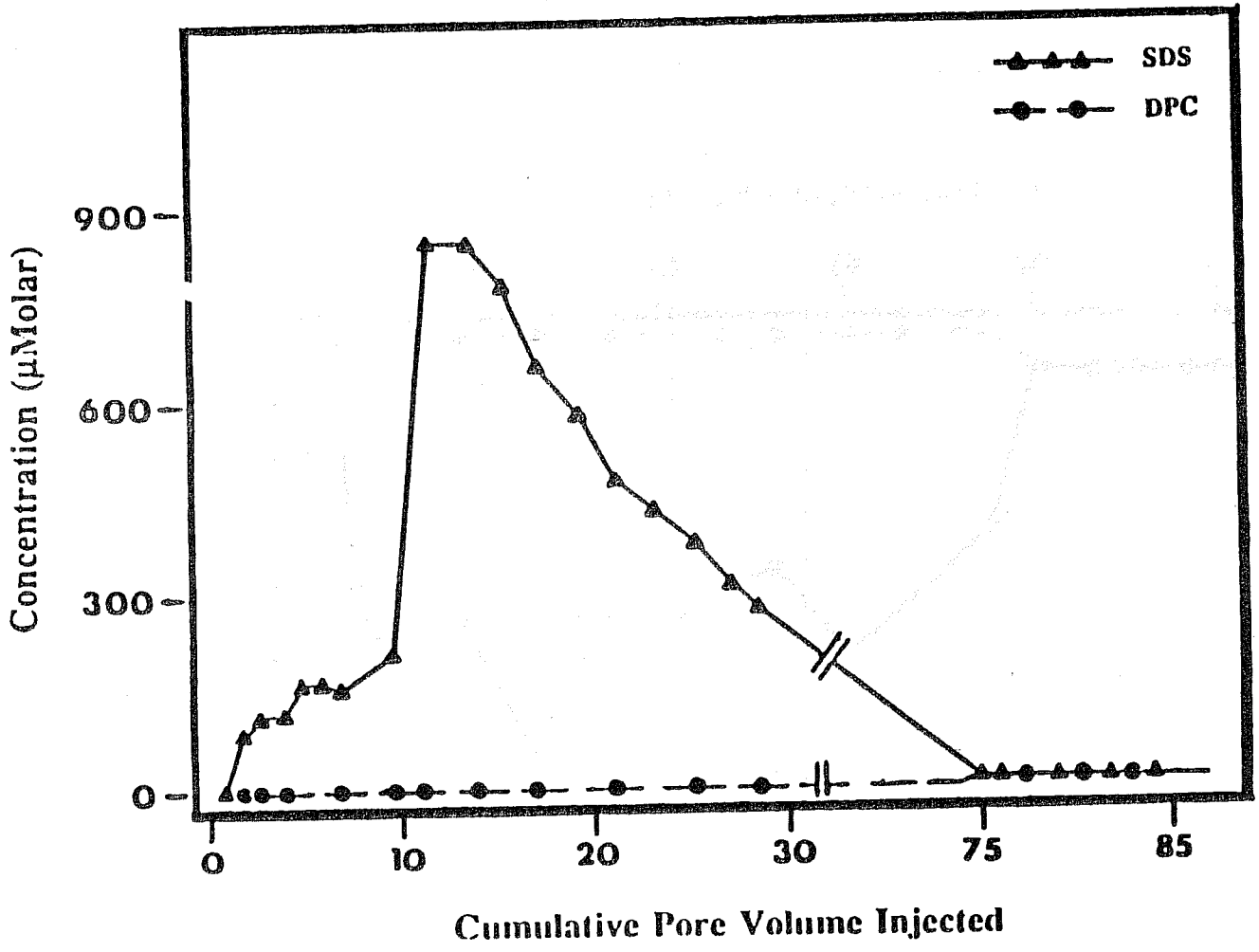

Figure 3 SDS and DPC Effluent Profiles (Experiment 3).

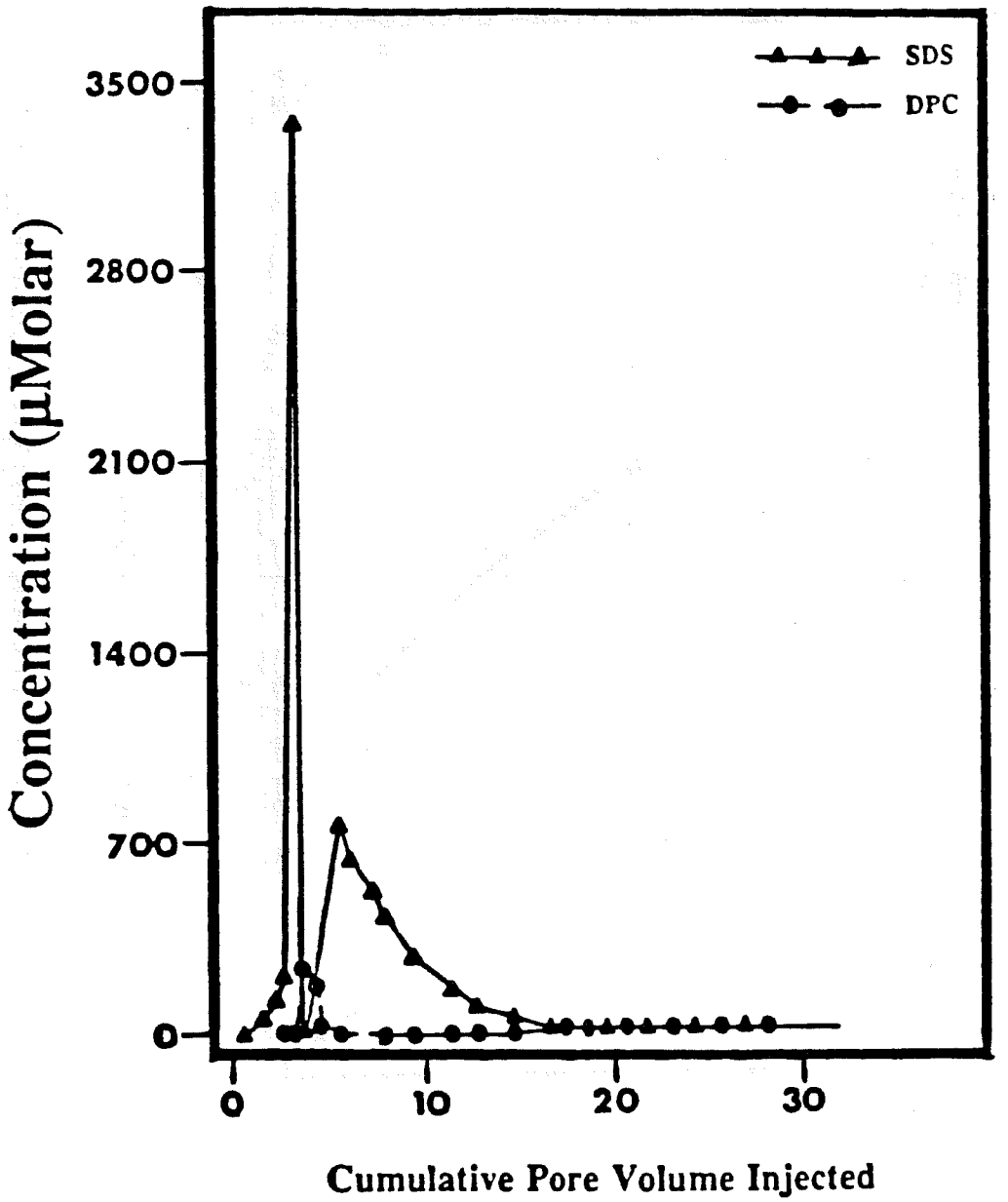

Figure 4 SDS and DPC Effluent Profiles (Experiment 4).

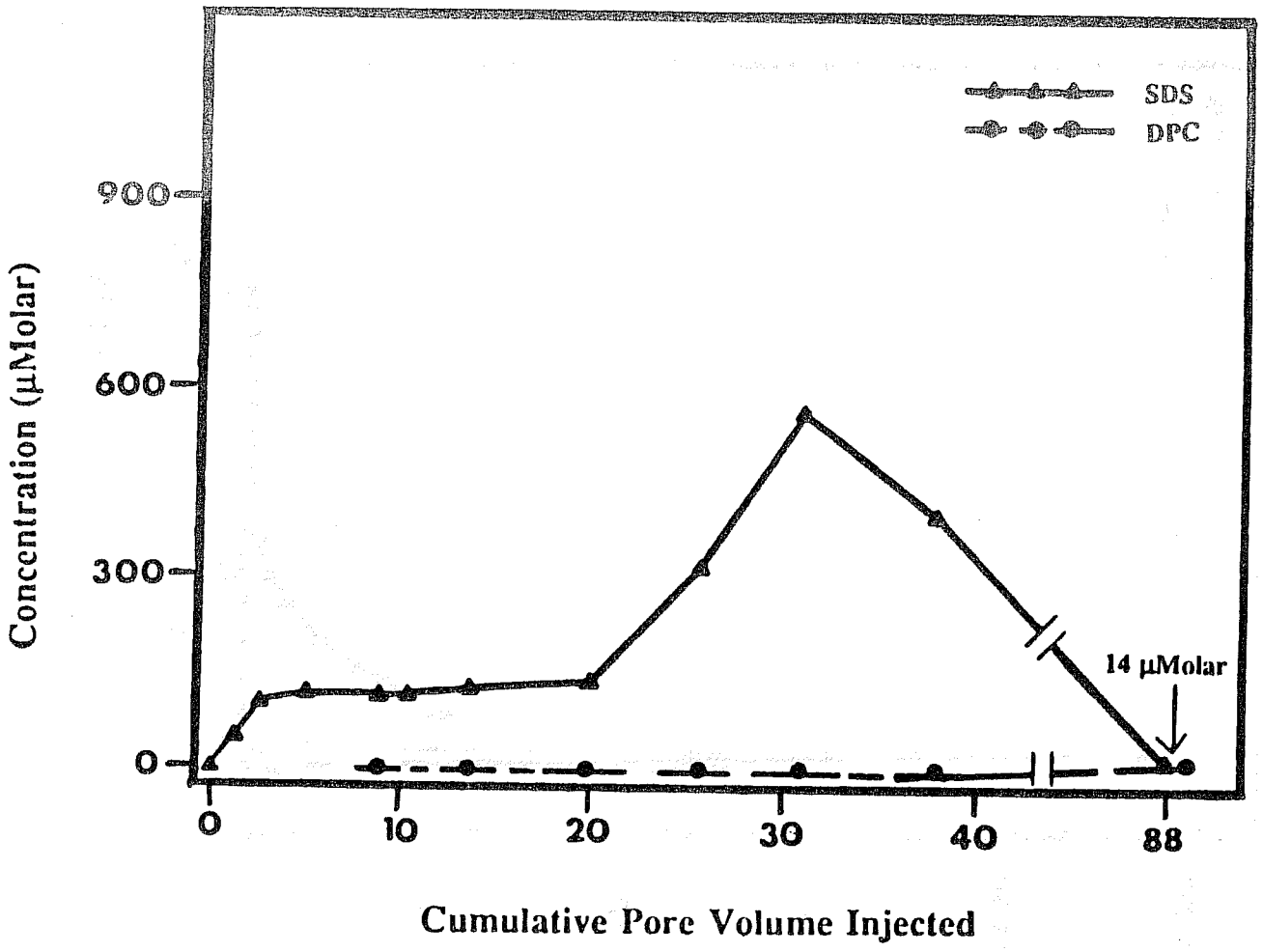

Figure 5 SDS and DPC Effluent Profiles (Experiment 5).

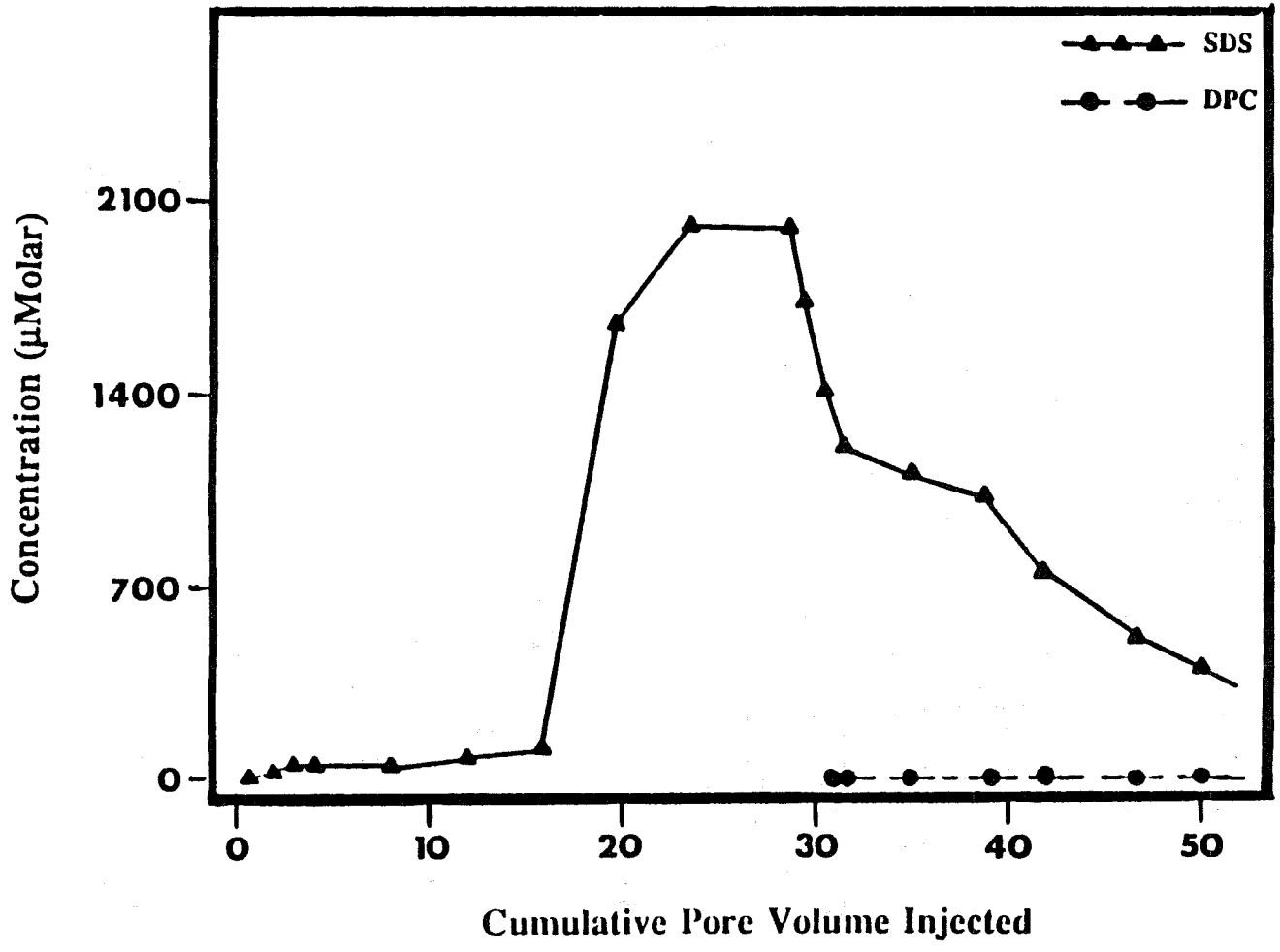

Figure 6 SDS and DPC Effluent Profiles (Experiment 6).

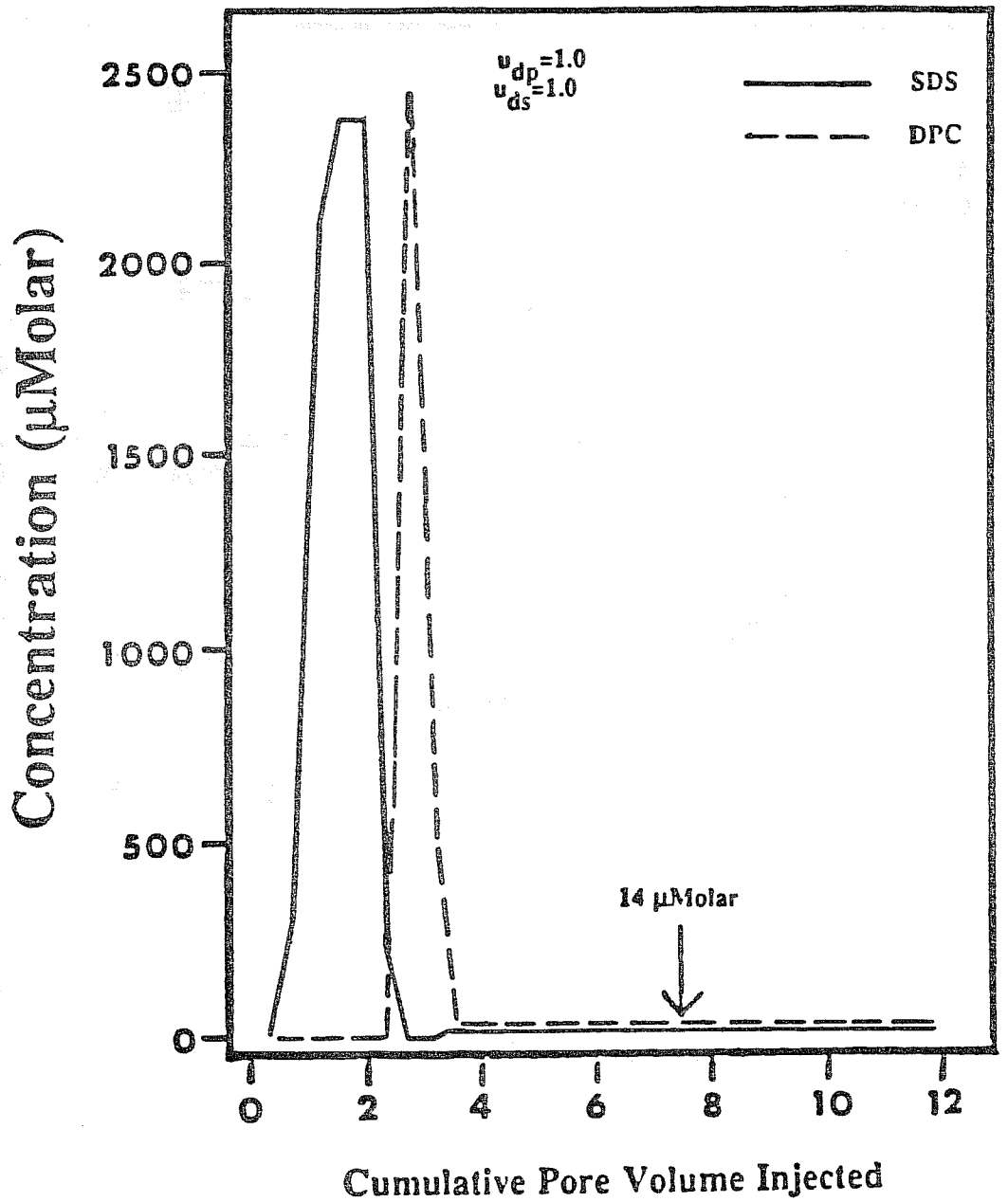

Figure 7 SDS and DPC Effluent Profiles.

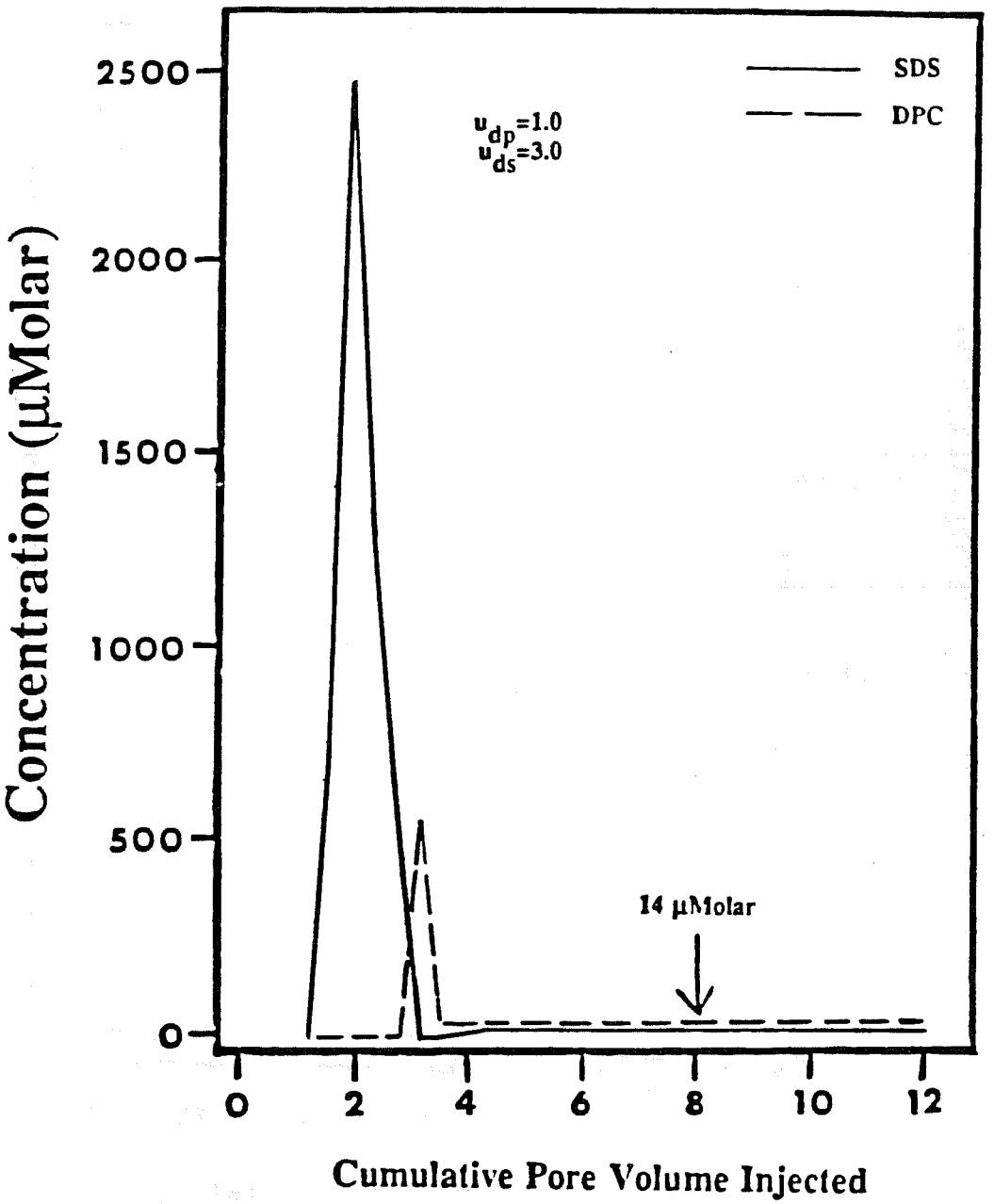

Figure 8 SDS and DPC Effluent Profiles.

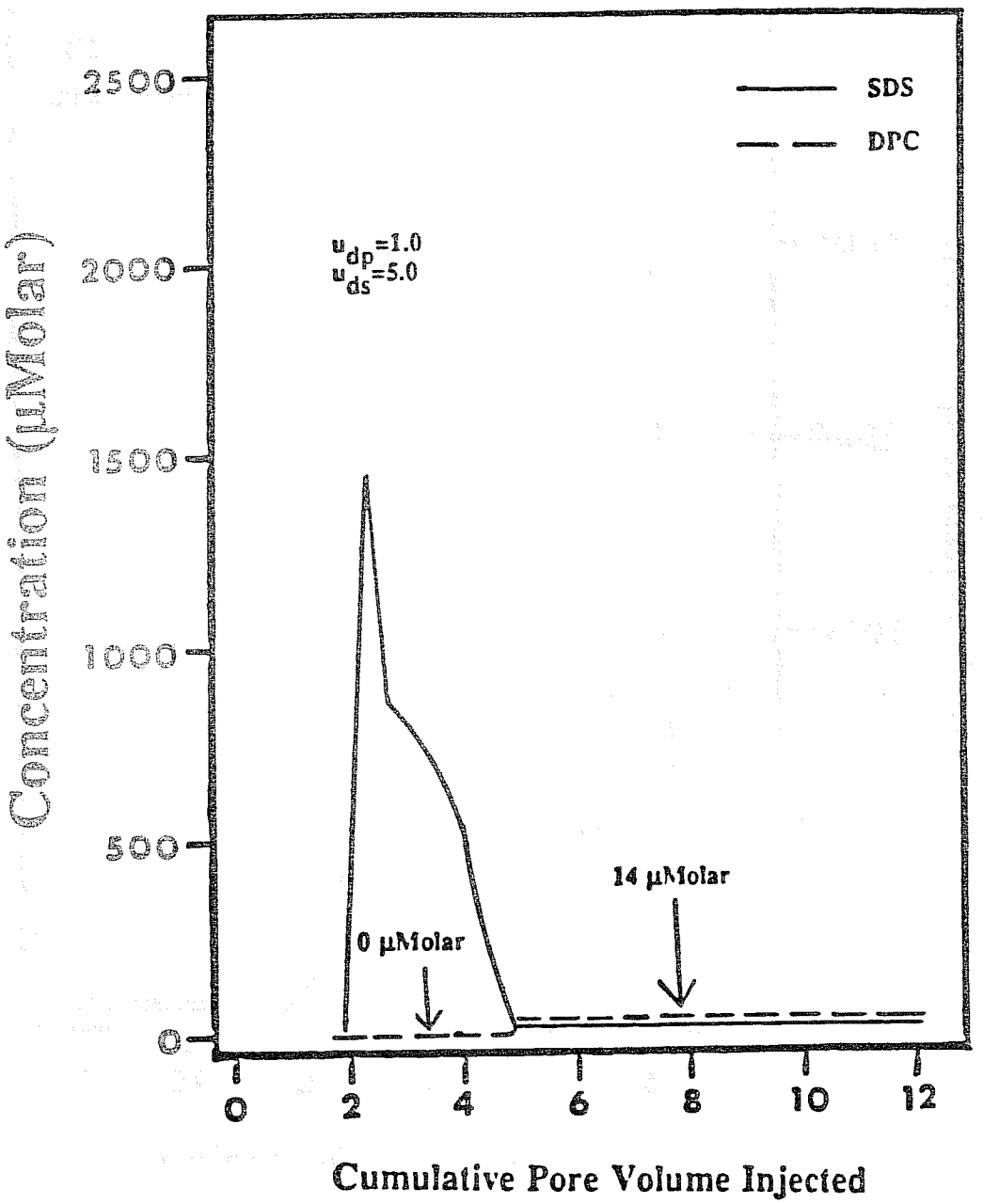

Figure 9 SDS and DPC Effluent Profiles.

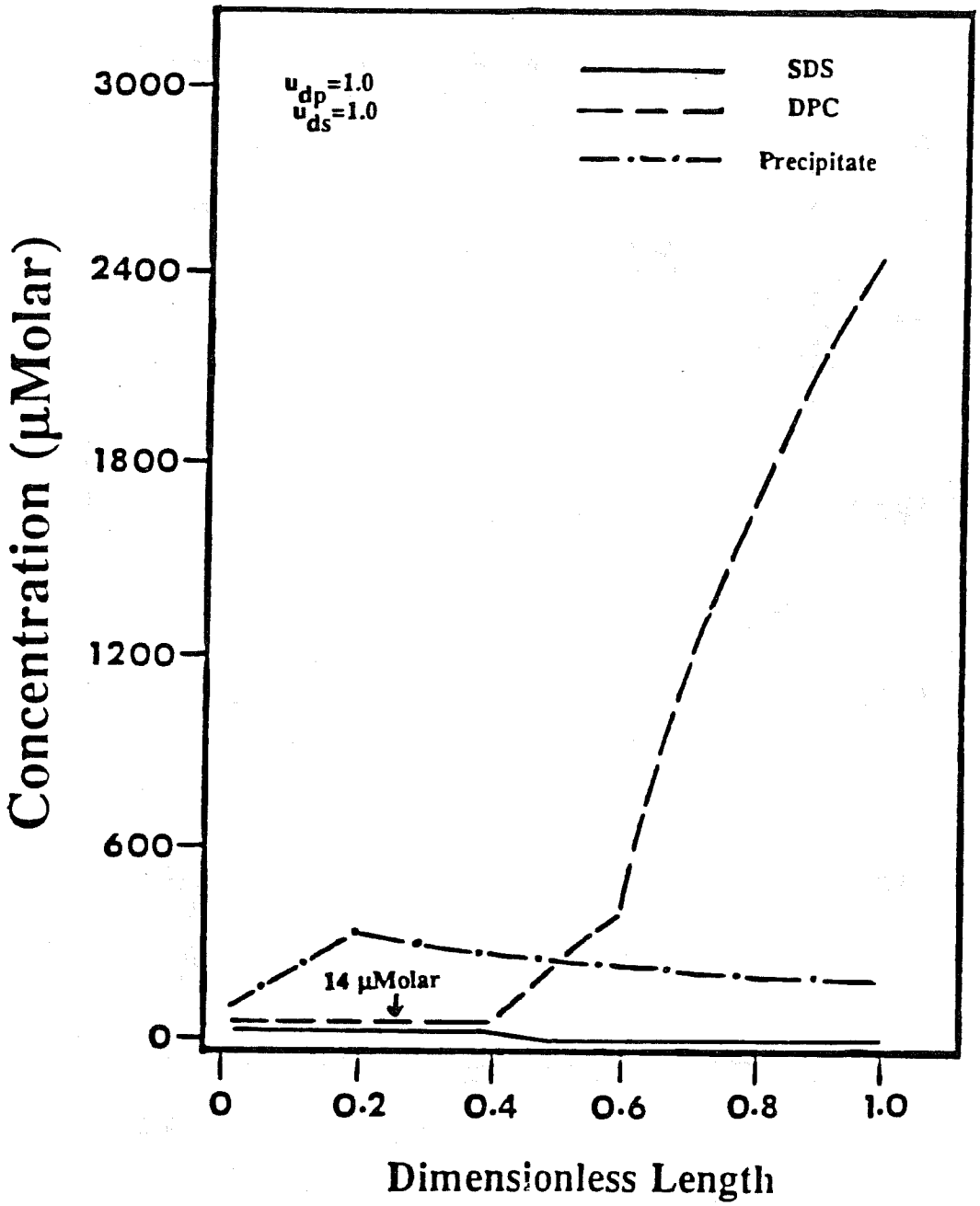

Figure 10 SDS, DPC, and Precipitate Concentration Profiles Within the Column (Pore Volumes Injected = 2.8).

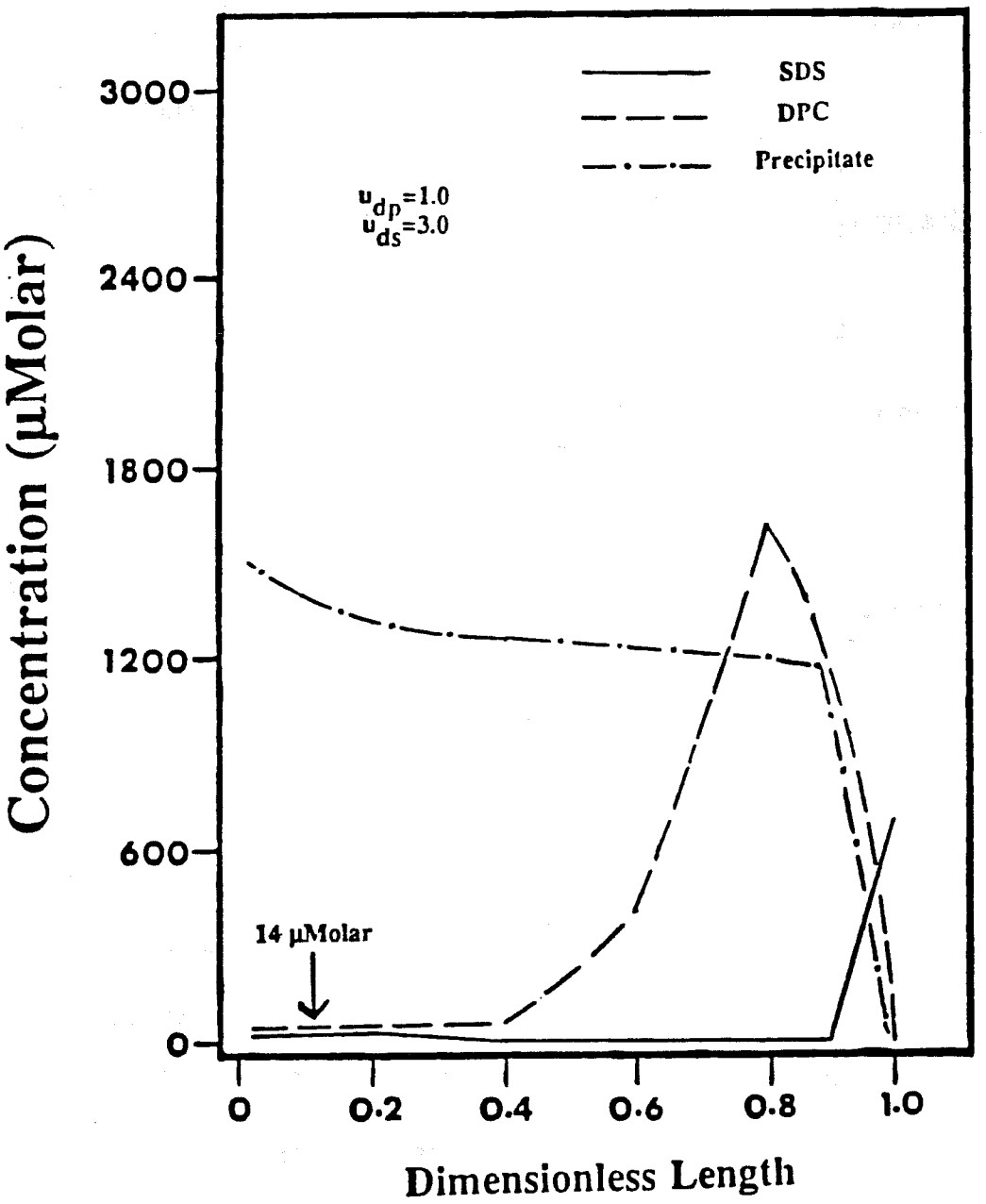

Figure 11 SDS, DPC, and Precipitate Concentration Profiles Within the Column (Pore Volumes Injected = 2.8).

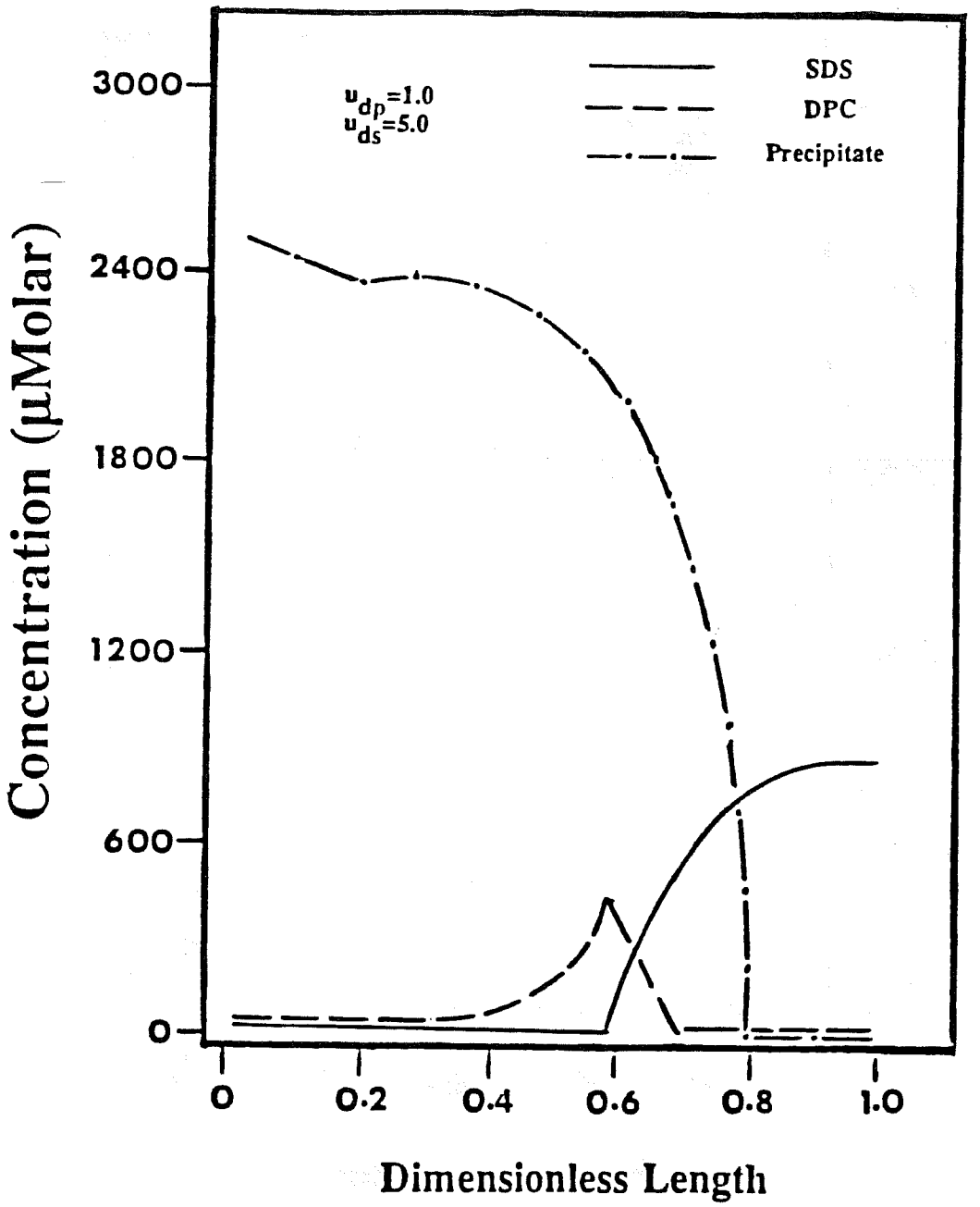

Figure 12 SDS, DPC, and Precipitate Concentration Profiles Within the Column (Pore Volumes Injected =2.8).

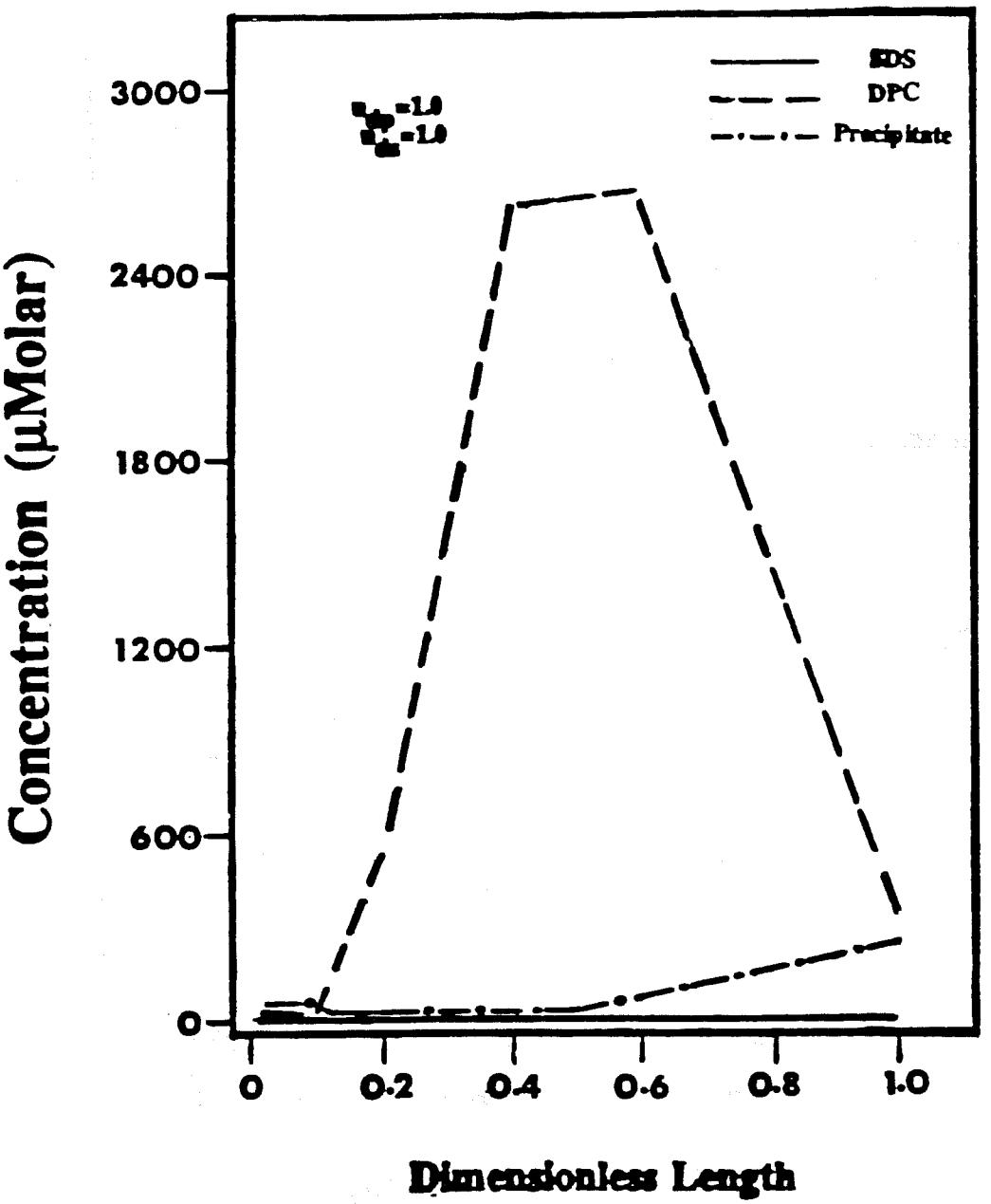

Figure 13 SDS, DPC, and Precipitate Concentration Profiles Within the Column (Pore Volumes Injected = 2.8).

CHAPTER 5

SIMULATION OF ENHANCED OIL RECOVERY BY SURFACTANT ENHANCED VOLUMETRIC SWEEP EFFICIENCY

ABSTRACT

A critical requirement in evaluating the technical feasibility of the process is the development of a mathematical simulation which is presented here. Case studies are presented which address different types of heterogeneous reservoirs. These studies examine the effectiveness of the plugs in enhancing the net oil recovery, so that types of reservoirs which are potential candidates for the process may be delineated.

INTRODUCTION

In this chapter, the development of a mathematical model to describe the proposed enhanced oil recovery process is described. The model will simulate a conventional waterflooding operation; the new process has been superimposed on the waterflooding model. The model will encompass the following; two-phase flow with oil mobilization by water displacement, the chromatographic movement of separately injected slugs, allowance for an arbitrary description of absolute permeability variation (directional dependence of permeability is allowed),and accounting for plug formation and permeability reduction upon phase separation.

The main physical assumptions made in the model are:

1. All fluids are incompressible.

2. Local phase equilibrium is assumed throughout.

3. No volume change occurs in the aqueous phase upon mixing or precipitate formation.

4. There are no important effects due to diffusion.

5. There is no partitioning of surfactant into the oleic phase.

6. "Trogus" type surfactant adsorption will apply.

7. The effects of gravity forces may be neglected (choose oil and water to be of equal density.)

8. The effects of capillary forces may be neglected.

9. Darcy's law applies.

10. The surfactant components react instantaneously and irreversibly to form a pore blocking phase so that reaction occurs at a single interface, and this leads to a fixed local permeability reduction.

The model is probably the first of its kind in applying the theory of "coherence" [1,2] to the waterflood and chemical flood of a black-oil reservoir. It allows the use of timesteps several orders of magnitude greater than those used in traditional finite difference models, whilst promoting the same accuracy and stability. The solution method allows the direct representation of water saturation distributions in terms of contour diagrams, and the edges of injected chemical slugs can be defined.It is also possible to define the edges of low permeability plugs.

DEVELOPMENT OF MODEL EQUATIONS

If a material balance for a surfactant component i is considered, it is apparent that:

$$\phi S_w \frac{\partial C_{i,w}}{\partial t} + \rho(1-\phi)\frac{\partial \bar{C}_i}{\partial t} + \phi v_x f_w \frac{\partial C_{i,w}}{\partial x} + \phi v_y f_w \frac{\partial C_{i,w}}{\partial y} = 0 \qquad \text{EQ.1}$$

Similarly, a material balance for incompressible water

yields:

$$\frac{\partial S_w}{\partial t} + v_x \frac{\partial f_w}{\partial x} + v_y \frac{\partial f_w}{\partial y} = 0 \qquad \text{EQ.2}$$

where

ϕ = porosity

S_w = volume fraction of aqueous phase

f_w = fractional flow of aqueous phase

$C_{i,w}$ = concentration of surfactant in aqueous phase, mol/l

$\overline{C_i}$ = concentration of adsorbed surfactant i in solid phase, mol/g

ρ = density of solid phase, g/l

$\vec{v}$ = interstitial fluid velocity vector

Equations 1 and 2 are first order hyperbolic partial differential equations and are amenable to a characteristic solution. A characteristic solution is one which tracks the movement of certain values of the dependent variables. It is easy to show that if a set of observation points is moved through the reservoir at a velocity given by the following:

$$\vec{V} = \vec{v} \frac{df_w}{df_w} \qquad \text{EQ.3}$$

then a constant "characteristic" water saturation will be observed. Similarly, the characteristic velocity for a given surfactant concentration (without coincidence of more than one component at a given place) is:

$$\vec{V} = \vec{v}\phi \frac{f_w}{\phi S_w + \rho(1-\phi)\frac{d\bar{C}_i}{dC_{i,w}}} \qquad \text{EQ. 4}$$

This "characteristic" approach can be extended to encompass binary interactive adsorption using the theory of "coherence", although this is not fully described here. It is known that surfactant solution compositions within chromatographic waves tend towards a form of propagational stability [3,4]. Such compositions remain intact within the wave and are termed "coherent." Their movement can be tracked.

In order to simulate the flow-field, we use Darcy's law for a multiphase system:

$$v_x = -K_{abs_x}\left[\sum_j \frac{kr_j}{\mu_j}\right]\frac{\partial p}{\partial x} \qquad \text{EQ. 5 \& 6}$$

$$v_y = -K_{abs_y}\left[\sum_j \frac{kr_j}{\mu_j}\right]\frac{\partial p}{\partial y}$$

Finally, the continuity condition requires that

$$\frac{\partial v_x}{\partial x} + \frac{\partial v_y}{\partial y} = 0 \qquad \text{EQ. 7}$$

Let

$$k_{eff_x} = -K_{abs_x}\left[\sum_j \frac{kr_j}{\mu_j}\right]$$

so that equations 5,6 and 7 give

$$\frac{\partial}{\partial x}\left[k_{eff_x}\frac{\partial p}{\partial x}\right] + \frac{\partial}{\partial y}\left[k_{eff_y}\frac{\partial p}{\partial y}\right] = 0 \qquad \text{EQ. 8}$$

For two surfactant components, and two phases, six equations in six unknowns are obtained:

$$S_w, C_{1,w}, C_{2,w}, v_x, v_y, p.$$

Relative permeability relations are based on simple power law models[5] involving water saturation, initial water saturation and capillary "trapped" oil saturation. Fractional flow relations as functions of phase saturations are then derived from the relative permeability expressions. The fractional flow curve for water is given in figure 1.

SOLUTION OF THE MODEL EQUATIONS

The simulation proceeds in several sequential stages.

a)

Using the values of water saturation at every grid point to calculate the effective permeabilities, the pressure equation is solved by using the usual finite difference discretization on a grid. The reservoir permeabilities for each grid point represent an average value. The solution method is direct, and proceeds by writing the finite difference equations and boundary conditions at every point. The resulting set of linear equations is then solved by an efficient banded structure Gaussian elimination. This method is extremely fast compared to Gauss-Seidel iteration, especially for long reservoirs. The interstitial fluid velocities are now calculated from equations 5 and 6.

b)

Curves of characteristic points, each curve representing a particular water saturation S_w, are now moved through the reservoir at a velocity given by equation 3. This is achieved using a fourth order Runge-Kutta method, where the interstitial velocities vary linearly in-between grid points.

c)

The value of the water saturation is now found at every grid point by interpolation from the positions of the characteristic curves. Linear interpolation is used for the interpolation scheme. The interpolation scheme will allow for arbitrary characteristic curve shapes, and is equivalent to finding spot high values from a "contour" map.

d)

Characteristic curves representing the chromatographic movement of injected surfactant slugs are moved through the reservoir according to equation 5 and analogous versions for the case of chromatographic " shock waves." Three such curves are associated with describing the chromatographic movement of each surfactant slug[4].

e)

Finally, a check is made of whether the leading edge of the second injected surfactant slug has overtaken the trailing edge of the first injected slug. The curve along which the two slugs first overlap represents the origin of a "reaction interface" which can be shown by material balance to move at a velocity given by:

$$\vec{V} = \frac{\vec{v}\phi f_w}{\phi S_w + \rho(1-\phi)\left[\frac{\Gamma_{CMC_1}+\Gamma_{C_{inj_2}}}{CMC_1+C_{inj_2}}\right]} \qquad \text{EQ.9}$$

The areas of the reservoir contacted by this reaction interface then experience a certain reduction in absolute permeability (i.e.plugging.) This permeability reduction factor depends on the ability of the precipitate formed to block the pore throats, and can be controlled to some extent by changing the concentrations at which the slugs interact. The new values for the absolute permeabilities are now calculated on a point by point basis.

Having completed the calculations for a given timestep, the simulation returns to step (a).

The computer code for the simulation consisted of two thousand lines of Fortran 77, and all the calculations were performed on an IBM-PC XT unit.

RESULTS OF CASE STUDIES

In this section, the results of computer simulations of the selective blocking process will be given. In all the simulations, the net pay-thickness of the reservoir was assumed to be 50 feet while the length of the reservoir was either 100 feet (corresponding to a short reservoir) or 5000 feet (corresponding to a long reservoir.) The first injected surfactant was anionic SDS and the second injected surfactant was cationic DPC. Both slugs were injected at a concentration of ten times the CMC. This enables large plugs to be formed from small injected slugs. Relevant data are given in table 1. The reservoir consisted of a narrow, high permeability zone along the center(y=20ft to 30 ft),surrounded by two low permeability zones. The transition in permeability was continuous.

a.Illustration of sweep efficiency.

In order to illustrate the problem of poor sweep efficiency a normal waterflood was simulated in a heterogeneous reservoir. Figure 2 and 3 represent the positions of the water saturation characteristics at an early stage in the flood. It is apparent that the high permeability zone is being depleted of oil at a more rapid rate than the low permeability zone, even for small permeability contrasts.

In figure 3, an order of magnitude difference in permeabilities has led to a large preferential invasion of injected water into the central, high-permeability zone, and this is reflected in the production history in figure 4. In this figure, the volume of oil produced as a result of waterflooding the reservoir is shown.Initially, the recovery of oil is rapid owing to a "piston-like" displacement of oil by the water in the high-permeability zone. However, after this point, injecting large amounts of water into the reservoir results in only an incremental increase in the recovery of oil.

The water to oil ratio in the production well reaches 50 at a point when the recovery of oil from the reservoir is

only 41% of the original oil in place. Furthermore, the flow-rate of displacement fluid through the highly permeable "thief-zone" is over 4 times that through the rest of the reservoir, even though it accounts for only 20% of the reservoir volume.

b.Selectivity of plug growth.

It is important to the feasibility of this process that the formation of low-permeability plugs as a result of surfactant phase separation takes place selectively in the watered out, high-permeability zones. The plugs should not enter zones of high oil saturation or low permeability. In zones where plugging occurs, in depth penetration is desired so that bypassing of fluids around the plug and back into the highly permeable streak is prevented.

As explained before, preferential diversion of injected surfactant should occur into the high-permeability zone. However, once that a low-permeability plug is formed, the flow pattern in the reservoir will begin to alter. Plug formation will have two possible self regulating effects:

(i) It may hinder the further interpenetration of the two surfactant slugs inside the high-permeability zone, hindering further plug development.

(ii) It may cause subsequent diversion of injected fluids into the low-permeability zones, leading to interpenetration of the surfactant slugs there, and blockage of the low-permeability zones.

The injection strategy for the surfactant slugs was chosen so that plug formation began at a fixed point deep inside the high-permeability zone, at a point when the ratio of water to oil produced from this zone exceeded 50.

Figures 5 and 6 represent the successive development of low-permeability plugs in a mildly heterogeneous reservoir.It is apparent in figure 5 that when plug formation is associated with a drastic permeability reduction (100),the selectivity of plug formation for the higher-permeability zone is extremely poor. The plug rapidly begins to bulge outwards into the low-permeability zone, and all zones of the reservoir are equally sealed off to injected fluids. In

figure 6, the permeability reduction factor is chosen to be 2, which is equal to the permeability contrast. In this case, selectivity is improved somewhat, but plug formation in the low permeability zones is still significant. Plug growth occurs somewhat faster in time.

The development of a plug in a strongly heterogeneous reservoir is shown in figure 7 and 8. The permeability contrast is 10 and the permeability reduction was chosen to be 100 and 10 respectively. In this case, the plug selectivity is improved. Since the permeability contrast is much larger, substantial interpenetration of the surfactants can occur before further plug development is hindered by blocking of the high-permeability zone. Several new phenomena are apparent.

1.

The development of a plug which is deep inside the highly permeable zone is associated with the formation of daughter plugs in the low-permeability zones which are very close to the injection well. However, this is found not to have a drastic reduction on injectivity since the fluids move initially into the high-permeability zone and are subsequently diverted into the low- permeability zone. Some reduction in injectivity is observed, once the high - permeability zone is blocked.

2.

After reservoir fluids containing the trailing slug have been forced into the low permeability regions long enough to bypass the plugged region, they return into the high permeability areas where they encounter the leading slug components and result in further blockage of the high permeability regions. This can be seen as the development of "lobes" or "jaws" at the leading edge of the plug in the high permeability zone.

3.

In figure 8, the permeability reduction matches the initial permeability contrast and here the selectivity is very good. The outgrowth of the plug into the low-permeability zone is much reduced compared with figure 7. In figure 9, the high-permeability zone is surrounded by a thin inpermeable layer which prevents flow of fluids across it.

This reduces the side growth of the plug, but the development of the "daughter plugs" is more apparent since fluids cannot enter the unblocked portion of the high permeability zone.

The previous phenomena are apparent in figure 10, where the permeability contrast is now two orders of magnitude. The permeability reduction in this case matches the permeability contrast and selectivity is good. In this case, the low permeability zones have a large c.ntent of residual oil and this prevents plug growth by virtue of high fluid viscosities.

Finally, figure 11 demonstrates the development of a plug in a very long reservoir (5000 feet.) In this case, the effect of bypassing of the plug is severe since the large length to pay-thickness ratio(aspect ratio) causes the flow pattern to adjust rapidly before and after a disturbance caused by blocking of the flow paths. Thus, in this case growth into the high-permeability zones is marked but this is associated with a marked side growth into the low-permeability zones. The plug selectivity quickly becomes very poor compared with figure 7.

c.Flow path diversion.

In figure 12, the effect of forming a small, very-low permeability plug on the flow pattern is shown. The plug is formed ideally inside the high-permeability zone at the point when it is watered out. The arrows on the figure represent the direction and magnitude of the fluid flow, and it can be seen that the low-permeability zone is only swept effectively in the vicinity of the plug. The fluid flow rapidly returns to the high-permeability zone after the plug, and is fully re-established 15% of the reservoir length downstream of the plug. This illustrates the importance of having in-depth penetration of the plugs inside the high-permeability zones.

CONCLUSIONS

I

Large permeability contrasts within an oil reservoir

lead to poor sweep efficiencies in waterflooding operations.

II

The development of low-permeability plugs with the proposed process is self influenced to a large extent. In reservoirs with small permeability contrasts, selectivity of low-permeability plugs for the high-permeability zones is very poor. This may be detrimental when the permeability variation is very gradual.

III

In reservoirs with large and distinct contrasts in permeability, plug selectivity is generally very good. However, it is poorer when the reservoir has a larger aspect ratio, or when the permeability reduction is large compared with the initial permeability contrast.

IV

A mechanism exists whereby new flow paths which form ahead of the plug are sealed off. In order for plugs to effectively improve the sweep efficiency, they must deeply penetrate the high-permeability zones.

REFERENCES

(1) Harwell,J.H., F.G.Helfferich, and R.S.Schecter,"Effect of Mixed Micelle Formation on Chromatographic Movement of Surfactant mixtures,"AICHE J.,28(3),448,1982.

(2) Harwell,J.H., R.S.Schecter, and W.H.Wade, "Surfactant Chromatographic Movement: An Experimental Study," AICHE J.,31(3),415,1985.

(3) Hales,H.B.,"A Reservoir Simulator Based on the Method of Characteristics",SPE 13219,1984.

(4) Arshad,A.,**Improving Sweep Efficiency In Oil Reservoirs Using Surfactant Phase Behavior,"** M.S.Thesis, School of Chemical Engineering and Materials Science, The University of Oklahoma, 1985.

NOMENCLATURE

C_i = concentration of surfactant, mol/l

C_{inj} = injected concentration of surfactant, mol/l

CMC = critical micelle concentration, mol/l

k_{abs} = absolute permeability, md

k_{rj} = relative permeability of phase "j"

p = pressure, psi

t = time, seconds

V_{wave} = wave velocity (ft/s)

x,y = depth, length (ft)

Γ_i = adsorption of component 'i' , mol/g

Γ_{CMC} = adsorption at CMC

μ_j = viscosity of phase 'j' , cp

TABLE 1.

Rock density = 2.65 g/cm^3

Porosity = 0.2

Oil viscosity = 5.0 cp

Water viscosity = 1.0 cp

Injection pressure gradient = 1.5 psi/ft

Fluid densities = 1.0 g/cm^3

Net pay thickness = 50 ft

Length of reservoir = 100 ft or 5000 ft

Trapped oil saturation = 0.2

Initial water saturation = 0.1

Henry's Law constant : DPC = 8.3×10^{-5} liter/g

or : SDS = 2.71×10^{-4} liter/g

CMC values : DPC = 800 micromole/l

or : SDS = 4000 micromole/l

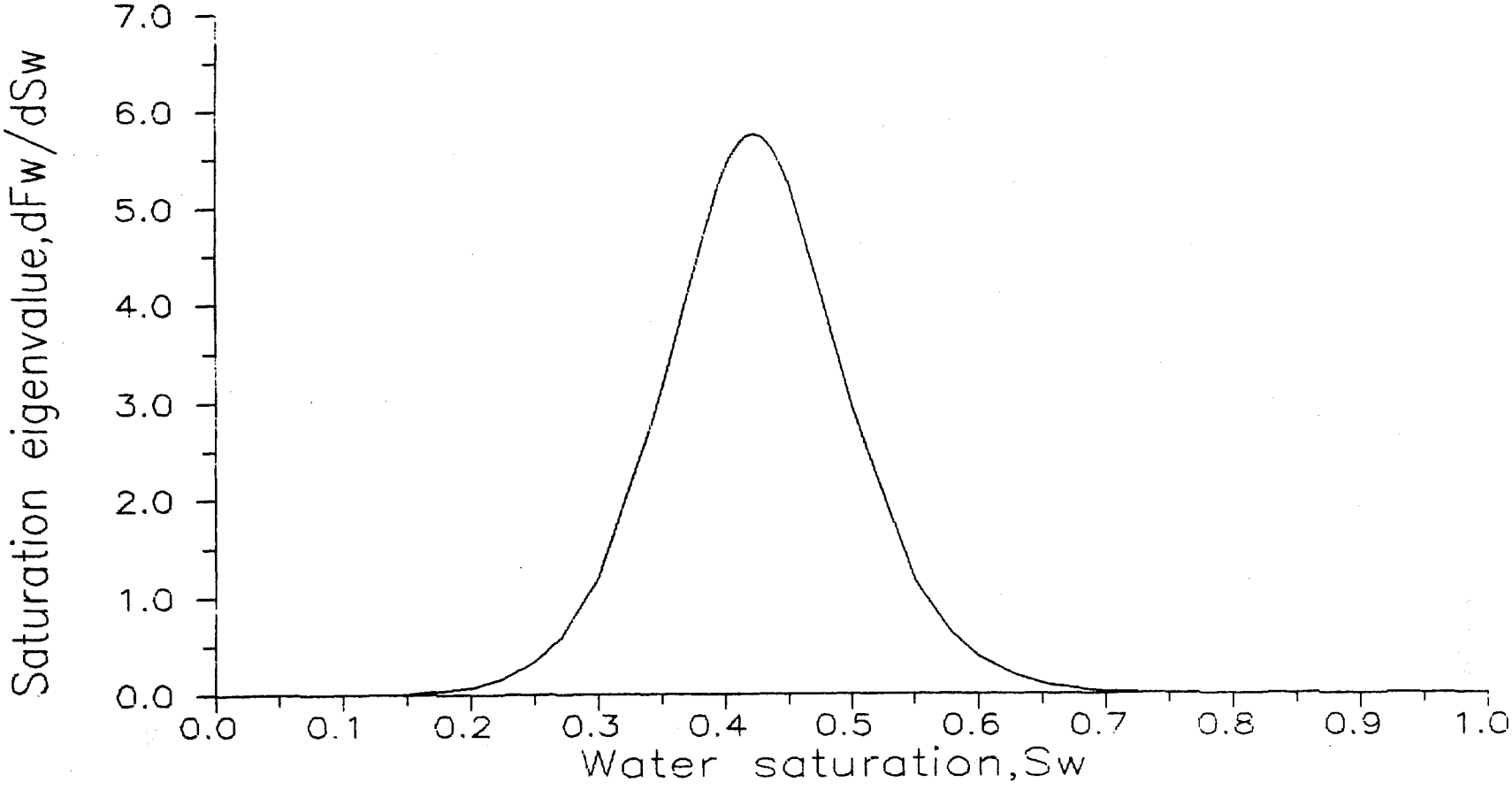

Fig. 1: Eigenvalue versus water saturation

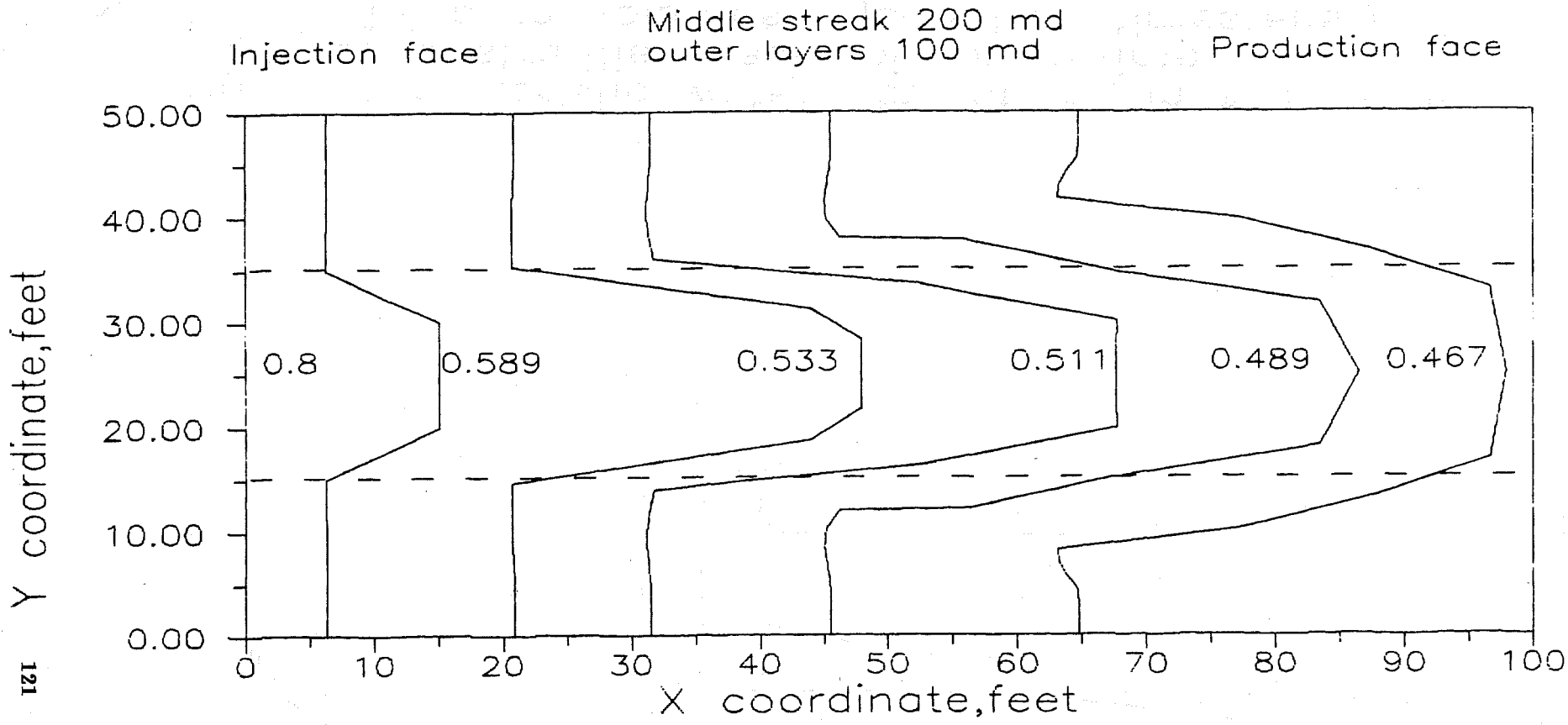

Fig 2:characteristic water saturations in the water flood of a stratified reservoir at a time of 35 days(0.17 pore volumes injected,10 timesteps.)

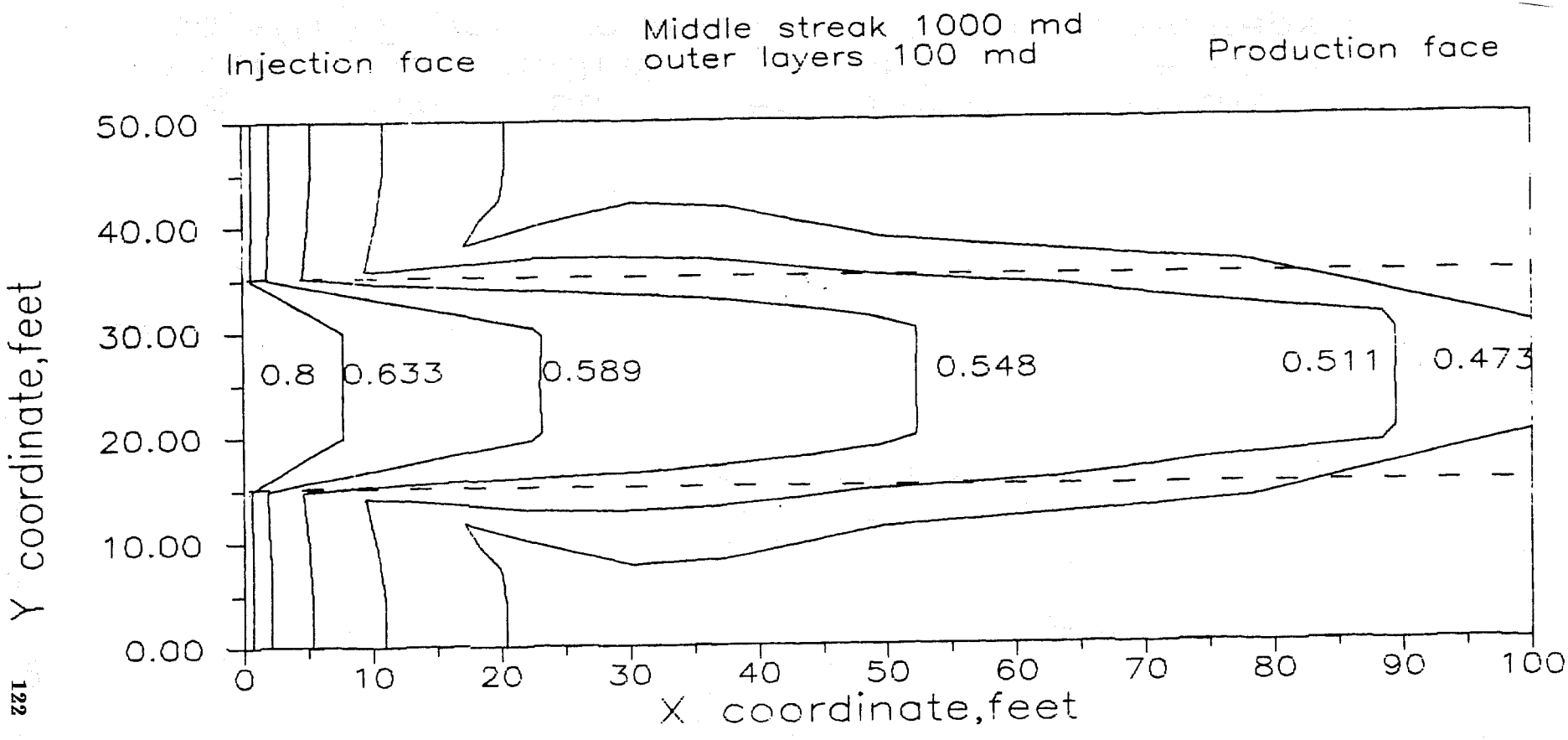

Fig 3:characteristic water saturations in the water flood of a stratified reservoir at a time of 11 days(0.17 pore volumes injected,10 timesteps.)

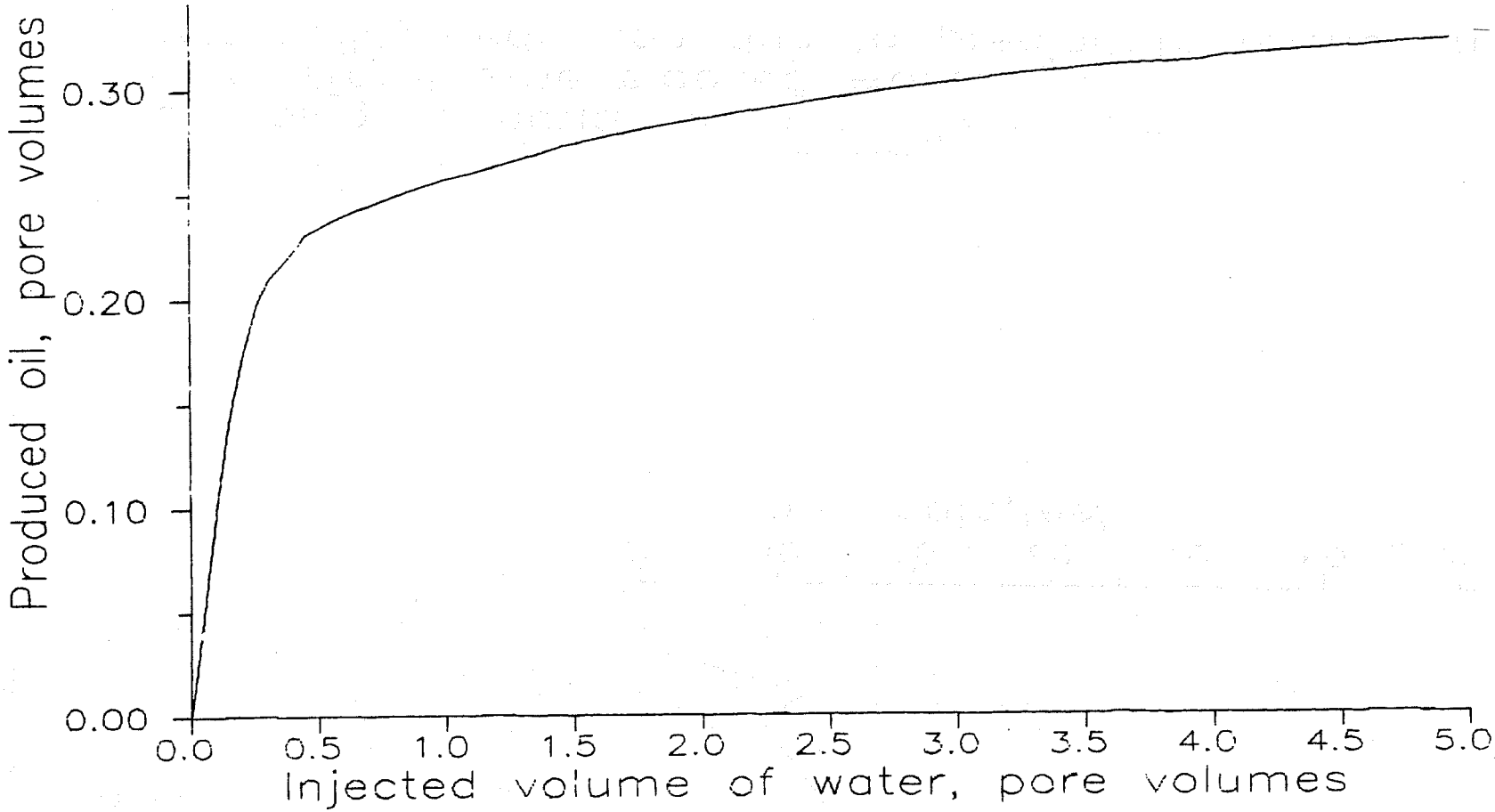

Fig.4: Production history for stratified reservoir (100 & 1000 md.)

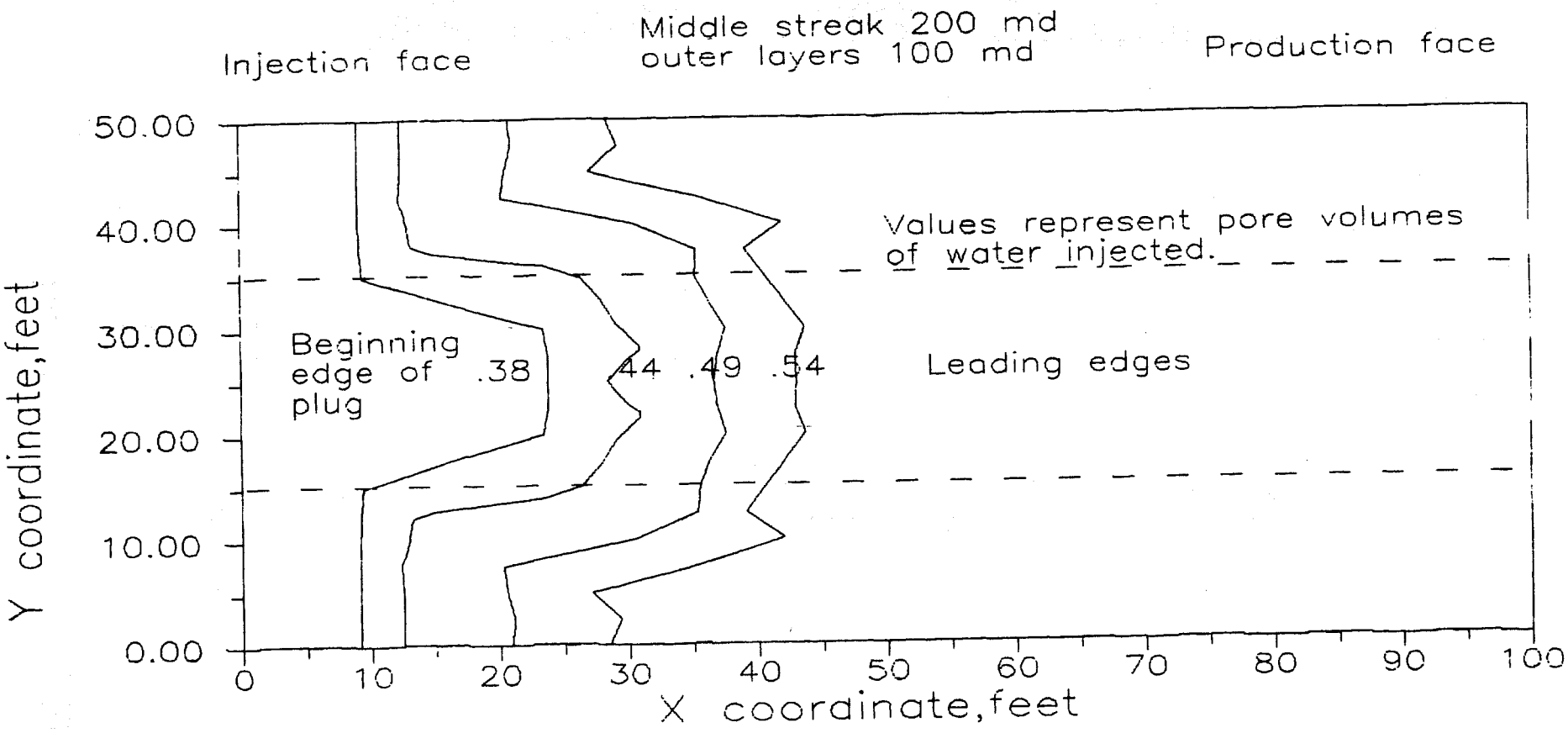

Fig 5:plug formation in a mildly heterogeneous reervoir.Total time elapsed =0.86 years.
Permeability reduction due to precipitate formation=100

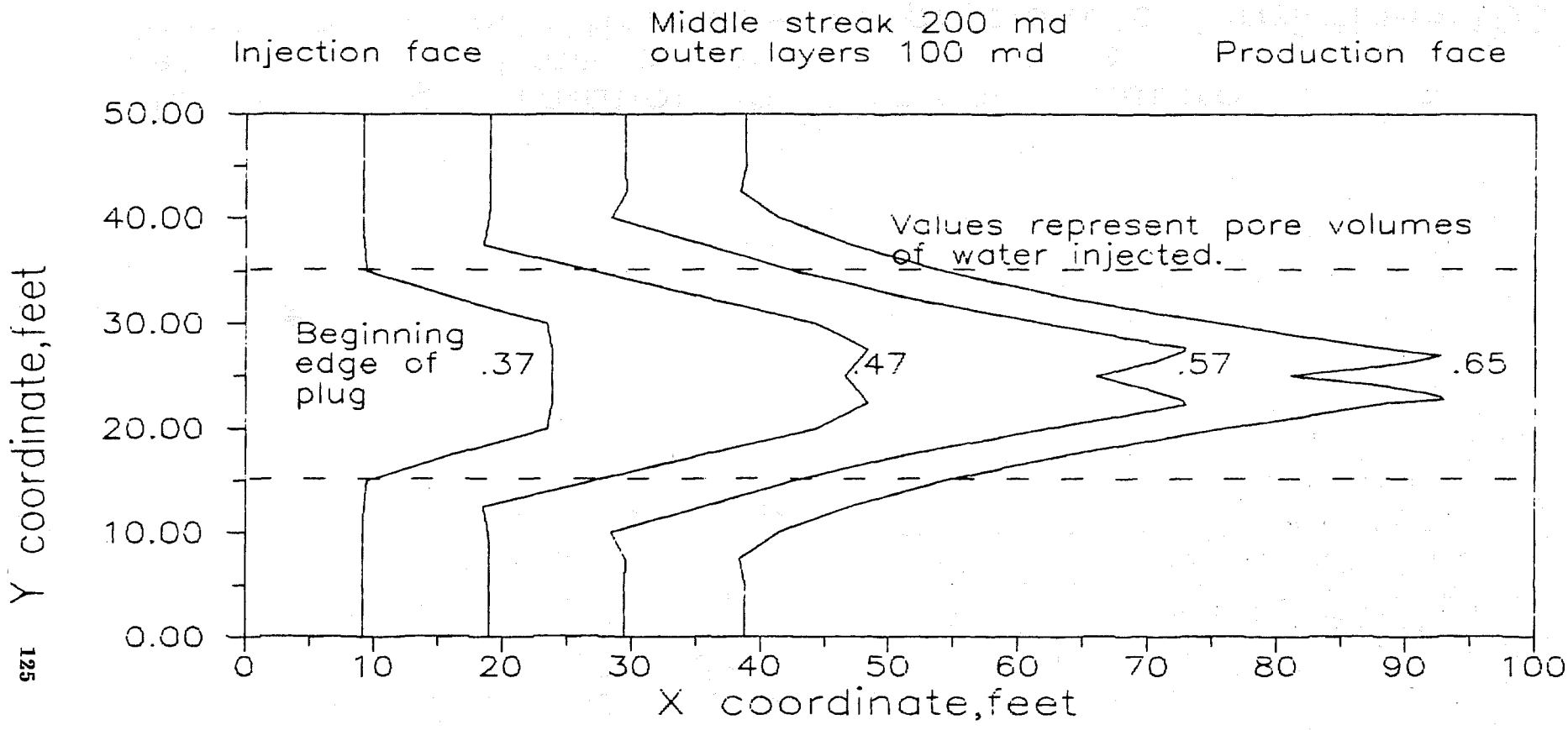

Fig 6:plug formation in a mildly heterogeneous reservoir.Total time elapsed=0.43 years.
Permeability reduction due to precipitate formation=2.

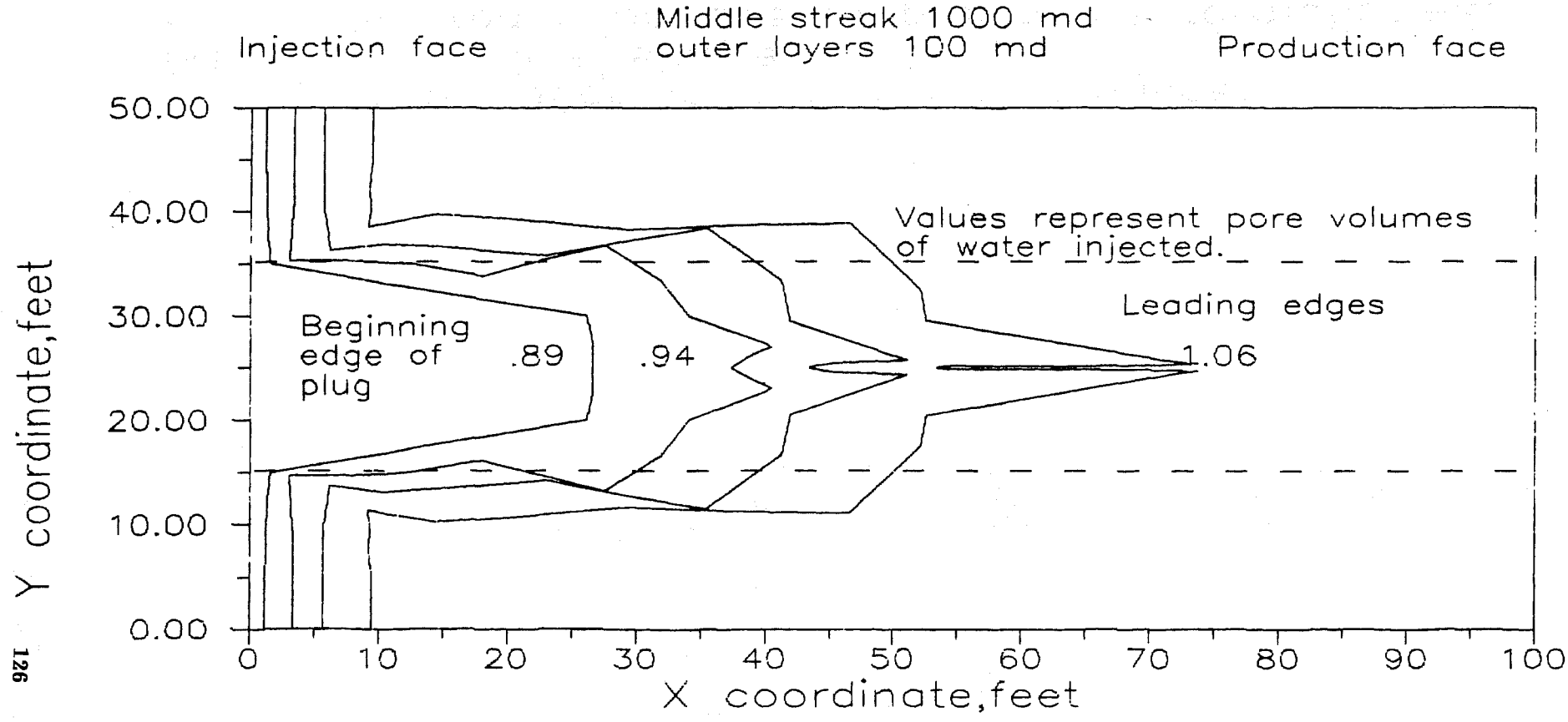

Fig 7: plug formation in a strongly heterogeneous reservoir.Total time elapsed=0.31 years.
Permeability reduction due to precipitate formation=100

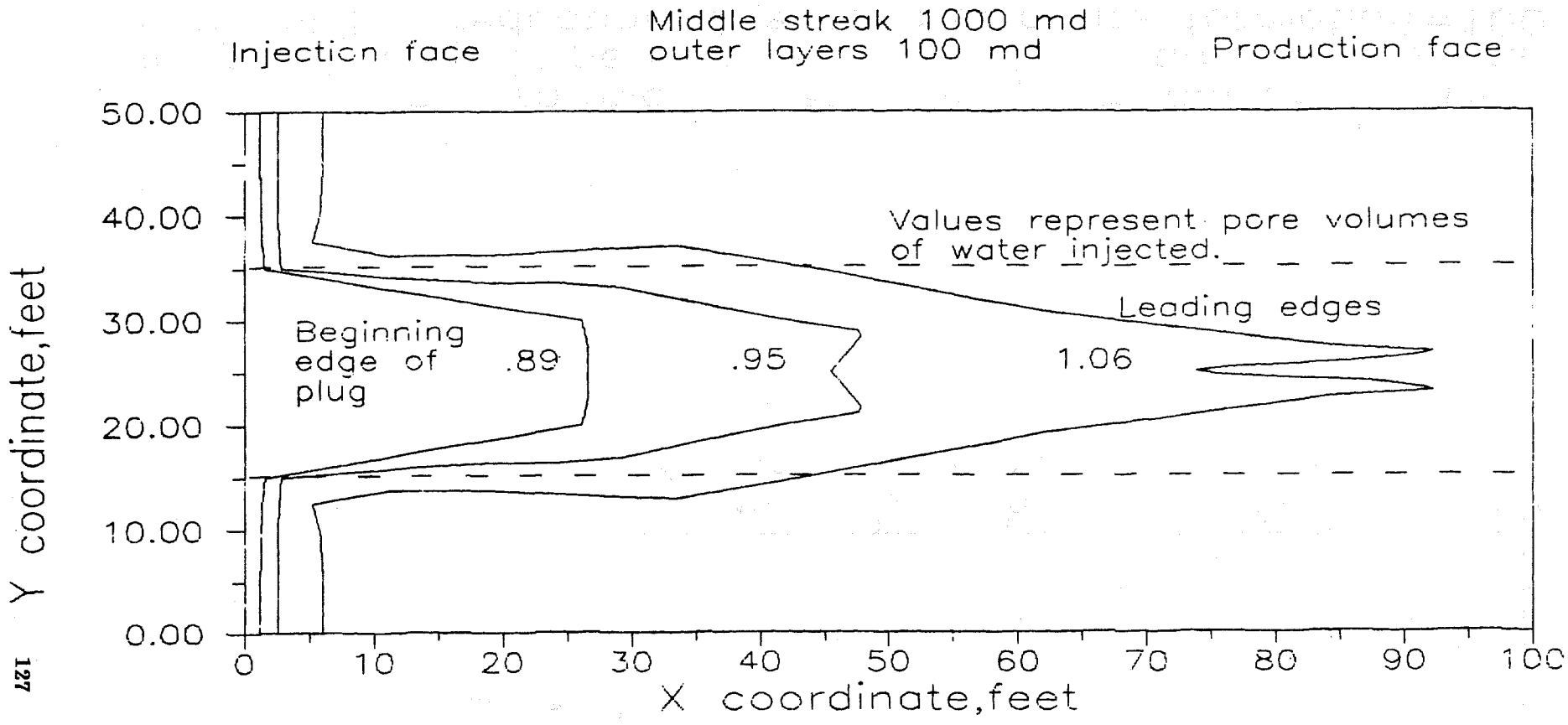

Fig 8: plug formation in a strongly heterogeneous reservoir. Total time elapsed=0.21 years.
Permeability reduction due to precipitate formation=10

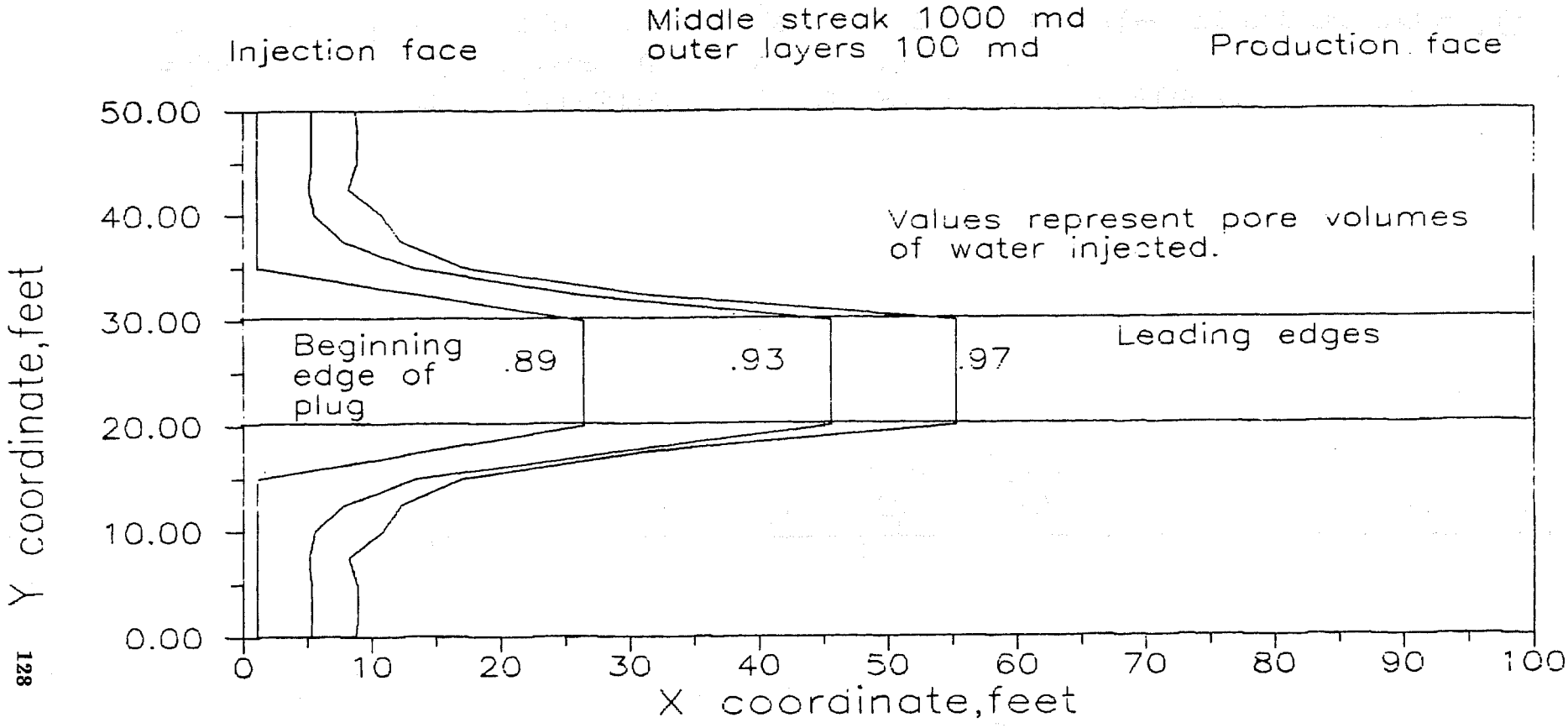

Fig 9: plug formation when high permeability streak surrounded by impermeable layers. Total time=0.3 years. Permeability reduction due to precipitate formation=100

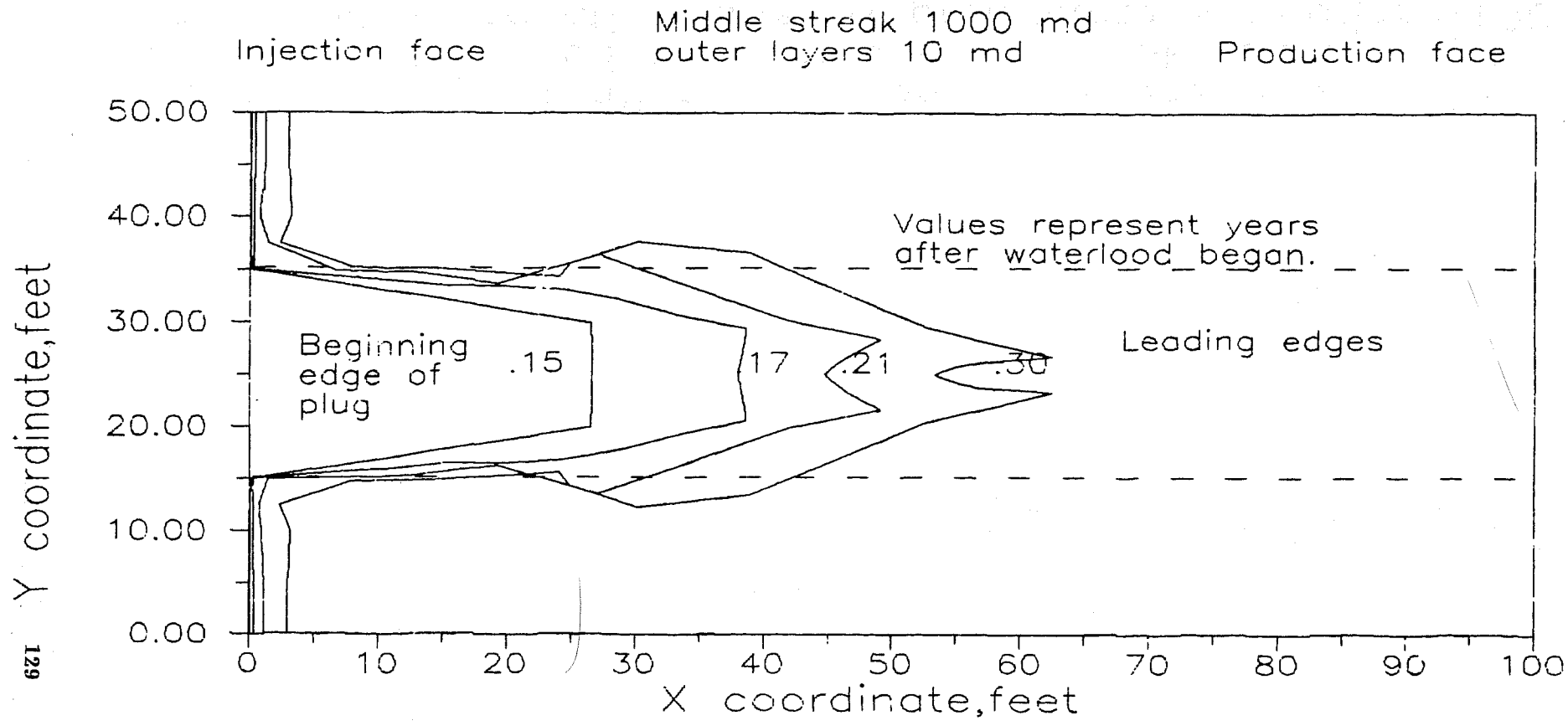

Fig 10: plug formation in a very strongly heterogeneous reservoir.Total flood time = 0.3 years. Permeability reduction due to precipitate formation=100

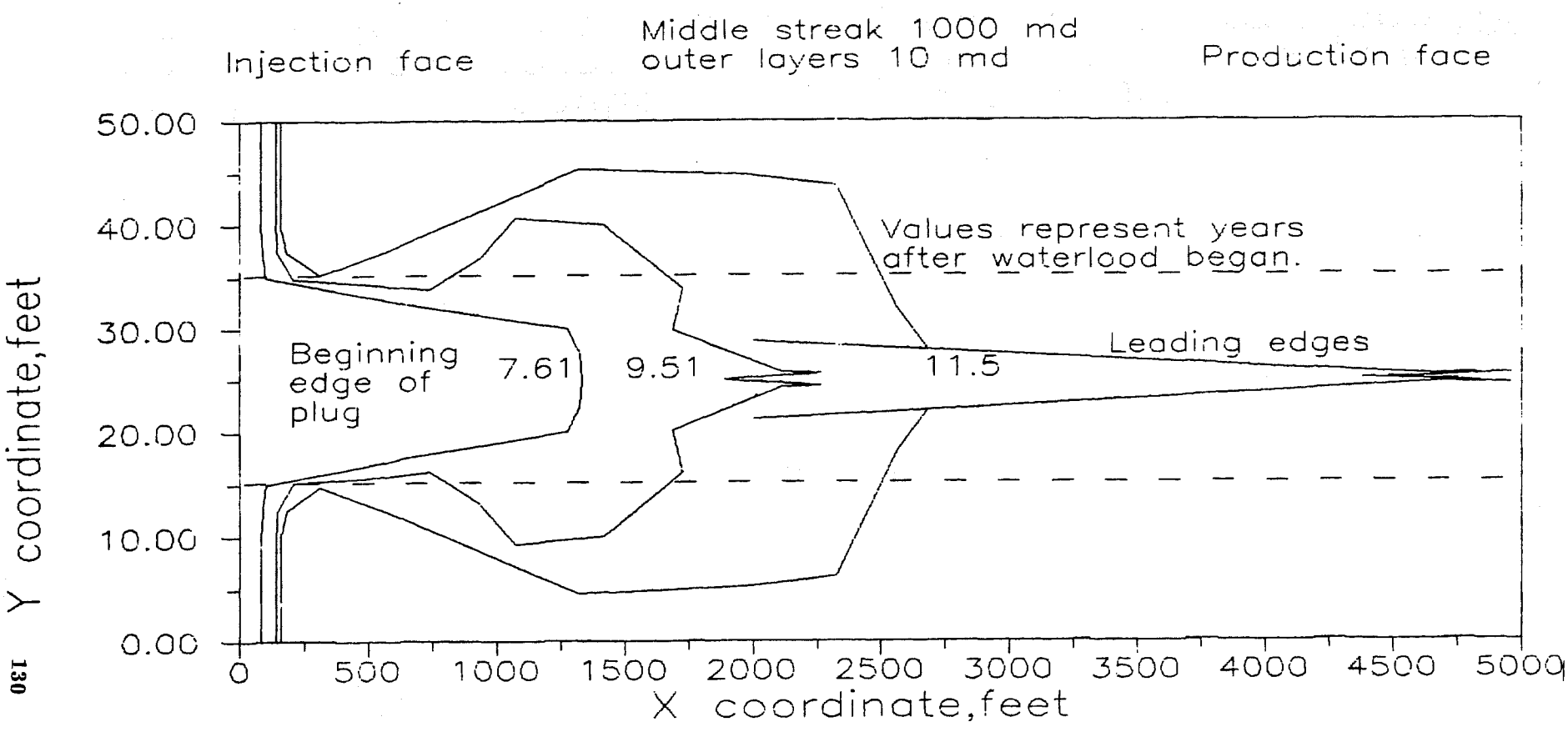

Fig 11: plug formation in a long heterogeneous reservoir.Total flood time elapsed = 11.4 years. Permeability reduction due to precipitate formation=10C

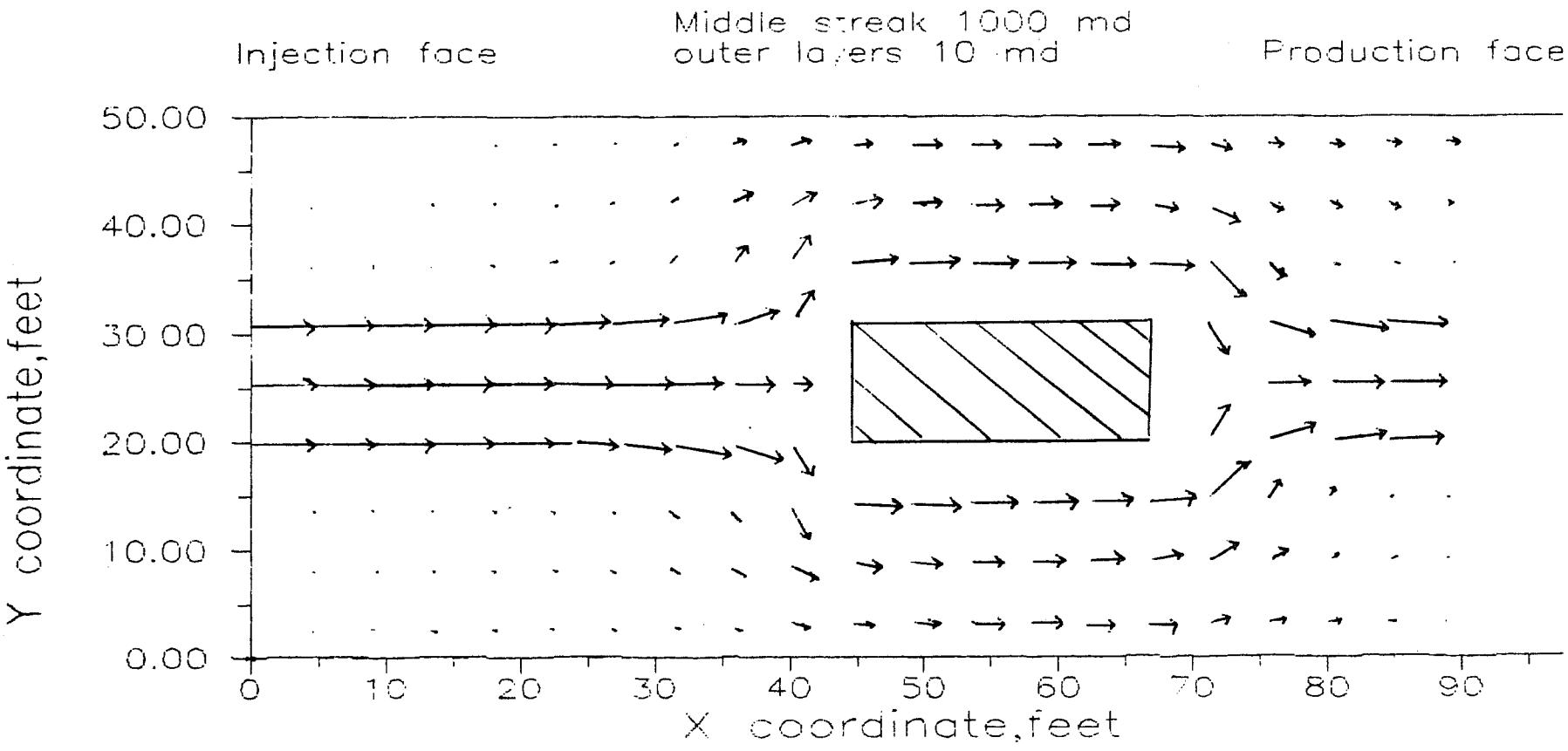

Fig 12: Nature of flow -field after plug formation.

★ U.S. GPO: 1988 561-025/80014